LA-UR-16-23972
Approved for public release; distribution is unlimited.

Title:	Limits on Subcritical Reactivity Determination using Rossi-Alpha and Related Methods
Author(s):	McKenzie, George Espy IV
Intended for:	Doctoral Thesis
Issued:	2018-04-30 (rev.2)

LIMITS ON SUBCRITICAL REACTIVITY DETERMINATION USING ROSSI-α AND RELATED METHODS

BY

GEORGE E. MCKENZIE

DISSERTATION

Submitted in partial fulfillment of the requirements
for the degree of Doctor of Philosophy in Nuclear, Plasma, and Radiological Engineering
in the Graduate College of the
University of Illinois at Urbana-Champaign, 2018

Urbana, Illinois

Doctoral Committee:

Associate Professor Tomasz Kozlowski, Chair
Professor Matthias Perdekamp
Professor James Stubbins
Professor Rizwan Uddin
Dr. William Myers, Los Alamos National Laboratory

ABSTRACT

The subcritical reactivity, ρ, of a neutron multiplying system is of interest to many factions of the nuclear community. The subcritical reactivity in a nuclear system can be inferred from measurements of the prompt neutron decay constant, α. Near critical, the reactivity is linearly proportional with α, but the linearity between these quantities does not hold in systems with low multiplication or significantly above prompt critical.

This work examines a large range of subcritical prompt neutron decay constant measurements on a thermal HEU metal system. This system is designed to mimic a solution system and to have the optimal H/^{235}U ratio to minimize the critical mass. The reactivity of these measurements varies between 0$ and 70$ below critical. In addition to experimental measurements on the thermal system, simulations are performed on both the thermal HEU system and a fast HEU metal system. Both the fast and thermal results are compared to baseline simulations performed using criticality eigenvalue (*KCODE*) mode in MCNP®6.2. These simulations are used for comparisons on the linearity between α and ρ.

Prompt neutron decay constant measurements in this work are performed using the Rossi-α method. The measurements are taken using a ^{3}He neutron detection system and a Los Alamos National Laboratory designed list-mode data acquisition system. A specially designed computer program determines α from list-mode data.

The α-eigenvalue, or α at delayed critical, for the thermal HEU system is $-199.4 \pm 4.4\ s^{-1}$ as measured during this work. The α-eigenvalue for the fast HEU system was previously measured to be $-8.5 \times 10^{-5}\ s^{-1}$. The results from the thermal HEU system study suggest that the relationship between ρ and α is linear when $k_{eff} > 0.80$ based on the simulation results. The experimental results also agree with this result, but have less fidelity. No experimental results are available for the fast HEU system.

ACKNOWLEDGMENTS

First, I would like to express my sincere gratitude to Dr. William "Bill Myers of Los Alamos National Laboratory, and Professor Tomasz Kozlowski for their support in making this dissertation possible. Their knowledge and encouragement have been invaluable as I developed my dissertation. Bill took me on as an intern in the summer of 2012. He motivated me to continue my education. He has been a dedicated mentor, listening to all my ideas, good and bad, and encouraging me to continue my education. I could not ask for a better advisor, confidant, or friend. In 2014, Professor Kozlowski took me on as a student. Since then, he has been everything I could have asked for in an academic advisor. Professor Kozlowski has been extremely helpful and patient; while, I made his job more difficult from 1500 miles away. Both Bill and Professor Kozlowski alleviated many of the stresses that arose during the execution of an experimental dissertation.

In addition to Dr. Myers and Professor Kozlowski, I would like to thank the rest of my committee: Professor Uddin, Professor Stubbins, and Professor Perdekamp for their insightful comments and willingness to assist me in my academic development.

I want to thank Dave Hayes, my group leader at LANL. Despite his busy schedule, he always found time to provide technical advice. I realize that without his hard work I would not have any work to present. I have not had many managers in my short career, but I know that I have been fortunate to work with Dave. He truly embodies everything to which a technical manager should aspire.

I owe Travis Grove, Jesson Hutchinson, Rene Sanchez, and Joetta Goda a huge thank you for their support in implementing my experiments. Most of all, I want to thank each of them for being an excellent sounding board as I worked through the meaning of my results. I would also thank them for providing an excellent work environment that inspired learning.

Rene, Travis, and Joetta, along with Sam Gonzales deserve recognition dedicating their time to my project. Rene, Travis and Joetta were the main operators for the critical assemblies during experimentation. Sam was a lifesaver by creating a method to remotely run then neutron generator with a critical assembly in compliance with all existing safety requirements. Sam was also the neutron generator operator during the Godiva scoping experiments. Without Rene, Sam, Travis and Joetta, none of this would be possible.

Jennifer Arthur, another PhD candidate, provided assistance in streamlining the simulations I had to run. Without her, everything would have taken much longer to complete. I wish her good luck in completing her own dissertation.

Finally, I want to thank Professor Roy Axford. I consider him to be my earliest mentor. He inspired my interest in reactor physics and provided introduction to Dr. Myers at LANL.

TABLE OF CONTENTS

LIST OF ABBREVIATIONS

ADS	Accelerator Driven System
CPSD	Cross Power Spectral Density
DAF	Device Assembly Facility
DC	Delayed Critical
DT	Deuterium-Tritium
GE	General Electric
HEU	Highly Enriched Uranium
LANL	Los Alamos National Laboratory
LLD	Lower Level Discriminator
MCNP	Monte Carlo N-Particle (Computational Software)
mil	One-thousandth of an Inch
MOX	Mixed Oxide (generally referring to Pu-U nuclear fuel)
NCERC	National Criticality Experiments Research Center
NIM	Nuclear Instrumentation Module
NNSS	Nevada National Security Site
PNS	Pulsed Neutron Source
SCA	Single Channel Analyzer
SNM	Special Nuclear Material
TTL	Transistor-Transistor Logic

LIST OF SYMBOLS

α	Prompt Neutron Decay Constant
α_{DC}	Prompt Neutron Decay Constant at Delayed Critical, α-eigenvalue
A	Average Count Rate of a System
B	Maximum Correlated Count Probability
β_{eff}	Effective Delayed Neutron Fraction
D_ν	Diven's Parameter
Δt	Time Difference Between Neutron Counts
ϵ	Efficiency of the Detection System
F	Average Fission Rate
k_{eff}	Effective Multiplication Factor
k_p	Prompt Multiplication Factor
k_{DC}	Multiplication Factor of the Calculation for the Delayed Critical Configuration
l	Neutron Lifetime
m	Mass
m_c	Mass at Critical
ν_p	Average Number of Neutrons Emitted Promptly from Fission
p(t)	Probability
ρ	Reactivity
σ	Standard Deviation
Σ_f	Macroscopic Fission Cross Section
Σ_a	Macroscopic Absorption Cross Section
υ	Velocity of Thermal Neutrons

CHAPTER 1

INTRODUCTION

The measurement of subcritical reactivity has become an expanding area of research in the past several years. This work discusses inference of subcritical reactivity using measurements of the prompt neutron decay constant, α. Prompt neutron decay constant measurements are rooted in the Manhattan Project where scientists wanted to measure reactor physics properties of uranium and plutonium. These measurements were used to determine the prompt neutron lifetime of these new materials. Today, these measurements are still used to give understanding of the prompt neutron lifetime in a system, and provide information on the hardness of the neutron spectrum in a system. Prompt neutron decay constant measurements provide a meaningful comparison between different experiments.

The renewed interest in determination of subcritical reactivity is due in part to the desire to build subcritical accelerator driven reactor systems that operate below critical using the neutron multiplication of the system to increase the total neutron flux from the accelerator. Measuring the reactivity in this type of system presents challenges because it falls between reactor measurements and conventional subcritical measurements. This work examines the application of deriving the subcritical reactivity of a system through measurement of prompt neutron decay constants.

1.1 Prompt Neutron Decay Constant Determination Methods

Neutron kinetics measurements give valuable insight into the dynamic behavior of a multiplying system. One such measurement is the prompt neutron decay constant, Rossi-α. The prompt neutron decay constant of a system is the rate at which the prompt neutron population changes as a function of time. For systems at delayed critical, this measurement

directly provides the prompt neutron decay constant at delayed critical or α-eigenvalue. The α-eigenvalue is the eigenvalue of the point reactor kinetics equation including delayed neutrons.

The α-eigenvalue is a standard metric used to benchmark the hardness of the neutron spectrum when performing criticality experiments. As the neutron spectrum hardens, the absolute value of the α-eigenvalue increases. The comparison of α-eigenvalues provides a consistent comparison among a wide variety of systems.

There are several methods for measuring the α-eigenvalue of a system. In general, these methods follow one of two different methodologies. The first methodology measures the time correlations between neutron detection events in a static neutron population. Then, it reconstructs the decay curve for the prompt neutron population using a statistical model. The second methodology uses neutron sources that are dynamic with respect to time to measure the decay in real time.

The first methodology includes techniques like the Rossi-α method and Feynman's variance-to-mean method. The Rossi-α method and Feynman's variance-to-mean method both statistically analyze the data to determine the value of the α-eigenvalue [1].

The second methodology includes techniques such as the source-jerk technique and the endogenous pulsed source technique. These techniques directly measure the prompt neutron population decay [1, 2]. The downside of these methods is that measuring prompt decay above delayed critical poses additional complications.

Prompt neutron decay constant measurements are best applied to configurations where the system is near delayed critical. All of the measurement techniques mentioned were developed using the point reactor kinetics model. These methods work best near delayed critical because the point reactor kinetics model assumes a point system near critical, so that the assumption of separability between spacial and temporal flux components is validated. For the measured quantities to retain their physical meaning, these techniques require the assumptions of the point reactor kinetics model to be adhered to.

This work examines the use of prompt neutron decay constant measurements to determine the subcritical reactivity in a system. The known range of applicability for relating the prompt neutron decay constant to reactivity is shown in Fig. 1.1. The red region in Fig.

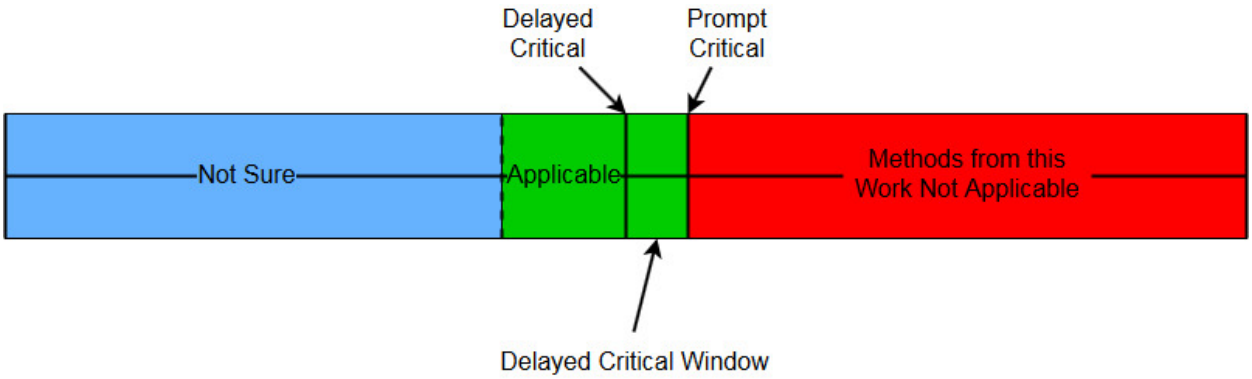

Figure 1.1: Range at which prompt neutron decay constants can be made and related to reactivity using neutron noise techniques.

1.1 consists of reactivities above prompt critical. Above prompt critical, the time constant becomes sufficiently fast that fission due to delayed neutrons occurs outside the frame of reference for the measurement; therefore, the inverse of the reactor period is the prompt neutron decay constant. Neutron noise measurements, like those discussed in this work, are not applicable above prompt critical. The green region of Fig. 1.1 consists of the region where a definitive linear relationship between α and reactivity has been established. The blue region in Fig. 1.1 consists of a region where measurements of α are possible but may or may not have a linear relationship to the systems reactivity.

This work will attempt to expand the green region from Fig. 1.1 into the blue region. This will be accomplished by comparing measurements taken in the green region to simulations of the same system to establish a baseline. Then subsequent measurements of α will be taken in the blue region and similarly compared to simulations to determine how well the measured quantity estimates the subcritical system reactivity using linear proportionality. These measurements seek to broaden the scope of the green region in Fig. 1.1 and provide a lower bound for subcritical reactivity determination using prompt neutron decay constants, α.

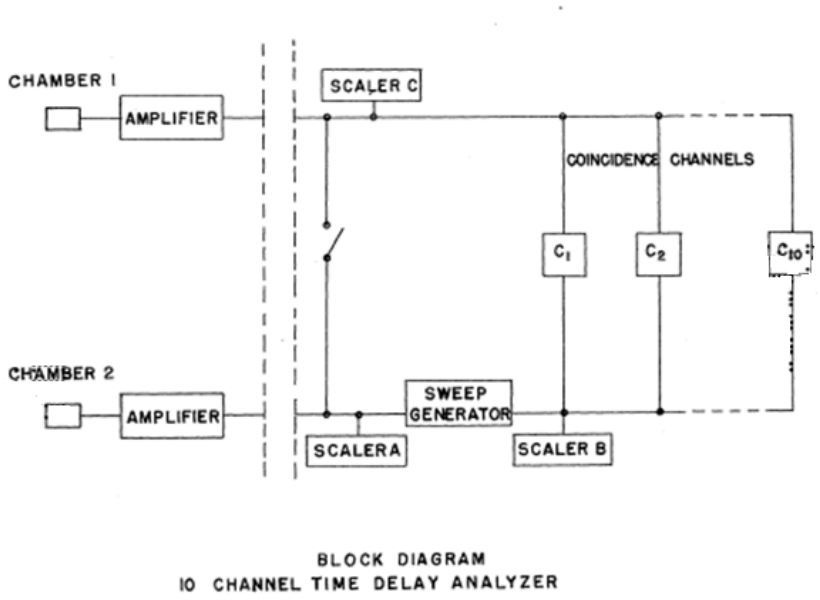

Figure 1.2: Schematic of Orndoff's Counting Circuit [4].

1.2 Past Experiments

The origin of α-eigenvalue techniques dates all the way back to the Manhattan Project, and more specifically to the work performed by the critical experiments team. The first prompt neutron decay constant measurement technique developed was the Rossi-α technique. The Rossi-α technique is an experiment originally proposed by Bruno Rossi in the 1940s. This experiment is accompanied by a heuristic, statistical analysis technique capable of separating prompt neutrons from delayed neutrons developed by Richard Feynman [3]. The experiment included a complex electronic configuration which captured the time neutron behavior through the use of gates and delay lines. A schematic of this system is shown in Fig. 1.2. This approach was most notably performed by John Orndoff [4]. Over time, advances in technology have changed the way this experiment is performed, but not affected the theory behind these measurements. An overview of neutron noise measurements and some of their history can be found in a paper by Muñoz-Cobo et al. [5].

Measurements using the Rossi-α technique were completed by Baker in 1947 on two UH_3 assemblies. Both assemblies were pseudo-spherical and used UH_3 cubes surrounded by tungsten carbide and beryllium oxide [6]. Orndoff also completed measurements at Los Alamos.

He measured time constants on an uranium metal assemblies called Lady Godiva and Topsy. Lady Godiva was a spherical uranium metal burst reactor and Topsy consisted of 0.5 in. by 0.5 in. uranium metal blocks [4, 7].

The pulsed source technique is a simplistic method of determining the prompt reactivity in a nuclear system. The pulsed source technique was developed in the 1940s during the Manhattan project. Its first applications were not used to measure the reactivity of a system, but rather to determine the neutron lifetime in reflector materials. These experiments were documented by Kupferberg [8]. The first experiments using a pulsed neutron source on a multiplying system were performed by Passell et al. at Livermore Radiation Laboratory [9] who measured the prompt neutron decay constant of a 13.1 cm enriched uranium sphere. Other early work was performed by Simmons and King [10] whose experiments included the measurement of the prompt neutron decay constant in a reactor with a $1/v$ poison in a hydrogen-moderated reactor. These measurements were completed with good accuracy to approximately 12$ subcritical. Additionally, measurements were performed by Brown on a slab geometry system consisting of water moderated ^{235}U [11]. These measurements covered a range of 30$ subcritical to a critical configuration. Another type of reactivity determination method also arose around this time, which utilizes a known configuration's value of alpha to determine a subcritical reactivity. This method known as the $k\beta/l$ method is derived and compared to data from a light water reactor in a paper by Garelis and Russell [12]. Their comparison analyzes data that is claimed to be 30$ subcritical. Garelis and Russell also provide useful information on the pulse rate required for good results stating that the repetition rate of the source must be much larger than the decay constant of the shortest lived precursor [12].

In 1965, a symposium on pulsed neutron research was held in Karlsruhe, Germany. Many papers in this meeting discussed different types of measurements using pulsed neutron sources, some papers of note were written by Garelis [13] whose work models the time profile of neutron density. Garelis' paper suggests that the prompt response of the reactor is essentially the Green's function of the reactor because the source is approximately a delta function neutron burst. Garelis' paper also suggests that the pulse rate needs to be small when compared to the decay constant to allow the population to decay between events.

Another paper of interest was written by Meyer [14] examines the pulsed source technique in light water assemblies (i.e. large central power stations). The experiments presented in Meyer's work show that meaningful results were obtained as far as 3.5$ subcritical. At the same symposium, a paper discussing modifications to the pulsed source method was presented by Gozani et al. [15]. The paper discussed modifications to the theoretical derivation to the pulsed source technique which included delayed neutrons. Gozani called this the modified pulsed source technique. Gozani et al. claim that these delayed neutrons are important for small cores which are heavily reflected by light nuclei. Gozani et al. applied their technique to a reactor system with a minimum reactivity near 1$ subcritical. Another attendee, Scott [16] presented a paper discussing pulsed neutron measurements performed on a subcritical reactor. Scott's measurements were performed with a minimum reactivity of 11$ subcritical. These prompt decay measurements were completed using a 1Hz source with 1000 pulses, and the paper concludes that measurements to 11$ subcritical were the lowest that could be achieved at the time with errors below 5%. Work presented by Storrer suggests that the lower limit for pulsed source measurements is based on k_{eff} rather than on reactivity in terms of dollars. This work suggests the lower limit is near a $k_{eff} = 0.7$ [17], although no experimental results are presented.

Increased interest in pulsed source measurements appeared again in the 1990s. The reasoning behind this resurgence is rooted in nuclear waste issues. One concept to reduce nuclear waste product is to transmute the actinides in the waste. The proposed transmutation reactors would never actually achieve criticality, but would rather be accelerator driven to increase reaction rates in a subcritical mass. These accelerator driven systems (ADS) drove a large resurgence in pulsed source techniques globally [18].

Before any new experiments could begin, some theoretical work was required to modify the methods to subcritical conditions, and non-stochastic sources [19, 20]. The first step was to modify many of the neutron noise techniques to be utilized during pulsed source operations. While this is interesting mathematics, its derivation is experimentally unnecessary as these measurements are still able to be performed on the steady neutron population between pulses where the population is both stable, and the source is stochastic. The majority of this work was performed by Pazsit and Yamane [21], Kuang and Pazsit [22], Degweker [20], Rugama et

al. [23], Baeten [24], and Kitamura et al. [25]. The delayed neutrons are considered to have a larger effect because fewer fissions are occurring in a subcritical reaction, so much effort was put into modifying many of the neutron noise techniques to include delayed neutrons. This work was primarily performed by Kitmura et al. [26] and includes one group of delayed neutrons.

In addition to new theoretical models, new hardware available to the modern experimenter improves the accuracy of the measurements and fundamentally changes how data acquisition happens. The progressive advancement of computer technology (i.e. the digital age) enabled new forms of data acquisition [27]. Instead of delay gates and physical counters, time-dependent data is recorded digitally. The data acquisition system used in this work is a list-mode module which is a LANL designed hardware capable of recording time stamps for up to 32 detectors at once with a resolution of 100 ns [28]. Examples of measurements using this technology are presented in articles written by Kitamura et al. [29] and by Jammes et al. [30].

The MUSE project built several different configurations measuring the kinetics properties of a mixed oxide system (MOX) at the MASCURA reactor in Cadarache, France. The MUSE-3 project was mainly interested in mapping the neutron flux in a source driven system [31].The MUSE-4 project is of more interest to this author because this project concentrated on different kinetic methods such as pulsed neutron source (PNS), fluctuation (Rossi-α or Feynman-α), and transfer function methods (Cross Power Spectral Density (CPSD)) for reactivity determination. Many of these papers suggest CPSD as the best method to determine the MASCURA core subcritical reactivity. As such, the measurement range for CPSD is far broader than for any other technique [32].

Although not the primary objective of the measurement campaign, some dynamics measurements of the MUSE-3 project were presented by Gadini and Salvatores [33] and Aliberti et al. [34]. Gadini and Salvatores compared the neutron density decline due to a burst of neutrons for several cases (between -42 and -1595 pcm), but did not perform the necessary analysis to separate the value of α [33]. Alberti et al. performed similar measurements with a low reactivity measurement at -5687 pcm ($\sim$-15\$) [34].

The MUSE-4 core was benchmarked by Messaoudi and Malambu [35] using neutron trans-

port codes with various nuclear data sets. Additional simulations were performed to compare the generation time of the system to experiments; this work was completed by Billebaud et al. [36] and determined the generation time for MUSE-4 to be 0.58 μs using neutron transport simulations. Pulsed source measurements are discussed by Villamarin and Gonzalez-Romero [37] using ^{237}Np and ^{235}U fission chambers, Soule et al. [32], Billebaud et al. [36], Jammes et al. [30], Rugama et al. [38, 39], and Baeten and Abderrahim [40], for configurations with a range of k_{eff} between 0.95 and critical using both 2.5 MeV and 14 MeV neutrons. Villamarin and Gonzalez-Romero discuss that a measurement of the system at its least critical state (k_{eff}=0.86) was attempted, but good results were not obtained due to what the authors claim as inadequate equipment [37].

One paper that should be addressed in this discussion was written by Grabezhnoi et al. [41]. Around the same time as the other ADS measurements, Grabezhnoi et al. published a paper on deeply subcritical Rossi-α measurements. These measurements were taken with calculated k_{eff} between 0.3 and 0.45 for a set of Pu blocks and 0.7 to 0.97 for the MATR subcritical assembly and the paper discusses using the area method to determine the value of α. The paper discusses how the results they obtained were related to α in the sense that these measurements would produce an incorrect correlation to the prompt reactivity without the use of fudge factors. The paper does assert that a delta change in reactivity can still be measured although the results are not linear with the α-eigenvalue [41].

The Yalina experiment is another European program working on ADS in Minsk, Belarus. The Yalina program ran in parallel to the MUSE program, but its subcritical core has a thermal neutron spectrum [42]. Experimental measurements using the pulsed source method were performed on this core down to about -9050 pcm [42].

The MYRRHA project is a collaboration in Belgium to work on ADS design for spent fuel transmutation. FREYA is a smaller piece of the MYRRHA project. Some computational analysis of the prompt decay has been completed by Saracco et al. [43]. This study examined reactivity states between k_{eff}=0.90 and k_{eff}=0.995 [43].

Recent developments in Rossi-α measurements have included a modern measurement system being added to the National Criticality Experiments Research Center (NCERC). A large range of systems have been measured including fast and thermal systems using both

uranium and plutonium metal fuel. The first experiment measured was a cylindrical HEU metal core reflected by copper [44, 45]. The second set of measurements was an interaction of the first but had lead interstitial used between the HEU plates [46]. The third system measured was another iteration on the HEU copper configuration which had both lead and natural uranium interspersed between the HEU plates. This core had an effective enrichment just above 20% and the results are currently unpublished. The fourth system measured was a thermal HEU system called the Polyethylene Class Foils which consists of HEU foils between polyethylene plates [47]. The fifth system measured at NCERC was a ball of HEU surrounded by a polyethylene reflector [48]. The sixth measurement made at NCERC was the first plutonium measurement completed since start-up of the facility, and consisted of a core of weapons grade plutonium, lead interstitial, and copper reflection. These results are not yet published. All of these results were used to calcualte the subcritical reactivity in the system. When possible, these reactivities were compared to control system calibrations. The results typically matched up extremely well. But, none of the measurements were more than 1$ subcritical. All of the measurements mentioned paved the way for the work presented here. Each case provided lessons learned, and improved the quality of Rossi-α measurements taken at NCERC. Evaluation of these measurements led to ideas explored in this work, and helped refine the experiment(s) necessary to reach a conclusion.

Recent developments in ADS technology were summarized in a report by Uyttenhove [49]. This report discusses the three current ADS testing systems MYRRHA, VENUS-F, and EFIT [49]. Uyttenhove suggests that the pulsed source method is beneficial to measure reactivity during start-up. Results of pulsed source measurements of the VENUS-F configuration suggest that the experiments overestimate the reactivity present in the range of operation k_{eff}=0.96-0.97 [49].

1.3 Innovation

Calculating subcritical reactivity is an interesting challenge in reactor physics. Reactivity for operating reactor systems is measured by calibrations performed above delayed critical and extrapolated to the region below critical. Only values near critical are accurate. Con-

ventional subcritical techniques like Feynman variance-to-mean, on the other hand, rely on assumptions that render them inaccurate for measurements near critical. As the system nears critical, the associated uncertainty rapidly increases. Techniques like Rossi-α or the endogenous pulsed source technique may be the best method to determine subcritical reactivity in a system that was never intended to go critical. One of the things that makes the prompt neutron decay constant a very powerful technique lies in the fact that subcritical reactivity may be determined without ever achieving a critical state. This thesis explores if and when measurements of the prompt neutron decay constant decouple from a linear relationship to subcritical reactivity. The idea is that one or more of the assumptions vital to the point-kinetics model is violated, such that the prompt neutron decay constant is no longer well defined by the model.

Many of the previous experiments recognize the existence of a breakdown of the linear relationship between reactivity and α at some unspecified large negative reactivity. This breakdown occurs when one of the assumptions fundamental to these measurements has been violated, and the mathematical model no longer agrees with reality. When this breakdown occurs, the current model of α is no longer sufficient, and a different model is required to properly represent the physics. These measurements will attempt to fully define the region of validity for the linear relationship between the prompt neutron decay constant and reactivity. Experiments up to this point have measured reactivity through various prompt neutron decay constant measurement methods to a $k_{eff} = 0.90$. This work will extend this range to a $k_{eff} = 0.64$. These measurements are beneficial to ADS system controllers as a check that their systems are performing in the intended manner, as well as to any individual who intends to build and safely measure a subcritical mass.

The breakdown observed is related to violation of one or more of the assumptions made in the development of the point reactor kinetics model. The assumption that is most likely violated is the assumption that the measurement is performed on a system that is in fundamental mode. Fundamental mode is the same assumption made during neutronic analysis that the flux or population spatial distribution will follow the mathematical representation of the first eigenfunction. This assumption is perfectly valid for a system at or near critical because an incident neutron will generate a chain reaction that does not rapidly die

away. The length of these chains allows an isotropic neutron population to build within the material driven by the decay products of previous fissions. As the reactivity of a system decreases, the length of time that fission chains exists decreases and the spread of decay products is not evenly distributed, so fundamental mode neutron population distribution cannot be achieved.

Measurements of subcritical reactivity based on the prompt decay constant complement other subcritical neutron multiplication methods, such as the Feynman variance-to-mean method. These methods complement one another in that prompt neutron decay measurements are most applicable near delayed critical while subcritical multiplication methods tend to break down as the system approaches delayed critical [50]. Although this complementary relationship is known, there is no distinct point where a turnover of techniques occurs. This work will place a lower bound on the applicability of prompt neutron decay measurements by prompt neutron decay constant methods.

CHAPTER 2

REACTOR KINETICS

2.1 Fission

Nuclear fission is an extremely useful but volatile process. When an atom fissions: daughter nuclei form, neutrons are liberated, photons and other particles are released, and massive amounts of energy are transferred to the surrounding media. A generalized fission reaction in uranium is shown in Eq. 2.1.

$$^{235}U + n^0 \rightarrow {}^{236}U^* \rightarrow fission\ fragments + n^0 s + other\ particles \tag{2.1}$$

In nuclear reactors, this fission reaction is sustained when the neutrons generated through the fission process live on to create another fission, and thus a neutron chain begins. A construct called the effective multiplication factor, k_{eff}, was developed to describe the average behavior of these chains. The effective multiplication factor is the ratio of the neutron population between the previous neutron generation and the current one. The effective multiplication factor is a construct designed to describe a nuclear chain-reacting system. The effective multiplication factor is not a directly measurable quantity. Although its value can be assumed to be 1 at delayed critical. The effective multiplication factor quantifies how close, or far, a neutron multiplying system is from being critical. When a system is critical, the value of k_{eff} is exactly one. Every neutron in generation i is replaced by exactly one neutron in generation $i + 1$. This creates a stable chain reaction. In reality, this process occurs over many generations, and will fluctuate with each generation. The average behavior of the system is what is important to defining the criticality of a system. Sub-critical configurations have values of k_{eff} less than one. Every neutron in generation i is replaced

by any number of neutrons less than one in generation $i+1$. This creates a dissipating fission rate. Supercritical configurations have values of k_{eff} greater than one. Every neutron in generation i is replaced by more than 1 neutron in generation $i+1$. This leads to an exponentially growing fission rate. The range of the effective multiplication factor is shown by Eq. 2.2.

$$k_{eff} \begin{cases} < 1 & subcritical \\ = 1 & critical \\ > 1 & supercritical \end{cases} \tag{2.2}$$

2.2 Types of Neutrons

During fission, two different categories of neutrons are produced. These categories are named prompt and delayed neutrons based on the time of birth of the neutron in relation to the fission that created it. Prompt neutrons are those released as a direct result of fission. The daughter nuclides, or fission fragments, born in fission are highly unstable and often produce more photons or even release neutrons themselves. Delayed neutrons are released on the order of milliseconds to seconds after the fission process and originate during decay of these highly unstable daughter nuclides.

Delayed neutrons account for a small portion of the total neutron population in a generation. The ratio of delayed neutrons to the total population of that generation is denoted by the symbol β typically referred to as the delayed neutron fraction. The delayed neutron fraction is in itself an approximation based upon the compound probability for each fission daughter to produce a neutron as part of its decay process and the probability for that fission daughter to be produced during a fission event. The energy at which a neutron is born is an important thing that needs to be accounted for because the probability for interaction between a neutron and a nucleus is inversely related to energy. Delayed neutrons are typically born in the keV energy range whereas prompt neutrons are born at approximately 1 MeV. Because delayed neutrons are born with lower energy, they are more likely to be absorbed by the uranium, and are therefore more likely to cause another fission. To account for the

originating energy, the effective delayed neutron fraction β_{eff} is introduced. The effective delayed neutron fraction takes into the account the effectiveness of a delayed neutron to cause another fission.

2.3 Effect of Delayed Neutrons on Criticality

Now that delayed and prompt neutrons are understood, the concept of k_{eff} can be further developed. The effective multiplication factor is a combination of the prompt multiplication component of the neutron population and the effective delayed neutron fraction. The prompt multiplication factor, k_p, is the component of the effective multiplication factor due only to the prompt neutrons as shown by Eq. 2.3.

$$k_{eff} = k_p + k_d \tag{2.3}$$

Typical power reactors operate with a $k_{eff} = 1$ which is also referred to as delayed critical. This is the point at which the nuclear chain reaction is sustained by both the prompt and delayed neutrons. One could also refer to a chain reaction sustained solely by the prompt neutrons as a prompt critical reaction. The effective multiplication factor, k_{eff}, at prompt critical is given by Eq. 2.4. The first two terms of the Taylor series expansion of Eq. 2.4 make for an extremely good approximation of the value of k_{eff} at prompt critical also shown in Eq. 2.4.

$$k_{eff,\,prompt} = \frac{1}{1-\beta_{eff}} \approx 1 + \beta_{eff} \tag{2.4}$$

The area between prompt and delayed critical is the delayed critical window. This region is shown in Figure 2.1. Figure 2.1 is used by the NEN-2 group, Los Alamos National Laboratory's Advanced Nuclear Technology Group, as a training tool when teaching about criticality. The delayed critical window is ideal for operating power reactors because the reaction rate changes on timescales of seconds to hours. Without delayed neutrons, these long timescales would not exist, and controllable nuclear power reactors would not be a reality. Delayed neutrons, while useful in other context, provide little insight into the time-

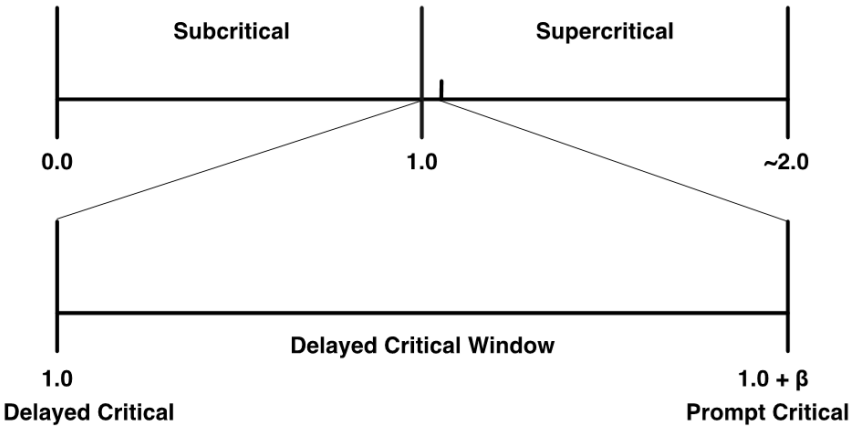

Figure 2.1: Criticality Range using k_{eff} as a guide [51].

dependent behavior of the fission process. For this reason, the delayed neutrons in such systems are often ignored during α-eigenvalue measurements because they have little effect on the dynamic system behavior. Insight into the time-dependent behavior of the fission process is attainable though measurement of prompt neutrons in a system during the implementation of α-eigenvalue experiments.

2.4 Reactivity

The reactivity of a system is the amount at which a multiplying system departs its critical state. Reactivity begins with a discussion of a unit-less fraction based on k_{eff} shown by Eq. 2.5.

$$\rho = \frac{k_{eff} - 1}{k_{eff}} \tag{2.5}$$

Reactivity is frequently quoted on a base 100 scale with the units of dollars and cents. Reactivity in terms of dollars and cents normalizes all systems to have the same values near both delayed and prompt critical. Reactivity in terms of k_{eff} converts to reactivity in dollars using Eq. 2.6.

$$\rho(\$) = \frac{k_{eff} - 1}{k_{eff}\beta_{eff}}. \tag{2.6}$$

In terms of dollars and cents, delayed critical is equal to $\rho = 0\$$, and prompt critical is equal to $\rho = 1\$$.

During reactor operation, it is essential to be able to dynamically report the reactivity of the system. Most reactors measure neutron population, which is proportional to the power in the reactor, with some sort of detection system. The rate power changes are then fit to find a period of the reactor. The fit period can then be converted to reactivity through use of the Inhour equation Eq. 2.7.

$$\omega \left[\frac{l}{\beta} + \sum_{i=1}^{G} \frac{\alpha_i}{\lambda_i + \omega} \right] = \rho \tag{2.7}$$

The Inhour relation uses a measured reactor period which becomes difficult to measure as the reactor approaches prompt critical and the period shortens. The Inhour relation uses the term ω which is related to the asymptotic reactor period, T_{as}, by $T_{as} = 1/\omega$. The reactivity, ρ, of the system is determined for the value of ω. The neutron lifetime l, and the delayed neutron fraction β are properties of a given system and are static in the calculation. The remaining constants α_i and λ_i are properties of each delayed neutron group. The constant α_i is not related to the Rossi-α, but rather is a constant $\alpha_i = \beta_i/\beta$. Where β_i is the fraction of delayed neutrons in group i and β is the total delayed neutron fraction. The number of delayed neutron groups is given by G. Typically, a six group approximation for the delayed neutron precursors is used.

2.5 Prompt Neutron Decay Constant

The prompt neutron decay constant, α, depends on both the prompt multiplication factor, k_p, and the neutron lifetime, l as shown by Eq. 2.8 [52]. Specifically, the prompt neutron lifetime mentioned in this context is the average length of time a prompt neutron exists in a system before a terminating event. Termination can be caused by leakage from the system, non-fission capture, or fission capture.

$$\alpha = \frac{k_p - 1}{l} \tag{2.8}$$

The model that created the relationship shown in Eq. 2.8 is based on the point reactor

kinetics framework. When using this model, the assumptions used to develop point reactor kinetics apply. The main assumption that carries over from point reactor kinetics deals with the assumption that the spatial flux distribution is not changing with respect to time and is thus separable from time. In systems where a constant, separable flux distribution cannot be established, this model and equation set will not apply. This assumption is often discussed as having a system that is near critical, as nearly critical systems will have a constant, separable flux distribution that is determined by the delayed neutron precursors decaying in the fuel region. Subcritical systems also have constant neutron fluxes in an integral sense, but over a short period of time in a single position the neutron flux has a large variance. The other important assumption made by this model is that the neutron population itself is not too large. This really means that relatively few fission chains exist at any one time in an assembly such that two neutrons from a single chain are discernible. This assumption comes from the fact that this model was developed considering only one fission chain existing in a system. For measurements made above delayed critical, where the neutron population is increasing as a function of time, cycling of the assembly is required to reduce the neutron population to avoid violating this assumption.

An understanding of the distinction between accidental and correlated neutron pairs is crucial to the comprehension of how α-eigenvalue methods were developed. Much like the distinction between prompt and delayed neutrons, dividing the detected neutrons into two groups is necessary to complete the analysis of the prompt neutron decay constant. In a single fission chain, the correlated and accidental pairs relate to the prompt and delayed neutron groups. Correlated neutron pairs refer to the prompt neutrons generated from a common fission ancestor. Accidental neutron pairs are defined to be neutrons originating from a random source such as the background, delayed emission, or other sources. When multiple fission chains are being analyzed, neutrons originating in a different fission chain are considered as accidental neutron pairs.

A visual representation of accidental and correlated neutron pairs is provided in Fig. 2.2 [53]. In Fig. 2.2, X is the common fission ancestor to correlated neutron pairs like C, D, and G. Correlated neutron pairs are also seen in the other chains at A and E or B and F. Any combination of neutrons from separate chains denotes accidental pairs, such as A and B.

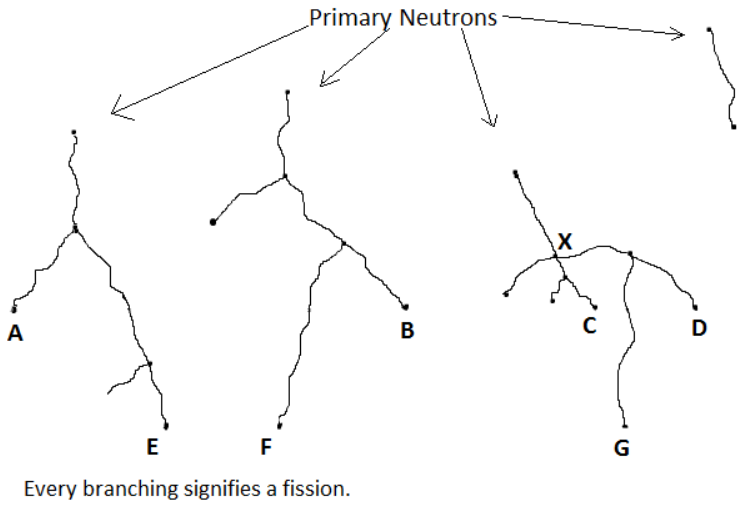

Figure 2.2: Visual representation of accidental and correlated neutron counts [3].

2.6 Derivation of the Prompt Neutron Decay Constant

The prompt neutron decay constant, often referred to as the Rossi-α or α-eigenvalue, is a dynamic variable of a chain-reacting nuclear fission system. The prompt neutron decay constant of a system is the rate at which the prompt neutron population changes. Like the Inhour relation, α-eigenvalue methods are another useful method of calibrating reactivity [1, 2, 54, 55], as long as the α-eigenvalue, the value of α at delayed critical, is well defined. The α-eigenvalue can additionally be used to create a dynamic model of a fissioning system as shown by the Transport Equation in Eq. 2.9 [56].

$$\frac{1}{v}\frac{\partial}{\partial t}\Phi\left(\boldsymbol{r},\boldsymbol{\Omega},E,t\right)+\boldsymbol{\Omega}\cdot\nabla\Phi+\sigma\Phi=q\left(\boldsymbol{r},\boldsymbol{\Omega},E,t\right) \tag{2.9}$$

The α-eigenvalue specifically fits into the time dependence of each flux term as shown by Eq. 2.10.

$$\Phi\left(\boldsymbol{r},\boldsymbol{\Omega},E,t\right)=e^{\alpha t}\Phi\left(\boldsymbol{r},\boldsymbol{\Omega},E\right) \tag{2.10}$$

The effective multiplication factor, k_{eff}, also fits into the Transport Equation as a part of the source term, $\boldsymbol{q}$, for a criticality source as shown by Eq. 2.11.

$$q\left(\boldsymbol{r},\boldsymbol{\Omega},E,t\right)=\iint\sum_{x\neq f}\sigma_{x}^{\prime}f_{x}v^{\prime}\Phi_{k}^{\prime}d\Omega^{\prime}dE^{\prime}+\frac{1}{k}\iint\frac{1}{4\pi}\nu\left(\boldsymbol{r},E^{\prime}\rightarrow E\right)\sigma_{f}^{\prime}v^{\prime}\Phi_{k}^{\prime}d\Omega^{\prime}dE^{\prime} \quad (2.11)$$

Measurements of the α-eigenvalue rely on a certain set of assumptions to be valid. The first and most important assumption is that the system is in a fundamental mode without significant fission chain overlap [2, 57]. The second assumption is that the measurement is taken at a point that is symmetric with respect to source and detector geometry, so that spatial correlations do not need to be considered [58]. The third and final assumption is that the system is not heavily reflected [1].

The Rossi-α and endogenous pulsed source methods are α-eigenvalue techniques that measure the correlation in neutron counts to determine α. Both methods apply the same theory, but have different experimental procedures for obtaining data. The theory consists of a model of the time behavior of the prompt neutron population. This model was developed by Richard Feynman congruently with Rossi's development of his experimental technique [53]. Rossi proposed that active fission systems are self-modulated; meaning that the emission rate of delayed neutrons is sufficiently slow that neutrons produced directly from two separated fission events are discernible [6].

Experiments using α-eigenvalue methods are performed subprompt critical. Measurements of α between delayed and prompt critical is often difficult because the power level and subsequently the neutron population of the neutron multiplying system are increasing. The increasing neutron population poses two issues to Rossi-α measurements. The first issue is the saturation of the detection system. The second issue is the increasing overlap of fission chains. Although the methods described are not strictly valid, measuring α above prompt critical is possible by measuring the prompt period of the reactor. Above prompt critical, α is defined as the inverse of the prompt period, as delayed neutrons are born to slowly too affect measurements in this regime.

To understand Feynman's derivation of the prompt neutron population in a neutron multiplying system, imagine the first fission in a chain reacting system occurring at some time

t_0. This fission emits several neutrons during the fission process. One of these neutrons survives to cause another fission which in turn emits several neutrons. This neutron chain eventually generates a fission where one neutron is incident on a detector, at some time t_1, and a separate neutron generates another fission. At some time t_2, another neutron is incident on the detector. The detection event at t_2 is either correlated to the event detected at t_1, or it has no correlation to the detection event at t_1 and is considered accidental [1, 4]. Using the statistics of the likelihood of this sequence of events, a distribution of the promptly born neutron population as a function of time is created. This process is completed over and over again until the distribution smooths and the distribution approximates a smooth, continuous function. When a system is subprompt, the prompt neutron population decays as a function of time because the likelihood of prompt neutron in any given chain surviving is low. Thus, all chains decay back to some constant background determined by the random neutron population at the time of the measurement. This background is related to the strength of the interrogating source, and the multiplication of the system. The multiplication of the system is important because delayed neutrons are born randomly in time, and are therefore treated as a random source of neutrons.

The probability that a fission occurs at time $t_0 = 0$ can be generalized by Eq. 2.12 to be equal to the average fission rate, F.

$$p_0(t_0)\Delta_0 = F\Delta_0 \tag{2.12}$$

In general p_x is the probability of detecting a neutron count number x at a time t_x. The time t_x exists within the time window Δ_x.

The probability of another fission originating from the same chain as the fission at t_0 and producing at least one detected neutron at some time t_1 is of interest. The probability of this neutron being detected can be quantified by Eq. 2.13.

$$p_1(t_1)\Delta_1 = \epsilon\nu_p\upsilon\Sigma_f e^{\alpha(t_1-t_0)}\Delta_1 \tag{2.13}$$

In Eq. 2.13, ϵ is the efficiency of the detector in counts per fission, ν_p is the number of prompt

neutrons emitted, υ is the velocity of thermal neutrons, Σ_f is the macroscopic fission cross section. When υ and Σ_f are combined they become the average fission rate per unit neutron density $\upsilon\Sigma_f$ [1].

The exponential including α has been shown in Eq. 2.13 and all subsequent equations with a positive sign. The prompt neutron decay constant has been modeled using many different sign conventions. The sign conventions used in this paper follow the sign conventions used by Orndoff [4]. Orndoff's convention defines α to be negative when below prompt critical. This convention is also important when examining Eq. 2.8, as the sign convention also has impact when defining α.

The probability of a detecting another neutron at time t_2 which is after the detection event at t_1 and from the same chain as the fission at time t_0 is quantified in Eq. 2.14.

$$p_2(t_2)\Delta_2 = \epsilon(\nu_p - 1)\upsilon\Sigma_f e^{\alpha(t_2-t_0)}\Delta_2 \tag{2.14}$$

Notice that the ν_p term has been modified to $(\nu_p - 1)$ to account for the neutron lost at t_1 to the fission chain [1].

All three of the probabilities calculated in Eq. 2.12, Eq. 2.13, and Eq. 2.14 are independent and can be joined to give the probability of occurrence of two chain-related, correlated (p_c) counts initiated by a fission at time t_0. This total correlated probability is shown in Eq. 2.15. The first subsequent count occurring at time t_1 in Δ_1 and the second happening at time t_2 in Δ_2 [1].

$$\begin{aligned} p_c(t_0,t_1,t_2)\Delta_0\Delta_1\Delta_2 = p_0(t_0)p_1(t_1)p_2(t_2)\Delta_0\Delta_1\Delta_2 = \\ F\epsilon\nu_p\upsilon\Sigma_f e^{\alpha(t_1-t_0)}\Delta_1\epsilon(\nu_p-1)\upsilon\Sigma_f e^{\alpha(t_2-t_0)}\Delta_2 \end{aligned} \tag{2.15}$$

The probability of the above-mentioned sequence occurring can be found by integrating the product of the probabilities for events at t_1 and t_2 over all time up until t_1. This integration is shown in Eq. 2.16.

$$p_c(t_1,t_2)\Delta_1\Delta_2 = \int_{-\infty}^{t_1} p(t_1)\Delta_1 p(t_2)\Delta_2 F\, dt_0 \tag{2.16}$$

This integration is performed because there is no way to know that a detected count is caused directly from the first fission. Instead, it is assumed that detected counts relate to the detection events at time t_1 and t_2. With a little simplification, Eq. 2.16 can be simplified into Eq. 2.17 which portrays the probability of two chain related events occurring as a result of a fission at time t_0.

$$p_c(t_1, t_2)\Delta_1\Delta_2 = F\epsilon^2 \frac{D_\nu k_p^2}{2(1-k_p)l} e^{\alpha(t_2-t_1)}\Delta_1\Delta_2 \tag{2.17}$$

Equation 2.17 is simplified using $\overline{\nu_p(\nu_p-1)}$ as an average of the number of prompt neutrons emitted and the identities shown in Eq. 2.18 and Eq. 2.19.

$$\overline{\nu_p} = \frac{k_p\Sigma_a}{\Sigma_f} = \frac{k_p}{\Sigma_f \upsilon l} \tag{2.18}$$

$$D_\nu = \frac{\overline{\nu_p(\nu_p-1)}}{\overline{\nu_p^2}} \tag{2.19}$$

These identities refer to the definitions of the average emission of prompt neutrons and Diven's parameter, respectively [1]. Diven's parameter accounts for the dispersion of the neutron emission [3, 59, 60]. Diven's parameter is a cleaner way of representing the information originally derived by Feynman [53].

Accidental neutron pairs have a constant rate with respect to time and are thus represented as a constant probability. The probability that the neutrons detected at time t_1 and t_2 are an accidental neutron pair is the same as the product of the average fission rate and the efficiency of the detector in the time bin. This probability can be seen in Eq. 2.20 [1, 2, 4].

$$p_r(t_1, t_2)\Delta_1\Delta_2 = F^2\epsilon^2\Delta_1\Delta_2 \tag{2.20}$$

The total probability for observing a pair of detections in Δ_1 and Δ_2 is the aggregate of the probabilities found above as shown in Eq. 2.21 [1].

$$p(t_1, t_2)\Delta_1\Delta_2 = F^2\epsilon^2\Delta_1\Delta_2 + F\epsilon^2 \frac{D_\nu k_p^2}{2(1-k_p)l} e^{\alpha(t_2-t_1)}\Delta_1\Delta_2 \tag{2.21}$$

The Rossi experiment guarantees an interaction in the time interval Δ_1 because the interaction at t_1 is the initiating event. This is also true of the endogenous pulsed source technique because the timing of the neutron generator is known. With some manipulation, the probability of the first neutron detection occurring in the time interval Δ_1, $F\epsilon\Delta_1$, can be separated as shown by Eq. 2.22 [1].

$$p(t_1,t_2)\Delta_1\Delta_2 = F\epsilon\Delta_1\left[F\epsilon\Delta_2 + \epsilon\frac{D_\nu k_p^2}{2(1-k_p)l}e^{\alpha(t_2-t_1)}\Delta_2\right] \tag{2.22}$$

As previously stated, the probability that a neutron is detected in time bin Δ_1 is 1, so $F\epsilon\Delta_1$ can be set to 1 as shown by Eq. 2.23 [1].

$$p(t)\Delta = F\epsilon\Delta + \epsilon\frac{D_\nu k_p^2}{2(1-k_p)l}e^{\alpha t}\Delta \tag{2.23}$$

In Orndoff's paper [7], a correction is made to Eq. 2.23 by the considering the effect of detecting multiple neutrons from the fission producing the count at $t = 0$. Consider δ to be the effective number of neutrons resulting from this fission and detection process, at $t = 0$. Since detection may involve capture, scattering, or fission, δ will depend on the type and placement of the detector and must be evaluated for a particular experimental setup [7]. The correction to Eq. 2.23 modifies the $\overline{\nu_p(\nu_p-1)}$ term hidden as a part of Diven's parameter. The correction term is shown in Eq. 2.24.

$$D_\nu\overline{\nu_p^2} \rightarrow \overline{\nu_p(\nu_p-1)} + \frac{2\nu_p(1-k_p)}{k_p}\delta \tag{2.24}$$

With the correction, the probability Eq. 2.23 becomes Eq. 2.25 [1].

$$p(t)\Delta = F\epsilon\Delta + \epsilon\frac{\epsilon[\overline{\nu_p(\nu_p-1)} + 2\nu_p(1-k_p)\delta/k_p]k_p^2}{2\overline{\nu}p^2(1-k_p)l}e^{\alpha t}\Delta \tag{2.25}$$

The correction added by δ is at most a few percent, and Orndoff suggests δ need not be evaluated precisely [7]. Uhrig suggests in Random Noise Techniques [1] that the correction itself is often neglected because of its small magnitude. Often for simplicity the total probability to detect a neutron event in some Δ_2 after detecting an event at Δ_1 is written in the

general form shown in Eq. 2.26. Equation 2.26 is fit to experimental data during analysis.

$$P(t) = A + Be^{\alpha t} \tag{2.26}$$

Using Uhrig's suggestion to neglect the δ correction, the parameters A and B are represented by Eqs. 2.27 and 2.28 [1].

$$A = F\epsilon \tag{2.27}$$

$$B = \frac{\epsilon D_\nu k_p^2}{2\alpha l^2} \tag{2.28}$$

2.7 Determine α-eigenvalue from Several Subcritical Measurements

The value of α at delayed critical, α_{DC}, or α-eigenvalue is often the number quoted when discussing the prompt neutron decay constant of a system. The α-eigenvalue is of interest because it relates to the eigenfunctions of the system, and because it is directly proportional to the effective delayed neutron fraction β_{eff} and the neutron lifetime l as shown in Eq. 2.29.

$$\alpha = -\frac{\beta_{eff}}{l} \tag{2.29}$$

The α-eigenvalue is typically determined in two main ways. The first is a direct measurement in which the value of α is measured on a system at delayed critical. The second extrapolates the value of the α-eigenvalue through several subcritical measurements of α very near delayed critical. The second method is often employed to verify the first measurement, or in situations where the neutron population even at the lowest achievable power is too high. The second measurement technique plots the value of α measured at several subcritical points against the inverse count-rate for each measurement. Typically, three or four points very near delayed critical are chosen. The line formed by fitting this data extrapolates the α-eigenvalue when it crosses zero, the y-intercept. This makes physical sense because at delayed-critical the theoretical count-rate is infinity.

2.8 Determine Reactivity from α

Determining the reactivity of a system using measurements of α is of interest because the subcritical reactivity of a system can accurately be measured. Because α is defined as proportional to the prompt multiplication factor ,k_p, α is inherently related to effective multiplication factor, k_{eff}, and the effective multiplication factor can be related to reactivity. This linear relationship is the crux of this work. So long as the definition of α presented in Eq. 2.8 is applicable; the linear extrapolation will be related to reactivity.

The linear extrapolation formula is given in Eq. 2.30.

$$\frac{y - y_0}{x - x_0} = \frac{y_1 - y_0}{x_1 - x_0} \tag{2.30}$$

For this application, y is the reactivity of the system in dollars and x in the value of α. The known points can be any two known points, but often the values at delayed-critical ($\rho = 0$) and prompt critical ($\rho = 1$, $\alpha = 0$) are chosen as they are known quantities. Using this knowledge, Eq. 2.30 becomes Eq. 2.31. The linear extrapolation described in this section is shown in Fig. 2.3.

$$\frac{\rho}{\alpha - \alpha_{DC}} = \frac{1}{-\alpha_{DC}} \tag{2.31}$$

Eq. 2.31 can be further simplified to Eq. 2.32.

$$\rho = \frac{\alpha_{DC} - \alpha}{\alpha_{DC}} \tag{2.32}$$

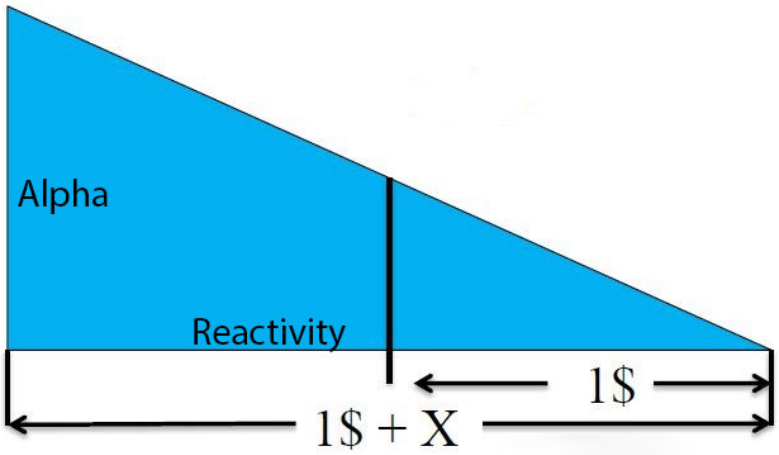

Figure 2.3: Linear extrapolation method used to determine reactivity from α.

CHAPTER 3

EXPERIMENTAL STUDY

3.1 Critical Experiments

Two different critical experiments are used during this project. Both systems have highly enriched uranium (HEU) fuel. The first system discussed is Godiva IV which is a critical assembly with a fast neutron spectrum. The second system discussed is the Polyethylene Class Foils which is a critical experiment with a thermal neutron spectrum.

3.1.1 Fast System: Godiva IV

Godiva IV is a fast burst assembly operated at NCERC. In this context, a burst reactor is able to assemble a super-prompt critical configuration and achieve a chain reaction exponentially increasing due to prompt neutrons alone for a fraction of a second before being thermally or mechanically quenched. Pulses of this type can be safely achieved by TRIGA research reactors. The Godiva assemblies are special because they have the hardest spectrum and smallest pulse width. Godiva IV is the fourth reactor in a line of fast bust assemblies operated by the critical experiments team at Los Alamos National Laboratory. The Godiva experiment series was originally designed to obtain the bare spherical critical mass of ^{235}U [61]. This first experiment named Lady Godiva (Godiva I) is shown in Fig. 3.1. Through the generations of the machine, the design has been modified to better support fast burst capabilities. The cylindrical shape and addition of molybdenum to Godiva IV are examples of such modifications.

The Godiva IV assembly consists of 65 kg of aluminum ion plated HEU (93.5% ^{235}U by weight). To improve the mechanical properties of the fuel, the HEU is alloyed with 1.5%

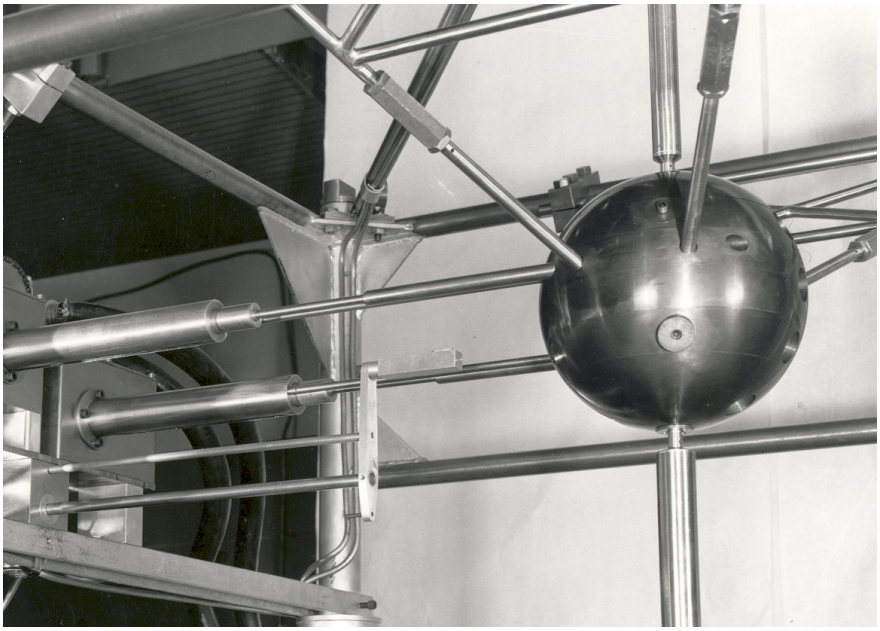

Figure 3.1: Lady Godiva (Godiva I) fully assembled.

(by weight) molybdenum. The fuel for the assembly comes in several pieces of which some are stationary and others can be remotely manipulated. The stationary fuel consists of six 1.00 inch tall rings which have a 7.00 inch outer diameter and 3.50 inch inner diameter as shown in Fig. 3.2. These rings give the core a total height of 6.00 inches, such that the total fuel exterior is slightly larger than a can of coffee, as shown by Fig. 3.3. Two additional stationary inner pieces fill up the top half of the central cavity shown by piece numbers 108 and 109 in Fig. 3.2. These pieces are 3.45 inches in diameter and 3.00 inches tall [62]. These two HEU pieces also have an inner cavity, typically referred to as the glory hole, which is capable of holding irradiation samples. The glory hole is 0.56 inches in diameter and 3.00 inches inside the active fuel. The movable HEU pieces of the system include the bottom inner half of the fuel called the safety block, and three control rods. The safety block is a 3.38 inch diameter cylinder with a height of 3.00 inches. The safety block is used as the main reactivity quench during operations, as its reactivity worth is large. The three rods are solid cylinders 5.00 inches long with an outer diameter of 0.86 inches [62].

Although identical in dimension, one of the three rods has a very different purpose. This lone rod is described as the burst rod and is typically only used during super-prompt critical burst operations. The other two rods are standard lead driven screw control rods. Unlike

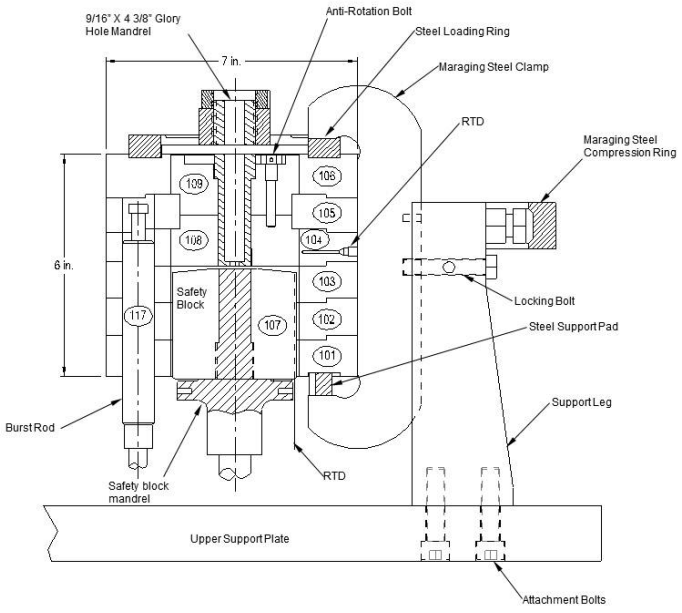

Figure 3.2: Godiva IV drawing.

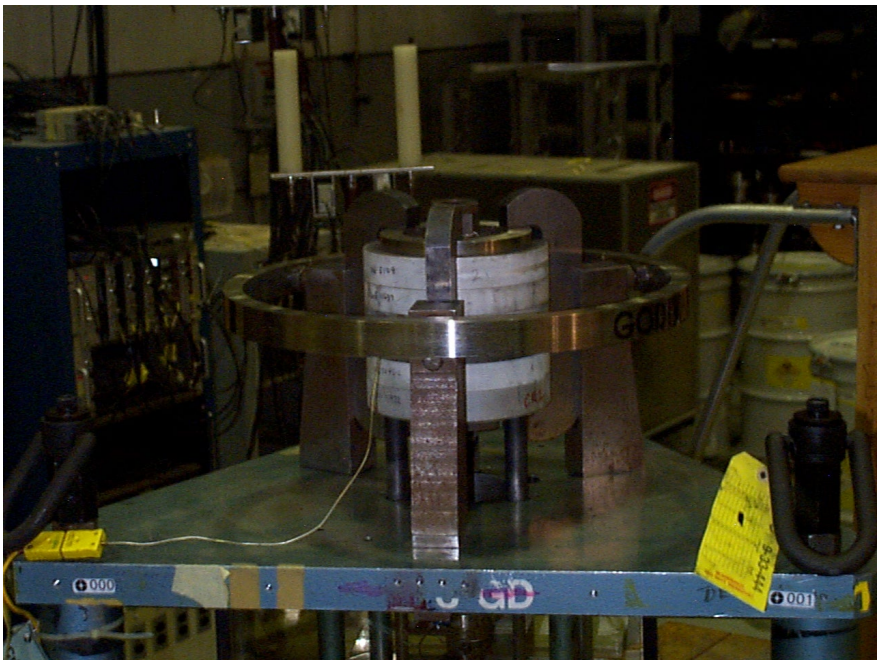

Figure 3.3: The Godiva IV critical assembly.

power reactors, the Godiva critical assembly controls reactivity by modifying the amount of mass and geometry of the assembly. These two control rods have fine control with positional accuracies near one thousandth of an inch (mil). Each of these rods would be worth about 1.5$ if allowed full travel. The burst rod only differs from the other two control rods by its control mechanism. The burst rod is pneumatically driven and cannot exist in any intermediate state. The rod can only be in or out. The travel on the burst rod is set such that from its out position to its full in position the change in reactivity is worth 1$ of reactivity. The burst rod travels by pneumatic injection approximately 3.5 inches in 70-90 milliseconds.

3.1.2 Thermal System: Polyethylene Class Foils

The Polyethylene Class Foils experiment is a stacking of 9 inch by 9 inch by 0.003 inch thick ^{235}U foils. These foils consist of thin highly enriched uranium (93 wt% ^{235}U) metal foils laminated in plastic; each foil weighs approximately 68 grams. The interstitial material is 14 inch by 14 inch by 0.500 inch thick polyethylene plates. These plates have a 10.125 inch by 10.125 by 0.026 inch deep recession machined into them to hold the ^{235}U foil in place. For alignment, the polyethylene plates have alignment pegs and holes machined into them. The top of the plate has four 0.500 inch pegs sticking out and the bottom has 4 0.500 inch holes drilled into it. To help visualize the plate, Fig. 3.4 is included. In addition to the stacking units described, 3 inches of polyethylene are also added onto the top and bottom of the stack as external reflector. This is shown by units 6, 4C, 4B, 11, 4A, and 5 in Fig. 3.5. This polyethylene has a larger axial height but similar dimensions to the interstitial plates for the other directions. Additionally, this polyethylene does not have recessions for foils. The membrane is the bottom plate supporting the stationary top half of the experiment. This plate also has different dimensions to help mate the experiment to the Planet critical assembly. This plate has similar dimensions to the interstitial plates except it is 18 inches by 18 inches by 0.500 inch thick. The source in this experiment is placed into an interstitial plate with a 0.406 inch hole drilled into the center of it. For all measurements performed in this work, the source unit was always the very bottom unit just above the bottom reflector

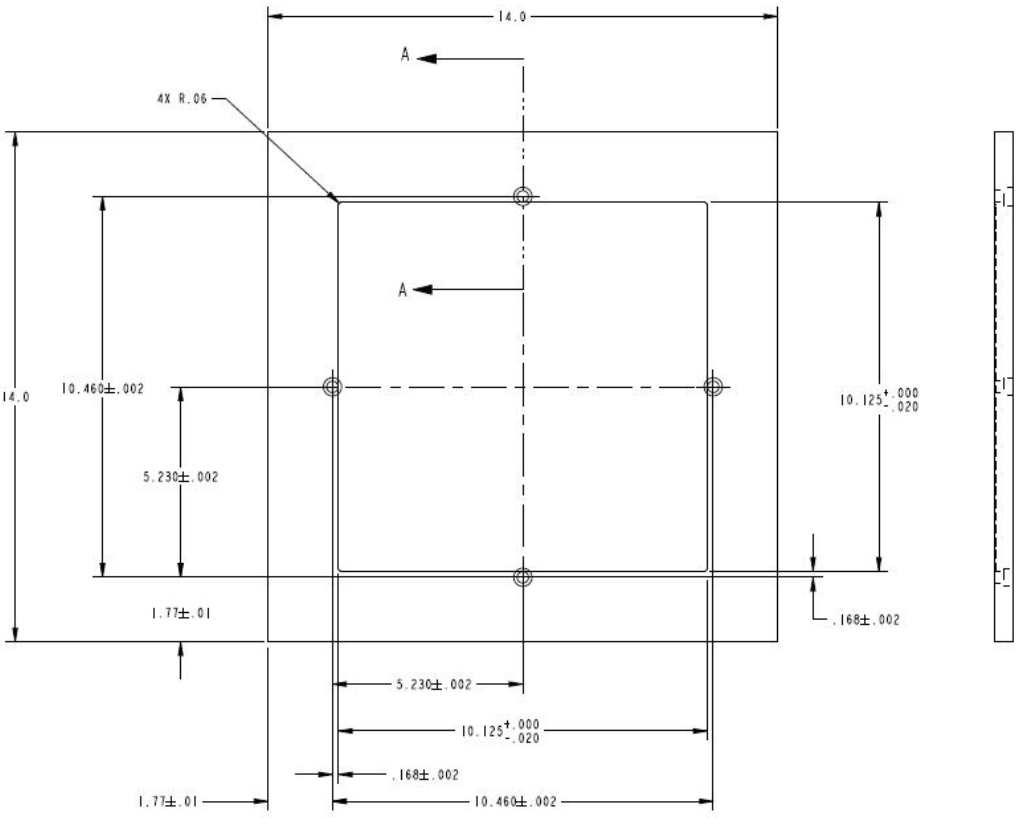

Figure 3.4: Drawing of a standard polyethylene interstitial plate.

in the stack.

The Class Foils experiment with polyethylene interstitial plates is one of the tools used to teach criticality safety at the National Criticality Experiments Research Center (NCERC). This set of polyethylene plates is designed to provide the optimal H/^{235}U ratio on the critical mass curve allowing the experiment to have the minimum amount of ^{235}U [63]. This experiment is a great teaching tool demonstrating how changing the ^{235}U mass or amount of moderation affects the critical mass [63]. For this experiment, adding additional mass or additional moderation increases the critical mass. This effect is possible because of the optimal ratio between H/^{235}U; either change shifts the "effective" concentration of ^{235}U in the assembly.

This experiment has been historically performed using either polyethylene or Lucite inter-

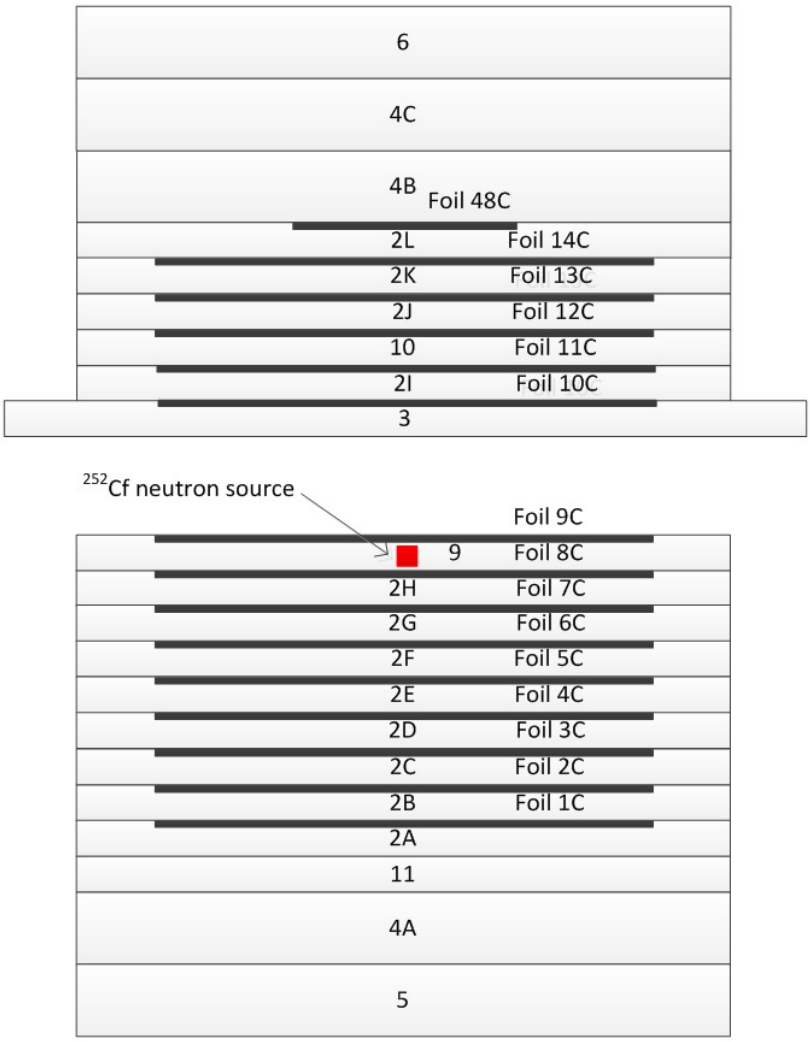

Figure 3.5: Critical Configuration of the Class Foils Experiment.

Figure 3.6: The Planet critical assembly with an older version of the Class Foils Experiment.

stitial moderating plates. The increased hydrogen density of polyethylene compared to the Lucite plates has reduced the critical mass for the polyethylene moderated experiment by 34% when compared to the same experiment using Lucite plates. The critical mass of the Class Foils experiment using polyethylene interstitial is 997.9 $\pm$ 0.65 g [63]. The system is shown in Fig. 3.5. The critical configuration requires 14.5 fuel foils.

The Polyethylene Class Foils experiment is typically performed on the Planet critical assembly. Planet is a general use vertical lift assembly which is shown in Fig. 3.6. In basic terms, vertical lift assemblies adjust reactivity through separation of two subcritical masses. Planet has a stationary top platform capable of holding about 2000 lbs which is well above the necessary amount for the Polyethylene Class Foils. Planet also has a movable section called a platen. The platen has two methods of control: the rams and the stepper motor. The rams act as coarse control and/or the safety system. The rams drive at about 400 mils (thousandths of an inch) per second. The stepper motor acts as fine control. The stepper motor drives at 50 mils per second, but can be adjusted to be slower. Fig. 3.7 shows the two subcritical masses of the Polyethylene Class Foils fully separated on the Planet assembly.

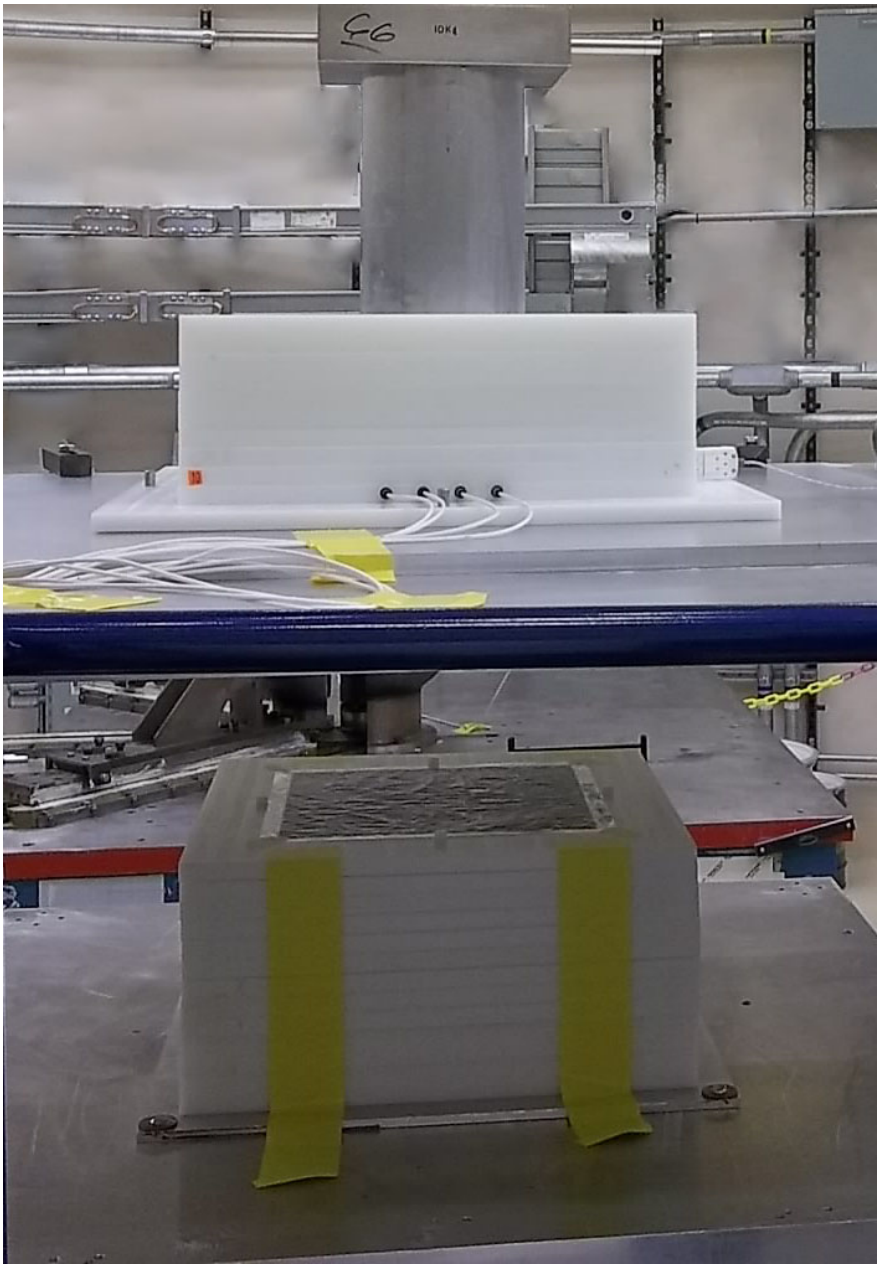

Figure 3.7: Photo of the Polyethylene Class Foils on the Planet assembly.

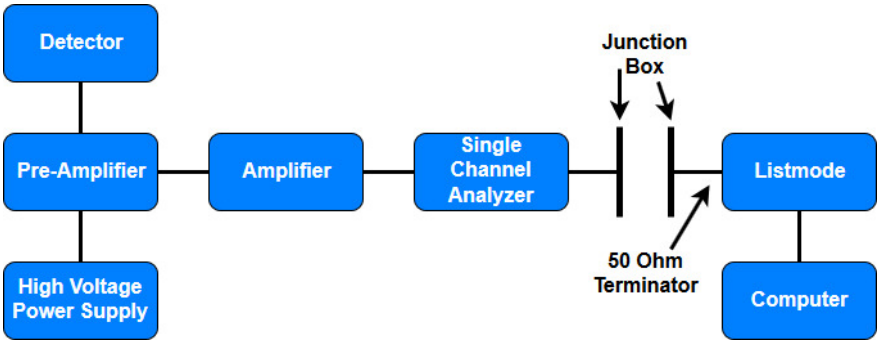

Figure 3.8: Wiring diagram used to connect the neutron detection equipment.

3.2 Neutron Detection Equipment

These experiments require the use of several pieces of hardware, most of which is commercial off-the-shelf. Equipment used in this experiment includes the following: helium-3 (^{3}He) detectors, pre-amplifiers, amplifiers, single channel analyzer (SCA), high voltage power supply, a nuclear instrumentation module (NIM) bin, a list-mode module, and computer.

The equipment was all standard NIM equipment connected using a wiring scheme similar to that shown in Fig. 3.8. As demonstrated by Fig. 3.8, the signal must travel through junction boxes between the building with Godiva IV or Planet to the control room. The distance this signal travels is significant, and distortion can occur to the signal. To reduce the distortion and potential for double pulsing of the signal, 50 Ω terminators were added to the cabling.

Rossi-α measurements can be performed with a wide range of neutron detectors. The detectors choosen for these experiments are ^{3}He detectors. The detectors are manufactured by Reuter-Stokes (RS-P4-0203-201), with a 0.25 inch diameter, an active length of 2.99 inches, and a ^{3}He pressure of 40 atm [64, 65]. These tubes may seem very small for many typical uses of ^{3}He neutron detectors, but their small size and quick recovery speed make them ideal for measuring prompt neutron decay constants in the assemblies at NCERC. The tubes recover fairly quickly because of their small volume; the typical pulse rate can reach 60,000 counts per second before saturation. A drawing and a photo of the detectors are shown in Fig. 3.9 and Fig. 3.10, respectively. To improve statistics and build in redundancy, four tubes are typically used for prompt neutron decay constant measurements. Additionally, the

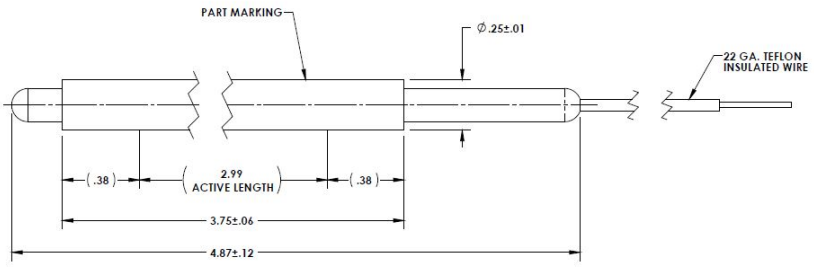

Figure 3.9: Drawing of the 0.25 inch diameter ^{3}He tubes used in the experiment.

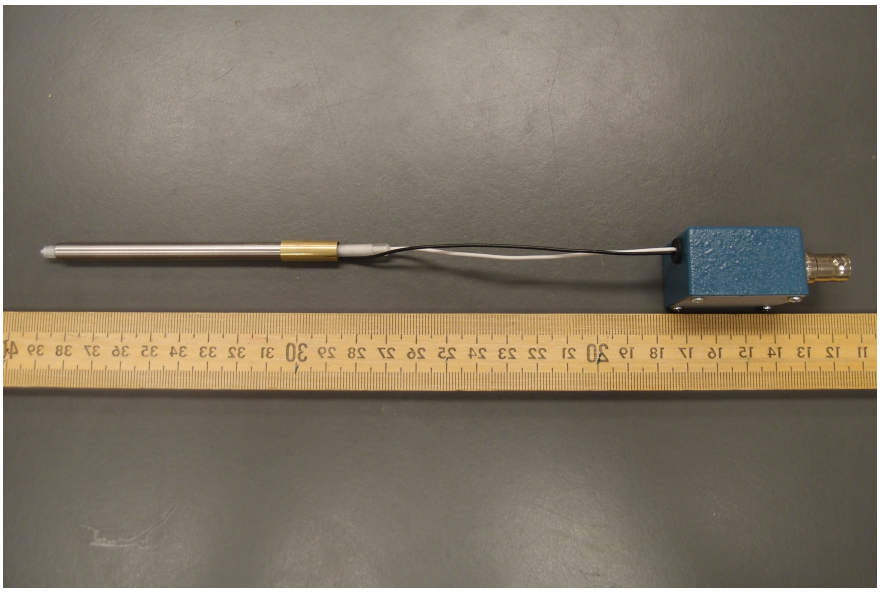

Figure 3.10: One of the 0.25 inch diameter ^{3}He tubes used in the experiment.

time stream from all four tubes can be combined during post processing to reduce detector dead-time and improve statistics.

The pre-amplifier used in this experiment is an Ortec 142-PC. This unit is a commercially available pre-amplifier. Four units are used in this experiment.

The amplifier used is an Ortec 572A. This unit is a commercially available amplifier. Four units are used in this experiment. The coarse gain used for these experiments was 20 and the fine gain was set near 10.0.

The SCA used during execution of this experiment is an Ortec 850. This unit is a commercially available quad SCA. This model is used because it can handle 4 separate channels

Figure 3.11: The front face of the LMM: Woody is shown.

in a single module. This works well as four channels are used during execution of Rossi-α or pulsed neutron source experiments at NCERC. The SCA for each channel were set to 5.00 V and the amplifiers adjusted so all detectors had similar signals.

The high voltage power supply used in this experiment is an Ortec 556 High Voltage Power Supply. This unit is a commercially available high voltage power supply. The tubes require a high voltage bias of 2100 V. This level was set based on a combined effort of manufacturer recommendation and a high voltage plateau performed before using the ^{3}He tubes.

The TTL pulses from the SCA were digitized and recorded by a LANL designed and built list-mode data recording module [28]. The particular list-mode used for these experiments is shown in Fig. 3.11 where LMM is the model number and WOODY is an identifier as to which unit in particular was used. The list-mode module is initiated by a computer program to begin saving the data it is receiving. When the module receives this signal, it opens 100 ns time windows (commonly referred to as tics). If any of the neutron tubes plugged into the LMM receive a count during a tic, the time and channel which received the count are recorded. This module generates a list of the times at which neutrons were incident upon the detection system, and is able to indicate which detector measured the event.

3.3 Neutron Source

The Rossi-α and pulsed neutron source methods differ in the neutron source used to perform the measurement. This section discusses the source used for each experimental technique.

3.3.1 Californium-252

The neutron source used for the Rossi-α experiments was a ^{252}Cf source which is a spontaneous fission neutron source. The particular source used during these experiments is designated D1-412. Source D1-412 was calibrated by Isotopes Products Laboratories on Feb. 15, 2006. On this date the source was 3.053E4 $\pm$ 5.8 % kBq with several impurities from other Cf isotopes as shown by Table 3.1. D1-412 is 1.45E6 Bq as calculated on Oct. 4, 2017 which was the day the source was used in these measurements. This activity level was calculated using standard nuclear decay and a half-life of 2.6 years for ^{252}Cf. Only ^{252}Cf is taken into account because it generates most of the neutron output. This activity level corresponds to 4.47E4 $\pm$5.8% spontaneous fissions per second which is a decay corrected value as calculated on Oct. 4, 2017 using a neutron emission rate 3.54E6 neutrons per second as measured by Isotope Products on Feb. 15, 2006 and a $\overline{\nu}$=3.77.

Table 3.1: D1-412 Radioimpurities as measured on Feb 15, 2006.

Cf Isotope	**Percentage (%)**
249	0.752
250	25.0
251	0.192

Because a spontaneous fission source is used there is a small amount of correlation relating to the source neutrons but this effect is assumed to be negligible as the fraction of detected source neutrons is small when compared to detected neutrons due to system multiplication. The real benefit of a spontaneous fission source is that the neutrons are born with a similar spectrum to the neutrons multiplied by the system.

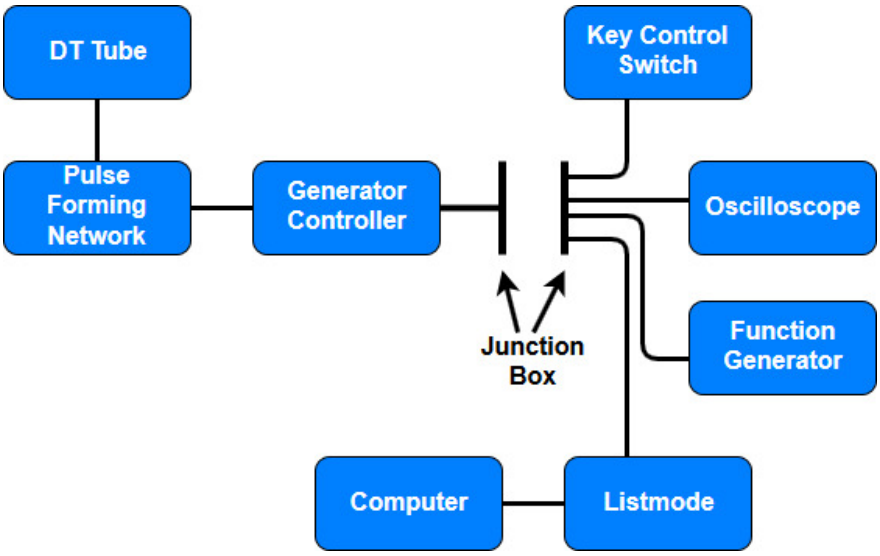

Figure 3.12: Wiring diagram used to connect the neutron generator.

3.3.2 Neutron Generator

The neutron generator used during pulsed source technique measurements is a deuterium-tritium (DT) neutron generator tube. The DT generator uses an accelerator to generate neutron from the deuterium-tritium fusion reaction. This fusion reaction creates 14 MeV neutrons an helium atoms as shown by Eq. 3.1.

$$ {}^{2}_{1}D + {}^{3}_{1}T \rightarrow {}^{4}_{2}He(3.5MeV) + n^{0}(14.1MeV) \tag{3.1} $$

In addition to the generator tube, a neutron generator controller, neutron generator pulse forming network, function generator, and pulse signal conditioner are required to run the neutron generator and send a trigger signal back to the LMM. A diagram of the electrical connections required to operate the neutron generator with a critical assembly are shown in Fig. 3.12. The DT generator used was a Physics Corporation A211-AC which is shown in Fig. 3.13. The DT generator produced pulses with a frequency of 50Hz and integrated pulse size of 10^6 $\frac{n^0}{pulse}$. Both of these were adjustable within reason, but the quoted numbers are those chosen for the pulsed source experiments.

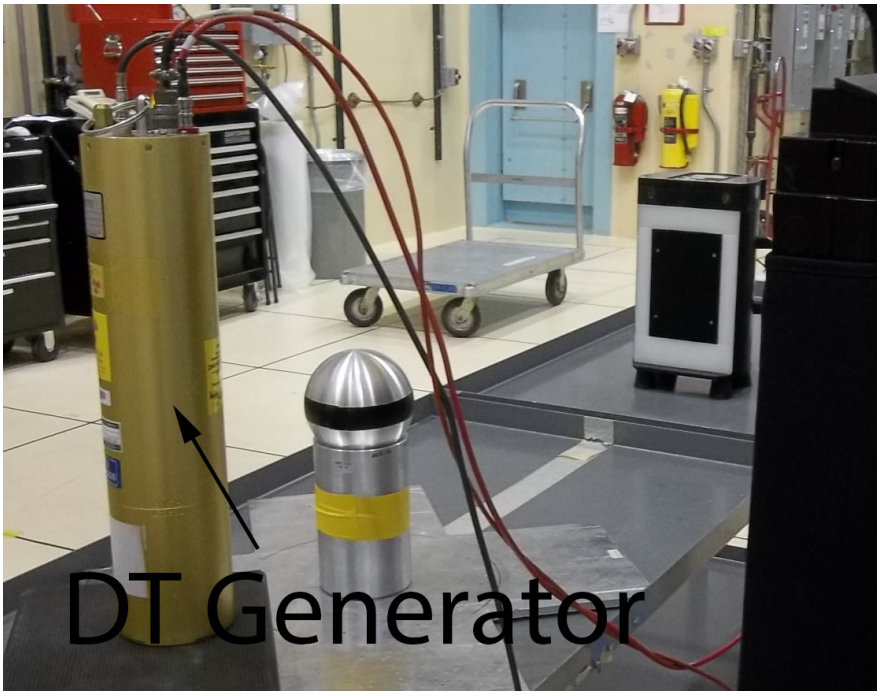

Figure 3.13: Neutron generator tube next to a different experiment.

3.4 Rossi-α and Pulsed Neutron Source Methods

Two α-eigenvalue methods have been discussed in the scope of this work. The first method, the Rossi-α method, was the original method used to determine the prompt neutron decay constant during the Manhattan project. The second is the pulsed source technique which was originally developed to determine neutron lifetime in non-fissionable materials. The pulsed source technique was quickly proven to also work for fissionable materials and is a valid method to determine α for chain reacting systems. Both techniques use the same theoretical considerations developed by Richard Feynman and Bruno Rossi in the 1940s for the Rossi-α experiment.

The Rossi-α technique measures an approximately constant fission rate from a chain reacting system, and measures the prompt neutron decay constant from an auto-correlation of the time distribution of neutrons. The constant fission rate for this method is increased for systems with a low intrinsic neutron source using an external source to reduce data acquisition time. The list-mode data file is processed using time based binning to develop a histogram that captures the response of the prompt neutron population to a fission.

The pulsed source technique is a method of directly measuring the prompt neutron decay constant of a multiplying system. The pulsed neutron source experiment measures neutron population response to a burst of neutrons. Typically, this experiment measures the die away of a neutron population in response to a pulse from a neutron generator. In this work, the pulse is supplied by a neutron generator and the response is measured by the neutron detection system. The list-mode data file is processed into a histogram based on time bins beginning when the neutron population begins to decay.

For both methods, the histogram developed through analysis is fit using the theoretical equation for the prompt neutron population, and the decay constant α is determined. Each method has its own advantages. The Rossi-α method is considerably less set-up and only requires time keeping for the neutron detectors. The advantage of the pulsed source technique is that the constant background is lower so more decay should be observable. The pulsed source technique also requires timing from the neutron generator to be recorded, which adds another layer of complexity. Since each method gives a similar result, each method is only used when its advantages outweigh the other.

3.5 Experimental Execution

Both Rossi-α and pulsed neutron source measurements are executed in a similar manner. The detectors are set-up in or around the system. The source is then placed such that no direct shine can be seen by the detection system to reduce the detection of neutrons that have not interacted with the system. Then the critical assembly is operated to amass the desired configuration. If the system is at or below delayed critical, the neutron population is allowed to stabilize. Then the measurement system records data until each detection channel detects more than one million counts per channel for Rossi-α or for a predetermined amount time for the pulsed neutron source method. Both of these selections are chosen based on operational experience with these type of measurements, and aim to reduce the statistical uncertainty between measurements. If the Rossi-α method is utilized, no additional action is required. If the pulsed source method is utilized, the time streams from the neutron generator and the data acquisition need to be linked. This is currently done by sending a

timing pulse from the neutron generator to the data acquisition at the beginning of each pulse. It should also go without saying the "on" and "off" time for the data acquisition should be at least as long as the total neutron generator run time.

In an attempt to obtain the data in the simplest way, Rossi-α measurements were attempted on both the fast and thermal system. In a case where the pulsed source technique would better fit the needs, the pulsed source technique was employed.

3.5.1 Fast System: Godiva IV Execution

Rossi-α measurements were attempted with ^{3}He detector for a separate project several years ago. The measurements did not provide sufficient quality results. The poor results were attributed to be a function of the extremely fast decay constant and the comparatively slow measurement system (^{3}He detectors). For the prompt neutron decay constant measurements on the fast system Godiva IV, the pulsed source method was used in hopes that a greater signal to noise ratio could be achieved.

For the pulsed source measurements, four ^{3}He tubes were placed on the Godiva IV clamps as shown in Fig. 3.14. This location was chosen because it is static and the closest location the detectors can be secured without actually touching the fuel elements. Each detector is centered on the clamp such that the center of the active region is centered relative to the Godiva IV fuel. The neutron generator was likewise centered relative to Godiva IV and directly opposing the ^{3}He tubes as shown by Fig. 3.15. This geometry was chosen to reduce the likelihood for direct shine from the neutron generator on the ^{3}He detectors.

The goal of the measurements on Godiva IV was to adequately measure a full range of prompt neutron decay constants between the least reactive state, all elements fully removed, and delayed critical. Each day the position of delayed critical was found and used as the starting point. Once delayed critical was determined, a 50 cent increment was removed using a control rod. This configuration would provide the first measurement point, and data was taken. The process of removing 50 cents, and taking data was repeated until the entire control rod travel was examined. This process would then continue by to removing the safety block in small increments until the entire range of travel was covered. During scoping

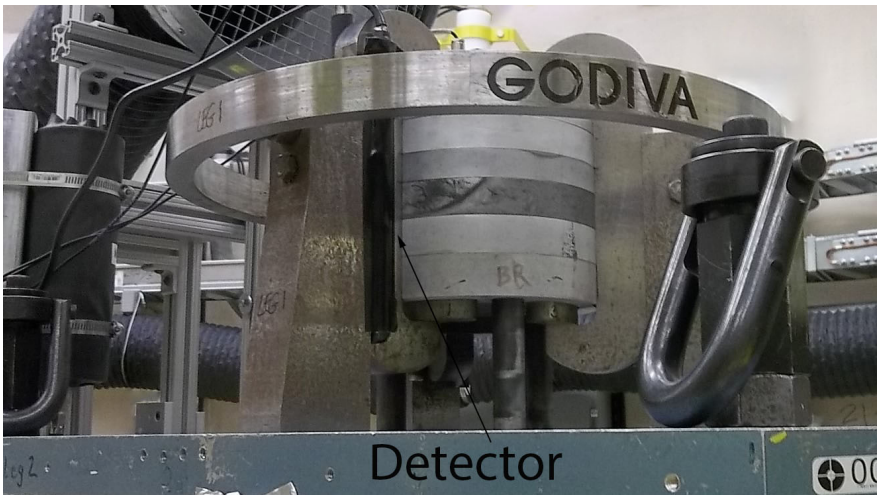

Figure 3.14: Detector placement on Godiva IV clamps.

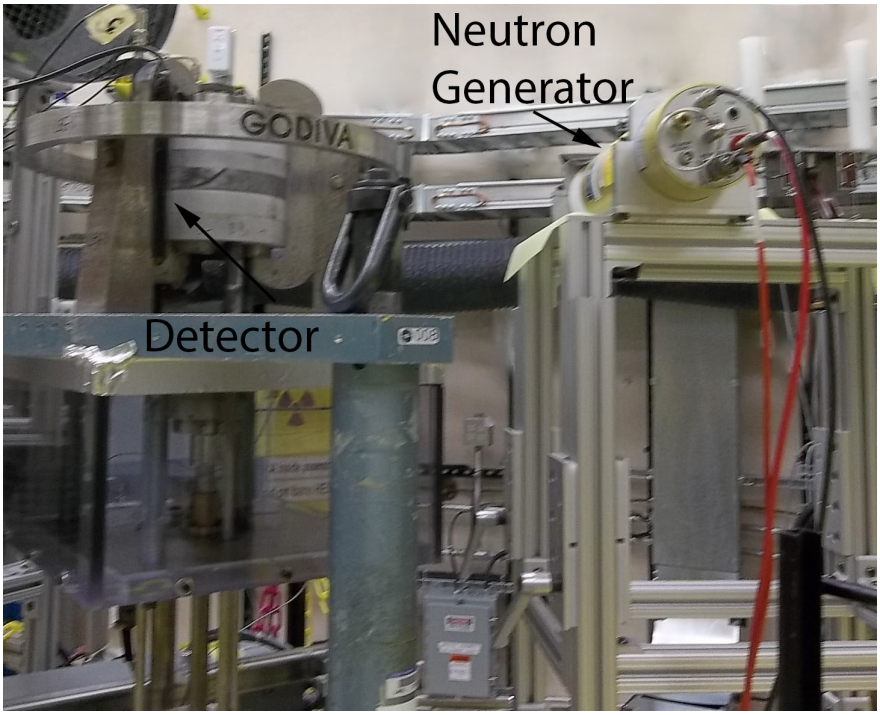

Figure 3.15: Neutron generator placement with respect to Godiva IV and ^{3}He detectors.

measurements, data was obtained at 50, 100, and 150 cents from critical, as well as at the least reactive state of the system. The control element positions for these configurations are given in Table 3.2.

Table 3.2: Measurement configurations on Godiva IV.

ρ (\$)	**Control Element Position (in.)**		
	SB	**CR1**	**CR2**
-0.5	-0.13	1.349	0.186
-1.0	-0.13	3.404	-0.48
-1.5	-0.13	4.164	1.047

3.5.2 Thermal System: Polyethylene Class Foils Execution

For the Rossi-α experiment on the Polyethylene Class Foils, a special moderator plate was designed to hold four detectors. The plate is identical to the interstitial polyethylene plates described, but has 4 holes drilled 8.25 inches into the side of the plate. The holes are 0.323 inch wide for the first 5.30 inches and 0.266 inch wide for the remainder. The plate is shown in Fig 3.16, and a drawing of the plate is shown in Fig. 3.17. This plate could theoretically be placed at any location in the stack. As a good practice, the special plate has been located only on the stationary half of the assembly during remote operations. A photo of the plate with the detection system in the assembly is shown in Fig. 3.18.

The addition of the Rossi-α experimental equipment added significant negative reactivity worth due to the absorption properties of the detectors. As such, additional fuel plates were added to counteract the negative reactivity worth. The critical configuration with the detection system consists of 16 units when the detectors are centered in the assembly. The critical configuration with the special modified plate and detectors is shown in Fig. 3.19.

To minimize the impact of source neutrons on the measurement, the source was placed at the bottom of the stack. The source was located in the center of the bottom unit in a specially designed polyethylene plate which has a small hole drilled through it which is large

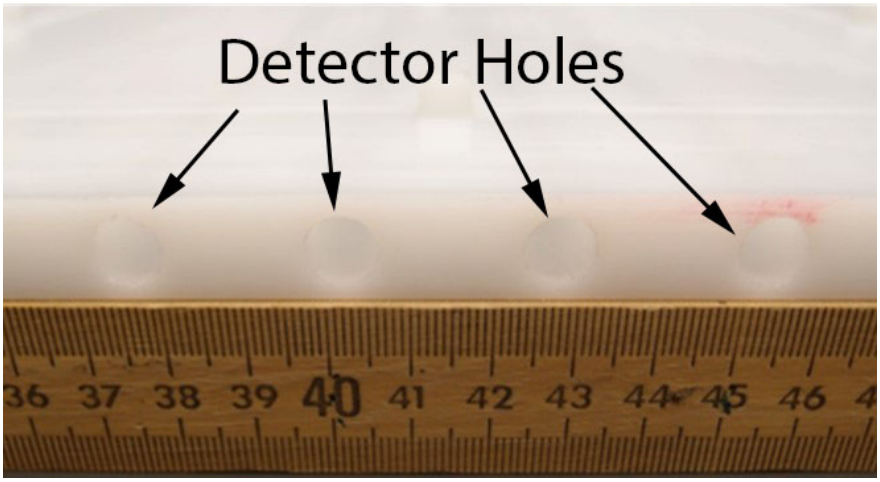

Figure 3.16: Holes in Specially Designed Plate added to the Class Foils for the Rossi-α Experiments.

enough to contain a small neutron source.

The experiment was performed using two methods of reducing reactivity. The first method was to use separation of the two halves using the assembly to adjust reactivity. The experiments performed as a function of separation were used to derive the value of α at delayed critical which can also be referred to as the α-eigenvalue. Measurements were taken at 34, 63, and 94 mils more separation than the critical separation.

The second method was to measure fully assembled stacks where units were removed. Measurements were taken containing 15, 14, 13, 12, 11, 10, and 5 units. The gap between 10 and 5 was unintended, but rather a result of limited time available. During these various configuration changes, the stack was shifted several times to ensure the detection system never strayed more than 2 units from the center of the stack. The stack was shuffled twice over the course of the experiment during the 13 unit and the 10 unit measurement cases. The order of the stacks is shown in Fig. 3.20 where the 13 unit case is shown in Fig. 3.20a and the 10 unit case is shown in Fig. 3.20b. All other measurements were completed on subsets of the stacks shown in Figs. 3.19 and 3.20 where the top unit was removed to form the next configuration. When the stack consisted of 15 units, the base would have been the stack shown in Fig. 3.19 without the polyethylene interstitial labeled 2N and the fuel labeled 10C.

When building an assembly where mass is used to control reactivity, an equation developed

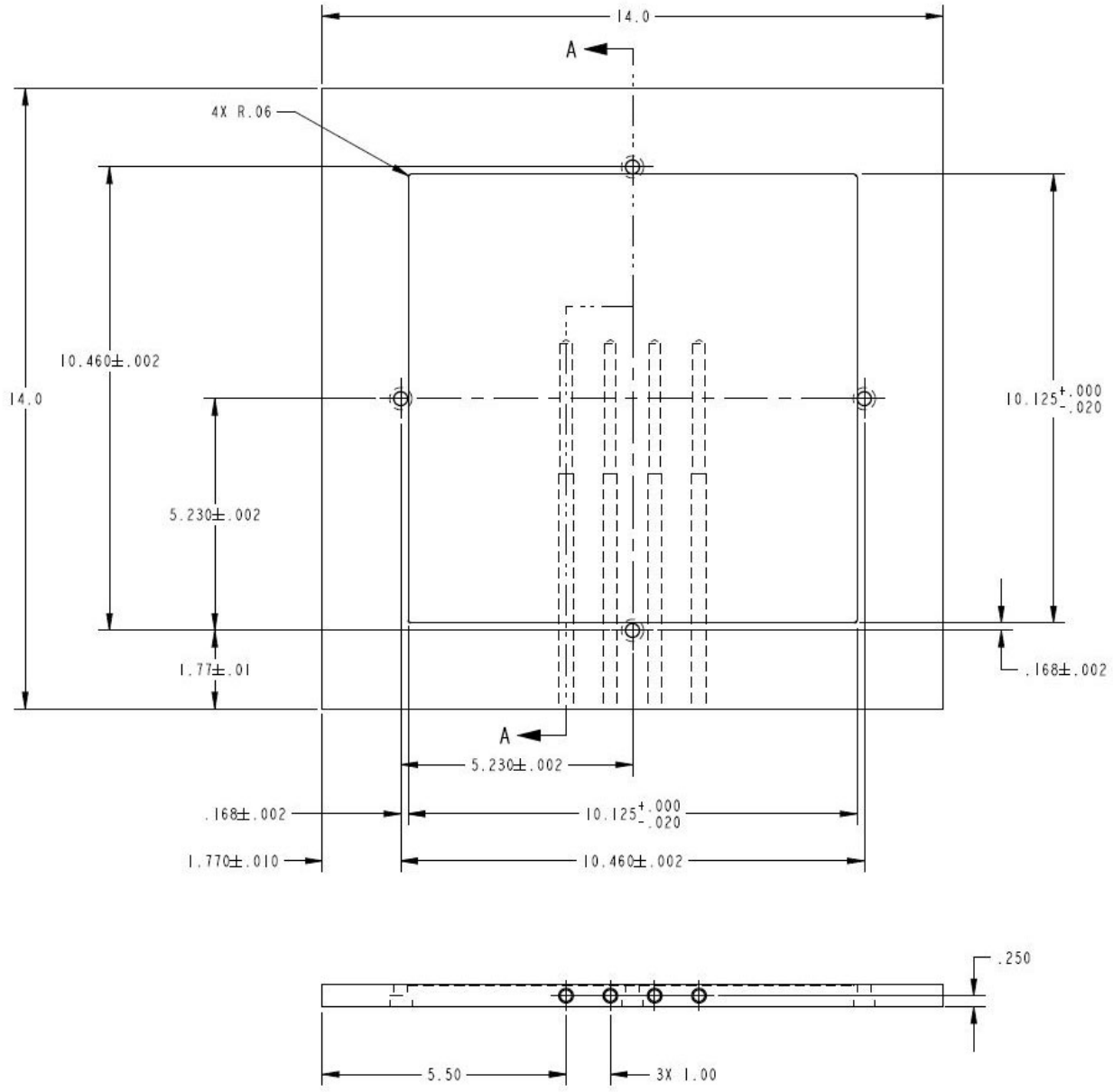

Figure 3.17: Drawing of the special plate designed to hold the ^{3}He tubes for the Rossi-α experiment.

Figure 3.18: Top Half of Class Foils on Planet Critical Assembly with the ^{3}He Tubes in Place.

by O'Dell can be used to estimate the multiplication factor of the assembly [66]. This relation can also be used to give an estimate of the expected multiplication factor for the experiment. This relationship only works well when the multiplication is greater than 20 (i.e $k_{eff} = 0.95$). Using O'Dell's equation and the exponent chosen using work of Hutchinson et al. [67], the k_{eff} of each of these cases was estimated using the mass comparison to the critical configuration using Eq. 3.2.

$$k_{eff} \approx \left(\frac{m}{m_c}\right)^{0.25} \tag{3.2}$$

In Eq. 3.2, the parameters used are m the mass in the system and m_c estimated mass of a critical system.

Once a critical configuration is established, the critical mass is known. The effective multiplication factor, k_{eff}, can then be determined using Eq. 3.2 for each subsequent case. The intended goal was to measure configurations between critical and a $k_{eff} < 0.8$. If this was not sufficient, more measurements would need to be completed. The estimated values of k_{eff} are listed in Table 3.3 along with the reactivity for each measurement and linearly

6 Poly		1"
4B Poly		1"
4C Poly		1"
2N Poly	10C HEU	0.5"
2M Poly	11C HEU	0.5"
2H Poly	12C HEU	0.5"
2G Poly	13C HEU	0.5"
2E Poly	14C HEU	0.5"
10 RTD	15C HEU	0.5"
Rossi Alpha Plate	16C HEU	0.5"
3 Membrane Poly	17C HEU	0.5"
2C Poly	18C HEU	0.5"
2I Poly	19C HEU	0.5"
2J Poly	20C HEU	0.5"
2K Poly	21C HEU	0.5"
2L Poly	22C HEU	0.5"
2F Poly	23C HEU	0.5"
2D Poly	24C HEU	0.5"
9 Poly Source	25C HEU	0.5"
11 Poly		0.5"
4A Poly		1"
5 Poly		1"

Figure 3.19: Critical Configuration of the Class Foils Experiment with the Specially Modified Plate and Detection System.

6		1"
4B Poly		1"
4C Poly		1"
2G Poly	18C HEU	0.5"
2E Poly	19C HEU	0.5"
2C Poly	20C HEU	0.5"
2I Poly	13C HEU	0.5"
2J Poly	14C HEU	0.5"
10 RTD	15C HEU	0.5"
Rossi Alpha Plate	16C HEU	0.5"
3 Membrane Poly	17C HEU	0.5"
2K Poly	21C HEU	0.5"
2L Poly	22C HEU	0.5"
2F Poly	23C HEU	0.5"
2D Poly	24C HEU	0.5"
9 Poly Source	25C HEU	0.5"
11 Poly		0.5"
4A Poly		1"
5 Poly		1"

(a) Polyethylene Class Foils configuration with 13 foils.

6		1"
4B Poly		1"
4C Poly		1"
2E Poly	16C HEU	0.5"
2C Poly	17C HEU	0.5"
2I Poly	18C HEU	0.5"
2J Poly	19C HEU	0.5"
2K Poly	20C HEU	0.5"
Rossi Alpha Plate	21C HEU	0.5"
2L Poly	22C HEU	0.5"
2F Poly	23C HEU	0.5"
2D Poly	24C HEU	0.5"
9 Poly Source	25C HEU	0.5"
11 Poly		0.5"
4A Poly		1"
5 Poly		1"

(b) Polyethylene Class Foils configuration with 10 foils.

Figure 3.20: Intermediate cases of Polyethylene Class Foils when re-stacking occurred to center the Rossi-α detection system.

related estimates of α. The values of k_{eff} in Table 3.3 are calculated using Eq. 3.2. The values of reactivity and α are determined using Eqs. 2.6 and 2.32, respectively.

Table 3.3: Estimates of the k_{eff} as a function of units using the O'Dell estimate.

# of Units	$\mathbf{k}_{effective}$	$\boldsymbol{\rho}$ **(\$)**	$\boldsymbol{\alpha}$ **($\mathbf{s^{-1}}$)**
15	0.995	-0.59	-317.4
14	0.978	-2.65	-727.6
13	0.960	-4.90	-1176.2
12	0.941	-7.38	-1670.1
11	0.921	-10.12	-2218.3
10	0.899	-13.21	-2832.7
9	0.876	-16.70	-3529.1
8	0.850	-20.71	-4329.6
7	0.822	-25.41	-5266.1
6	0.791	-31.03	-6386.9
5	0.756	-37.96	-7769.5

CHAPTER 4

COMPUTATIONAL STUDY

4.1 Monte Carlo Simulations

Simulations are performed using a Monte Carlo neutron transport code for comparison to experiment. The simulations discussed here are performed using MCNP®6.2[1]. MCNP, Monte Carlo N-particle, is a robust and well validated stochastic neutron transport code developed by Los Alamos National Laboratory [68]. For this computational study, it is important that the code be able to perform stochastic neutron transport because several of the configurations are extremely subcritical.

MCNP is used to determine the prompt neutron decay constant for several configurations of two different systems. The ENDF/B-VI.6 cross sections (.66c) are used for all calculations quoted in this dissertation, unless otherwise noted. The first system is a fast system named Godiva IV. The second system is a thermal system named the Polyethylene Class Foils. For both systems, criticality eigenvalue, *KCODE*, calculations are used to determine the multiplication factor of the system for each configuration. In addition to the simulations to determine multiplication factor, simulations to determine the prompt neutron decay constant are performed for both systems.

[1]MCNP® and Monte Carlo N-Particle® are registered trademarks owned by Los Alamos National Security, LLC, manager and operator of Los Alamos National Laboratory. Any third party use of such registered marks should be properly attributed to Los Alamos National Security, LLC, including the use of the designation as appropriate. For the purposes of visual clarity, the registered trademark symbol is assumed for all references to MCNP within the remainder of this paper.

4.1.1 Fast System: Godiva IV Simulations

To perform a computational experiment on the value of the prompt neutron decay constant, an MCNP input deck is modified beginning with the MCNP input deck given in the Godiva IV Benchmark HEU-MET-FAST-086 [62]. The modifications made include both correcting the errata included in the benchmark as well as other issues identified by the critical assembly principal investigator (PI). The modifications include changing the size of the glory hole (internal sample space), adding a shim beneath the safety block to correct for oxidation over the years, and correcting the safety block density. Additional modifications made include updating to more current cross sections, and moving the control rods to their critical positions on Apr. 17, 2014. This date is selected because in addition to the critical rod heights, the position of the both rods fully inserted into the assembly was also measured. This removes potential uncertainty from the zero positions indicated by the control rod encoders which measure their positions. The system is shown in the critical configuration in Figs. 4.1, 4.2, and 4.3.

This MCNP input deck is then run to determine the k_{eff} and neutron lifetime of the computational study where the calculation geometry matches the experimental geometry of delayed critical. All further calculations depend on this value as a baseline. Additional MCNP input decks are created adjusting both control rods and the safety block in an attempt to determine α over the entire range of reactivity of the Godiva IV assembly, which is approximately -25\$ to $+1.15$\$.

This reactivity range is covered by performing calculations on the following configurations. Starting with the critical benchmark input deck, control rod 1 is moved out from its critical position in 500 mil increments until the rod is in its full out position. This procedure is then repeated for control rod 2. The study of reactivity on control rod 2 begins using an input deck with control rod 1 fully withdrawn. Then a study is completed by moving the safety block. The safety block is moved out from its delayed critical position in 100 mil increments until the block is fully removed from the assembly. This study begins with an input deck where both control rod 1 and control rod 2 are fully withdrawn.

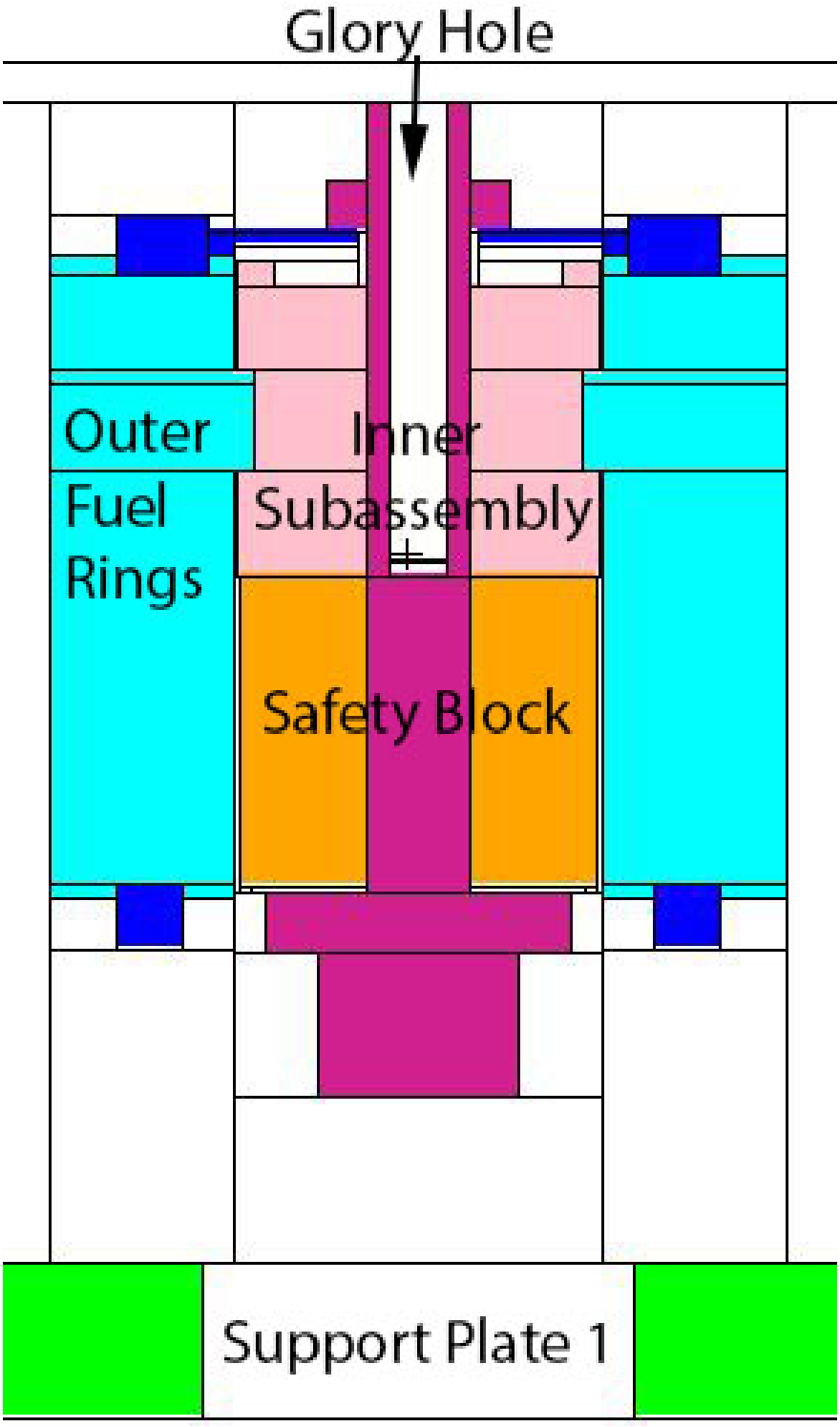

Figure 4.1: The yz plane of Godiva IV from the centerline.

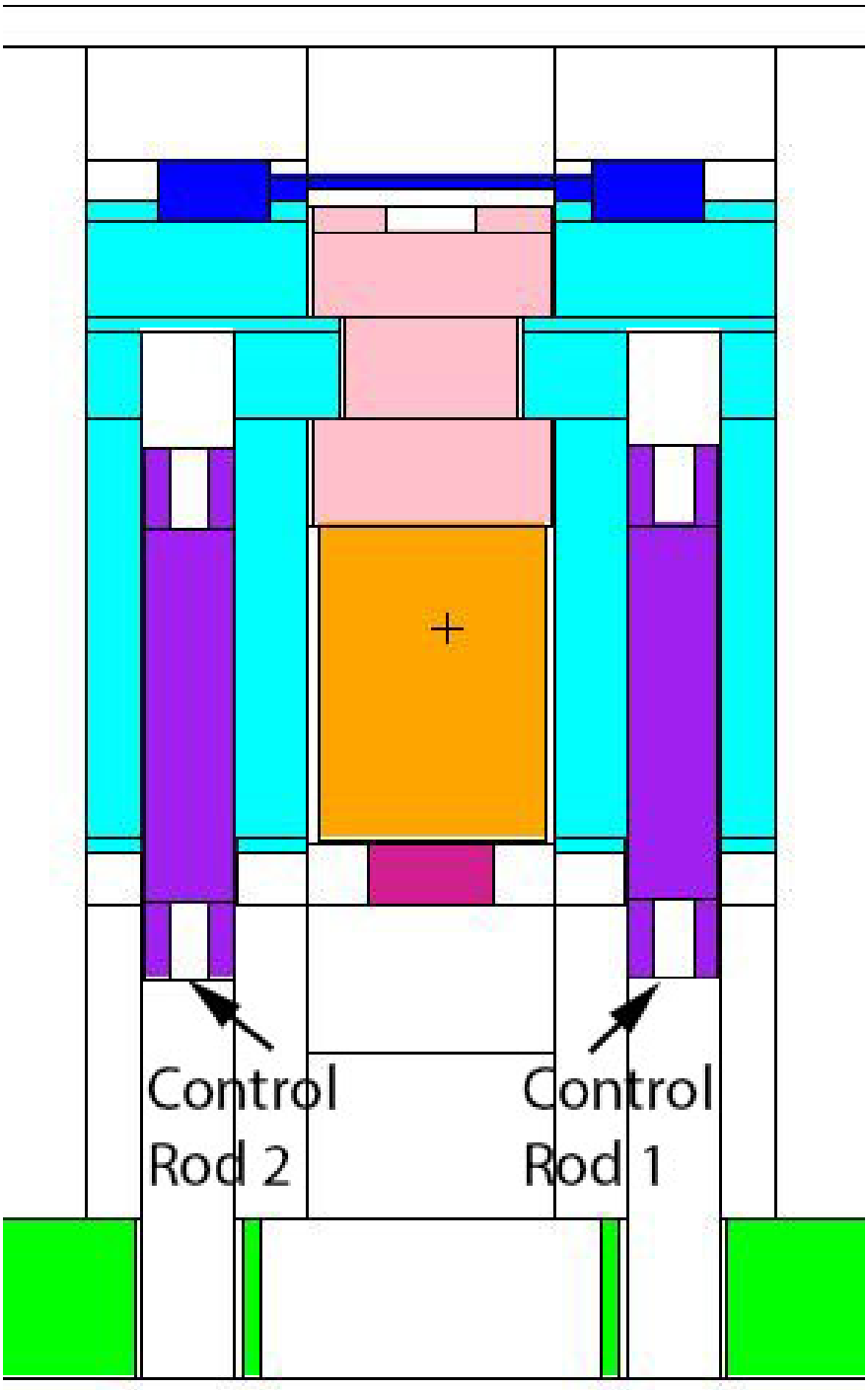

Figure 4.2: The yz plane of Godiva IV in the plane of control rods 1 and 2.

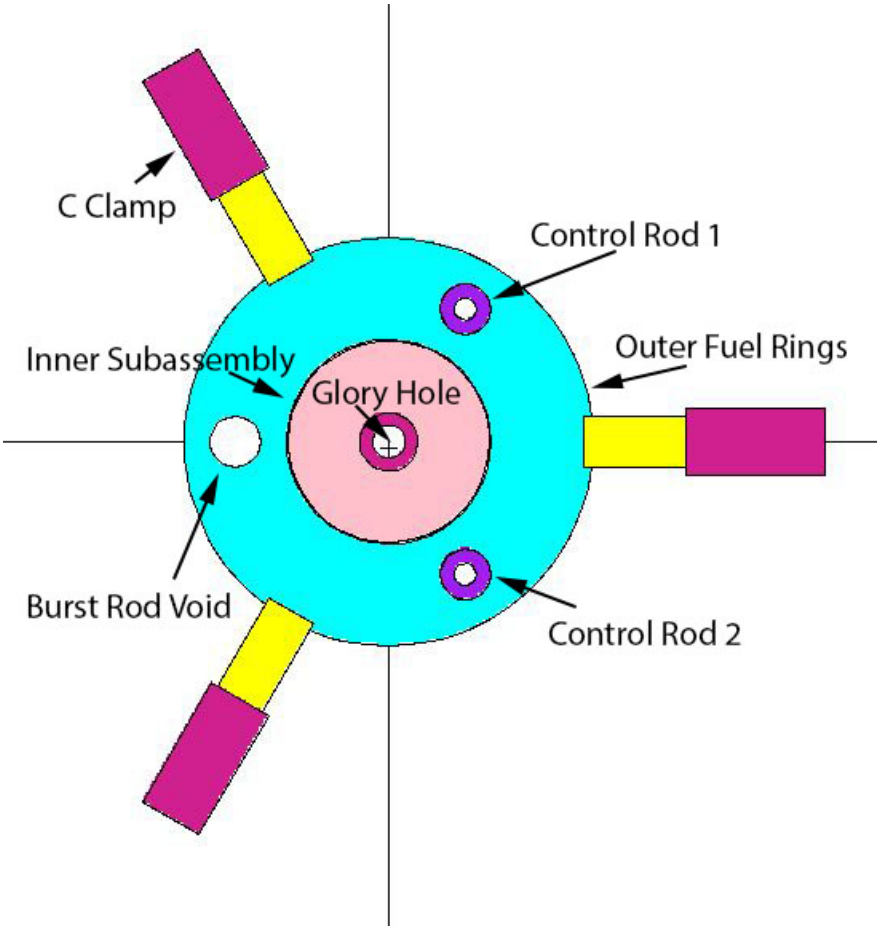

Figure 4.3: The xy plane (top looking down) of Godiva IV from the centerline.

4.1.2 Thermal System: Polyethylene Class Foils Simulations

The simulations performed on the Polyethylene Class Foils started from the MCNP input deck used when the foils were designed. The Rossi-α experimental plate is added to the center of the assembly. At this point, the system is well subcritical, so additional foils are added to compensate for the lost reactivity. The xy profile of the model is shown in Fig. 4.4. In Fig. 4.4, the green circles are the cross section of the ^{3}He detectors, and the black lines are where the uranium foils are located. Because the fuel is difficult to discern, a zoom of the fuel region is also included in Fig. 4.6. An enlarged cross section of the detectors is shown in Fig. 4.5. The yz profile of the model is shown in Fig. 4.7 at the centerline of the detectors. Because the detection system is quite small in Fig. 4.7, a zoom of the region containing the detectors is provided in Fig. 4.8. Then individual cases are run removing one foil each time. The total range of reactivity examined was -70$ to 0$. This reactivity range corresponds to configurations containing 5-15 units.

4.2 Methods to Determine Prompt Neutron Decay Constant

Two different methods to simulate the value of α are examined. The first method used *KCODE* MCNP simulations to calculate k_p for the system, and backs out α using known values for the neutron lifetime in the Godiva IV assembly. This calculational method is attempted because it should give the linear expectation of α for a given k_p. The second method uses fixed source MCNP simulations to measure neutron absorptions in ^{3}He which is nearly identical to the experimental measurements. This method uses a time based tally calculating the fluence in the detection volume to obtain time tallies of neutron events during the simulation. This calculational method is used because it closely follows the experimental method.

4.2.1 Definition of α Method

For the *KCODE* simulations, each MCNP input deck is run twice. The first run is completed using delayed neutrons to determine the configurations k_{eff}, and subsequently calculate

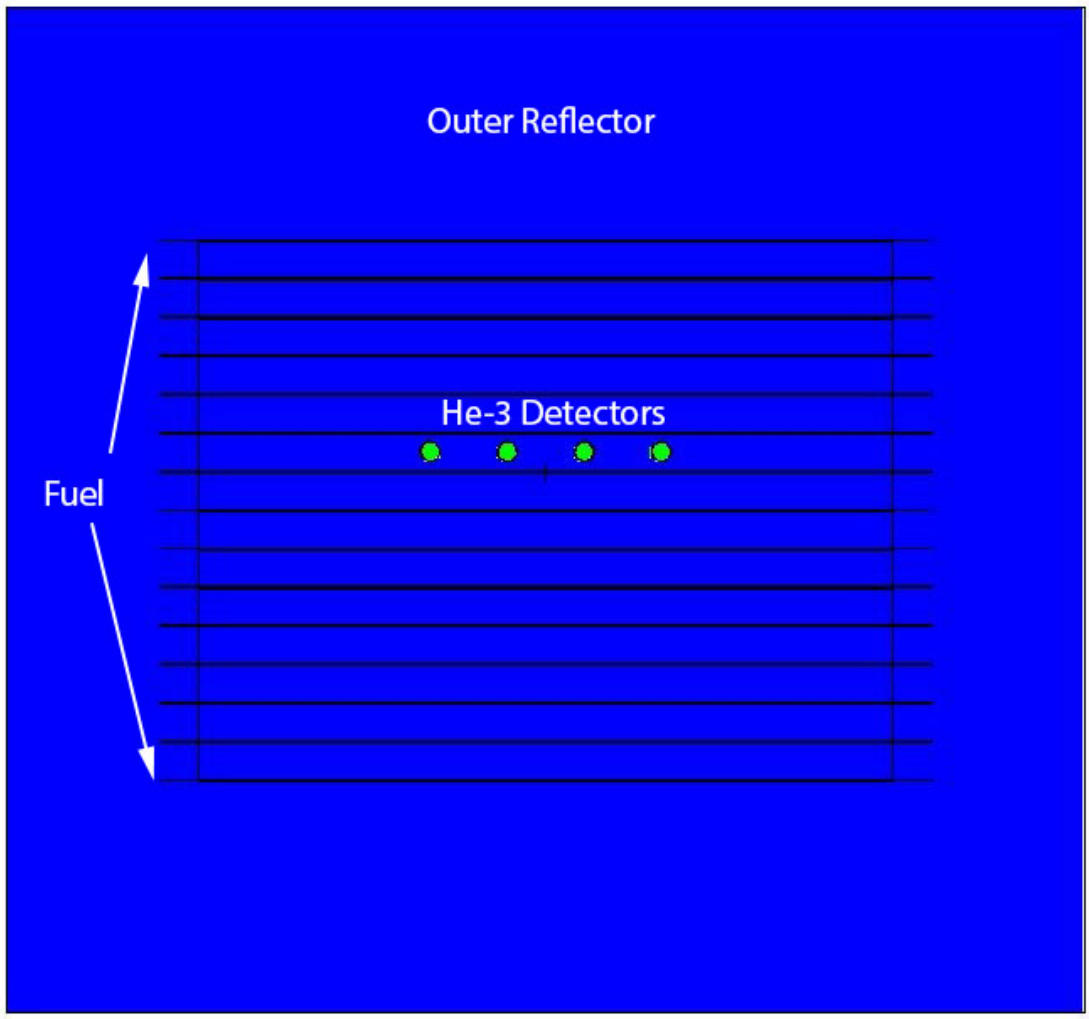

Figure 4.4: The centerline of the xy plane for the 15 unit configuration of the Polyethylene Class Foils.

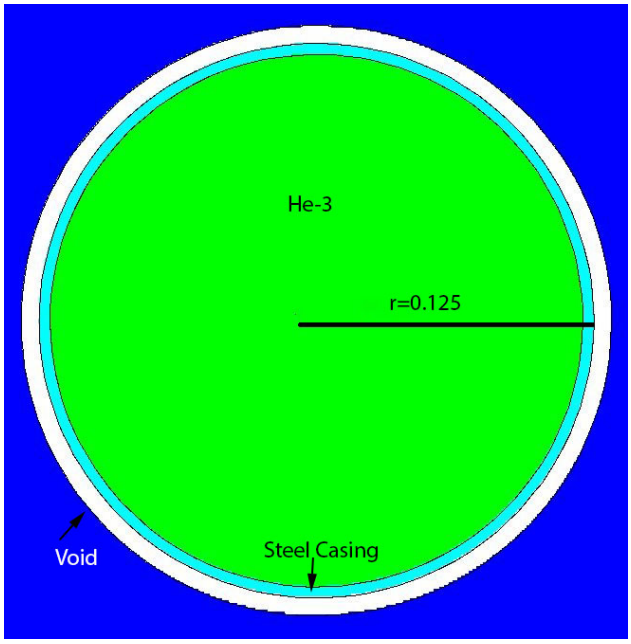

Figure 4.5: This figure shows a zoomed xy plane of the ^{3}He detector with dimensions in inches.

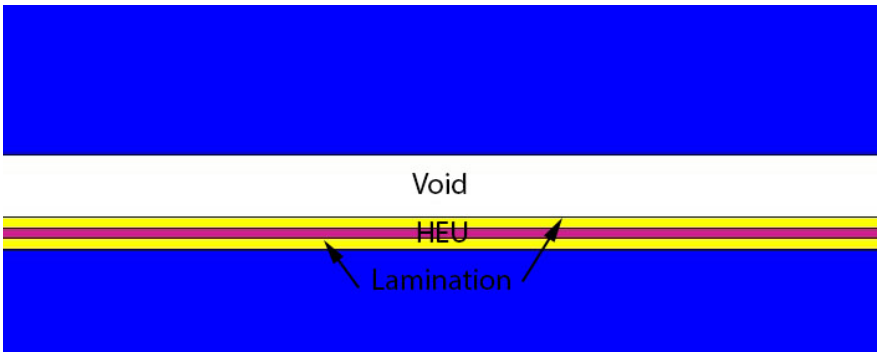

Figure 4.6: A zoom of the fuel region of the Polyethylene Class Foils.

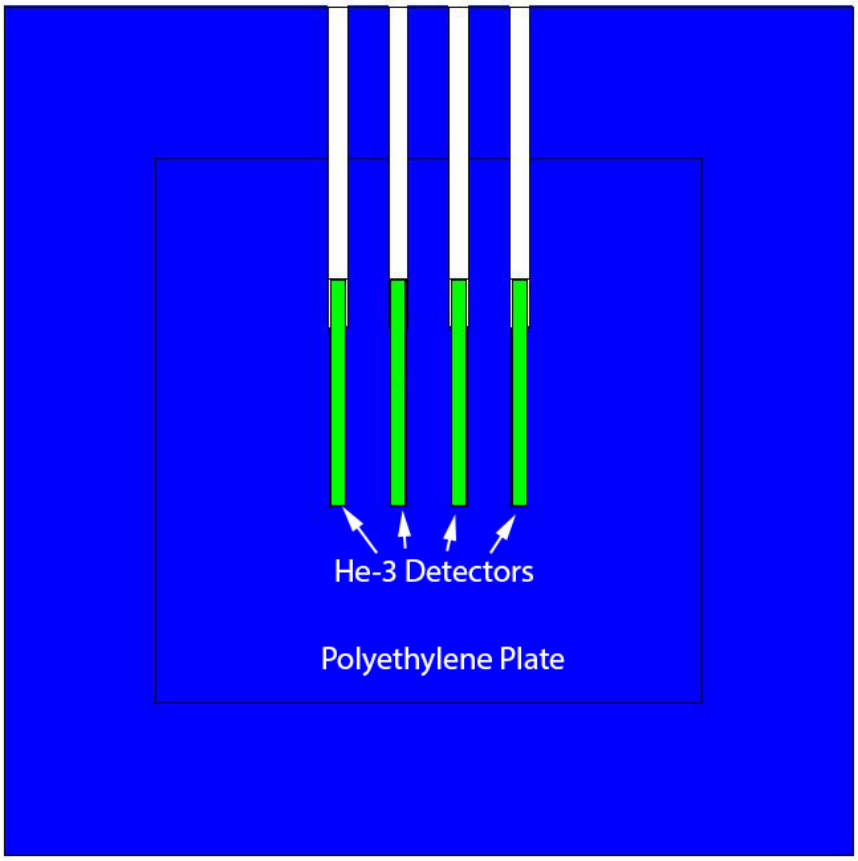

Figure 4.7: The yz plane for the 15 unit configuration of the Polyethylene Class Foils at the centerline of the detectors.

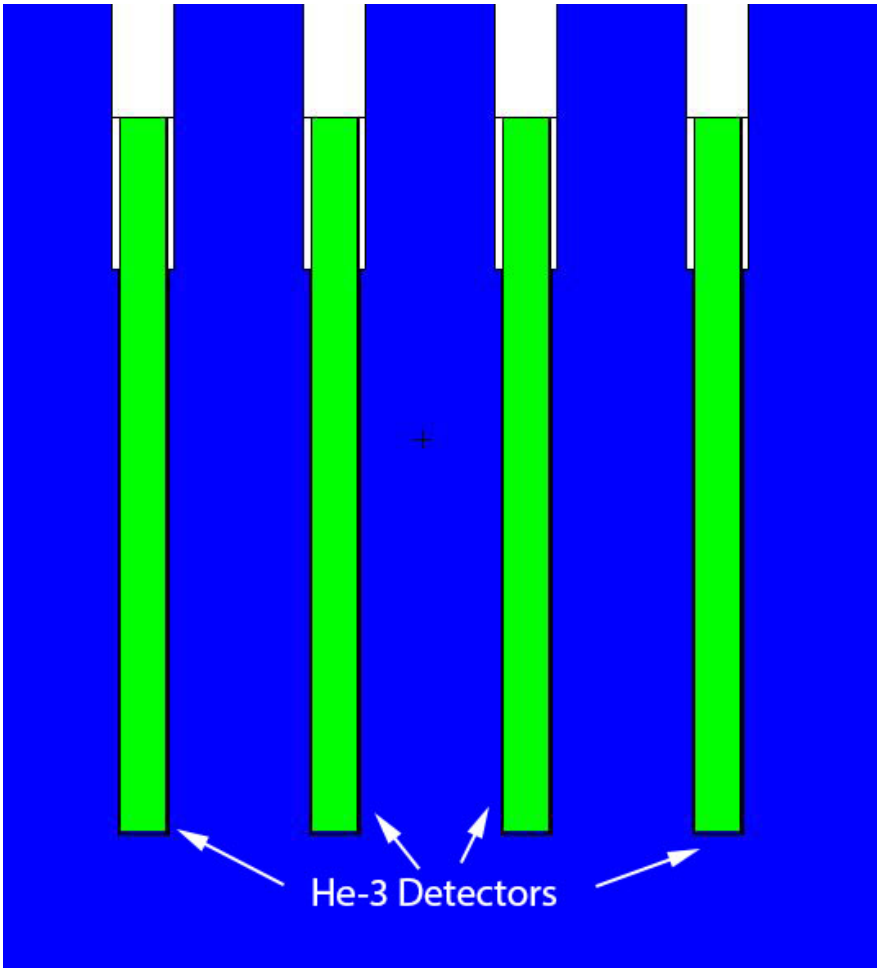

Figure 4.8: A zoom on the region of the yz plane containing the detection system.

the reactivity of that configuration. The reactivity of each configuration is found using the traditional conversion from k_{eff} to ρ shifted such that the delayed critical effective multiplication will give a reactivity of zero. This modified reactivity equation is given by Eq. 4.1.

$$\rho = \frac{k - k_{DC}}{k k_{DC} \beta_{eff}} \tag{4.1}$$

This equation includes β_{eff}, which for this computational study, is determined from the calculations at delayed critical. The value of β_{eff} is determined using Eq. 4.2.

$$\beta_{eff} = 1 - \frac{k_p}{k_{eff}} \tag{4.2}$$

For this study, the value of $\beta_{eff} = 0.00649$ which agrees extremely well with the assumed β_{eff} for fast systems , $\beta_{eff} = 0.0065$.

The second run is executed with the delayed neutrons turned off. This run gives the value of k due only to prompt neutrons, referred to as the prompt multiplication factor k_p. Its relationship to k_{eff} is shown in Eq. 4.3.

$$k_p \approx k_{eff} - \beta_{eff} \tag{4.3}$$

This value is used to determine the computational estimate of the prompt neutron decay constant for the configuration of interest. The prompt neutron decay constant is computed using a modified version of its traditional definition. The traditional definition is given by Eq. 2.8 in chapter 2 section 2.5. The modified definition of alpha was suggested by the group that creates the MCNP code. The modified version normalizes the reactivity of the delayed critical position to match the reactivity, k_{eff}, of the delayed critical MCNP input deck to account for differences between the real world and the model. These include: physical differences like machining tolerances and physical gaps; errors or gaps in the nuclear data; and the code itself. This modification is shown in Eq. 4.4.

$$\alpha = \frac{k_p - k_{eff,dc}}{l} \tag{4.4}$$

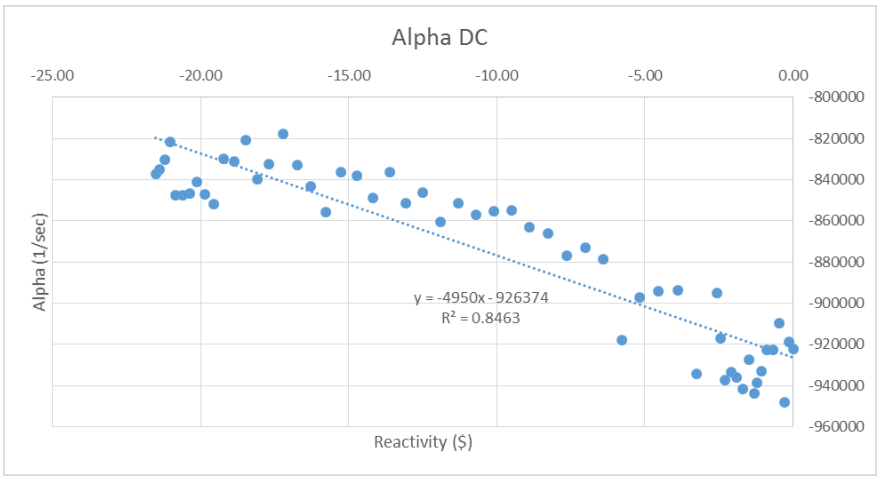

Figure 4.9: Study of the α-eigenvalue given directly from the *KOPTS* card in MCNP.

A shift of this type ensures the computational values of the prompt neutron decay constant more closely resembles the experimental prompt neutron decay constant for a given reactivity.

Seasoned MCNP users may wonder why go to the additional trouble of running multiple input decks when the *KOPTS* card gives a value of the α in the output file. Although this is in fact true, the value of the α reported is actually determined by the code using Eq. 2.29.

Since the goal of this study is to determine the value of the prompt neutron decay constant for the entire reactivity range of a system, the assumed value of the α-eigenvalue at delayed critical is not useful. The value of the α-eigenvalue at delayed critical is a useful quantity and MCNP will give favorable results if your input deck has a k_{eff} near 1, but can give misleading results as reactivity is increased or decreased. The misleading result is not a result of the code performing in an improper manner, but rather caused by the fact that the lifetime of the system is changing as reactivity is increased or decreased. This is especially important in systems like Godiva IV where moving control rods increases surface area and subsequently the system leakage, but also has an effect with the Polyethylene Class Foils as the size of the system is changing. A plot of the α-eigenvalue determined by MCNP for each case examined during the Godiva IV simulations is shown in Fig. 4.9.

4.2.2 Simulated Experiment Method

This method of determining the prompt neutron decay constant performs the same steps as the experiment performs, but uses a simulation for the input to the detectors. The results of this method can easily be converted into list-mode data. These simulations are performed using the same input decks as the other method, but include a Cf-252 source and are run in fixed source mode with no variance reduction. An important thing to note is that all cases examined must be subcritical for the simulations to finish because neutrons are tracked to extinction. The Cf-252 source is added to each input deck to be a match to the Cf-252 source described in Chapter 3, so that the simulations match the experiment as closely as possible. This source could not be defined by the ENDF/B-VI.6 cross sections because ENDF/B-VI did not include spontaneous fission distributions. The Cf-252 source in these simulations is defined using ENDF/B-VII.1 cross sections (.80c). Regions of interest are defined in the input deck where all termination events are tracked. to the code. Inside these regions of interest, individual particle interactions are tracked and the time of each absorption is recorded in a file called a *PTRAC*. For this series, the regions of interest defined are the active regions inside the ^{3}He detectors. These simulations liken the experiment completely by producing list-mode data using the *PTRAC* file in MCNP. The detectors in the simulations do not have the same physical limitations as the experiment in terms of dead time. The data from the simulations assumes a perfect detector which distinctly recognizes each absorption event. The list-mode data is then analyzed in the same manner as the experimental data.

These simulations need to be executed without any variance reduction because only complete particles can be counted in real life. Because these simulations must be run without variance reduction, they are computationally expensive and time consuming.

These simulations are completed for each case experimentally measured so that a direct comparison can be made.

4.3 *KCODE* and Fixed Source Simulations

The computational experiment is performed on both a fast and a thermal HEU system. For the fast system, only the results for the definition of α method are presented. This will be addressed in the results. For the thermal system, both methods are compared.

The procedure for the definition of α method includes computations of the effective multiplication factor, k_{eff}, for a series of configurations. One base case is compared to the experiment to determine the bias, and determine the value of $k_{eff,DC}$. The other cases k_{eff} is used to determine the system reactivity using Eq. 4.1. Then a second set of calculations are completed. Turning off delayed neutron emission, the prompt multiplication factor, k_p, for each configuration is calculated. The lifetime of the system is determined from Eq. 2.29 where the assumed value of β_{eff} is divided by the α-eigenvalue to determine the neutron lifetime. This result is combined with the previously calculated $k_{eff,DC}$ and lifetime to determine α using Eq. 4.4.

CHAPTER 5

DATA ANALYSIS

To determine the subcritical reactivity of a system of interest, first the prompt neutron decay constant needs to be measured. This α is then converted to a reactivity, and compared to reactivity determined using another method. The analysis has several steps. The first is to reduce the measured data into a more manageable form. The second is to generate the prompt neutron population decay curves. The third is to obtain the α parameter. The fourth and final step is to convert the α into a reactivity value, so that a comparison can be made.

5.1 Data Reduction

Data reduction simplifes large listmode data files and creates Rossi-α specfic analysis files. Data reduction is only used on the Rossi-α experimental data and simulated experiment data. The definition of α method does not require data reduction. The pulsed source method data also does not require data reduction.

5.1.1 Simulated Experiment Method

The data for the simulated experiment method comes from MCNP in a file called a *PTRAC* file which tracks specified particle interactions in a volume. As discussed in Chapter 4, the tracked interaction for these simulations is the absorption of neutrons in ^{3}He gas. This mimics the reaction measured by the detectors in the experiment as if these volumes were detectors with no dead-time. This data needs to be organized into the same format as the experimental data, so that it can be turned into a measurement of α. A python script

written by the MCNP team at Los Alamos National Laboratory was used to process the *PTRAC* files and turn them into an unordered list of times interactions occurred in each tracked volume. This list is very similar to the experimental data, and can be processed by the same algorithm.

5.1.2 Rossi-α Method

Once data has been collected, each measurement contains a list of times at which neutrons were absorbed and counted by the detection system. This list is then reduced into a list including only the time when neutrons were detected. Prior to execution of the code to reduce the list, the specific detectors desired in the output can be chosen. The user can choose to include a single detector or several combined to generate the reduced list.

5.2 Generate Prompt Neutron Decay Curve

For each method, the reduced data is analyzed by a C++ program designed to generate the histogram depicting the detected prompt neutron population as a function of time after a fission event. Each analysis methods assume that this histogram is proportional to the true prompt neutron population. An example of one of these histograms is shown in Fig. 5.1. The data from the Rossi-α and simulated experiment methods is now in the same form, so only one explanation will be given. The definition of α method does not generate prompt neutron decay curves, so no explanation is given.

Pulsed Neutron Source Technique

Once the data has been collected, each measurement contains a list of time at which neutrons were absorbed and counted by the detection system. This list also includes the time at which the neutron generator was pulsed. The list of times was reduced into a histogram that is proportional to the prompt neutron population after a fission event by adding the events after each pulse into a histogram with user defined bin widths of 18 ms. A bin width of 18 ms is chosen because it is slightly smaller than the period of the neutron generator (20 ms).

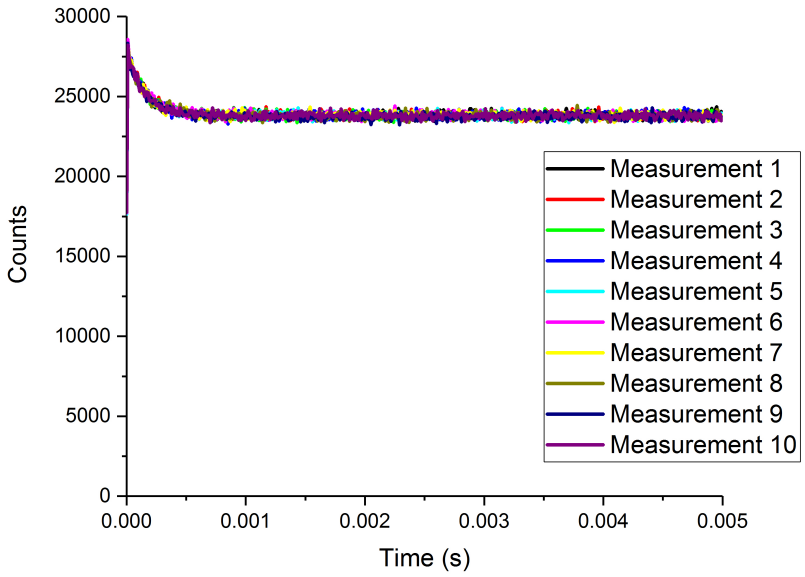

Figure 5.1: An example of a prompt neutron population histogram taken from the 5 unit configuration of the Polyethylene Class Foils.

For the pulsed source work, the histogram is created by adding together times after the neutron generator pulses. A flow chart highlighting the logic of this code is shown in Fig. 5.2.

5.2.1 Rossi-α and Simulated Experiment Methods

The reduced list is then processed by another algorithm designed to create the histogram that is proportional to the prompt neutron population as a function of time after a fission event. This description explains the process followed by both the Rossi-α and simulated experiment data as they are the same. This histogram is created by measuring the time difference between neutron counts and placing those time differences in a histogram. In Hansen's paper, he discusses three different potential binning schemes [69]. For this work, Type I binning is employed. With type I binning, each neutron count is treated as an initiating event, the event at t_1 as described in Eq. 2.13. Then the time difference between this event and each subsequent event is placed into a histogram. To save time and resources, a limit on the maximum time difference placed into the histogram is chosen. This limit

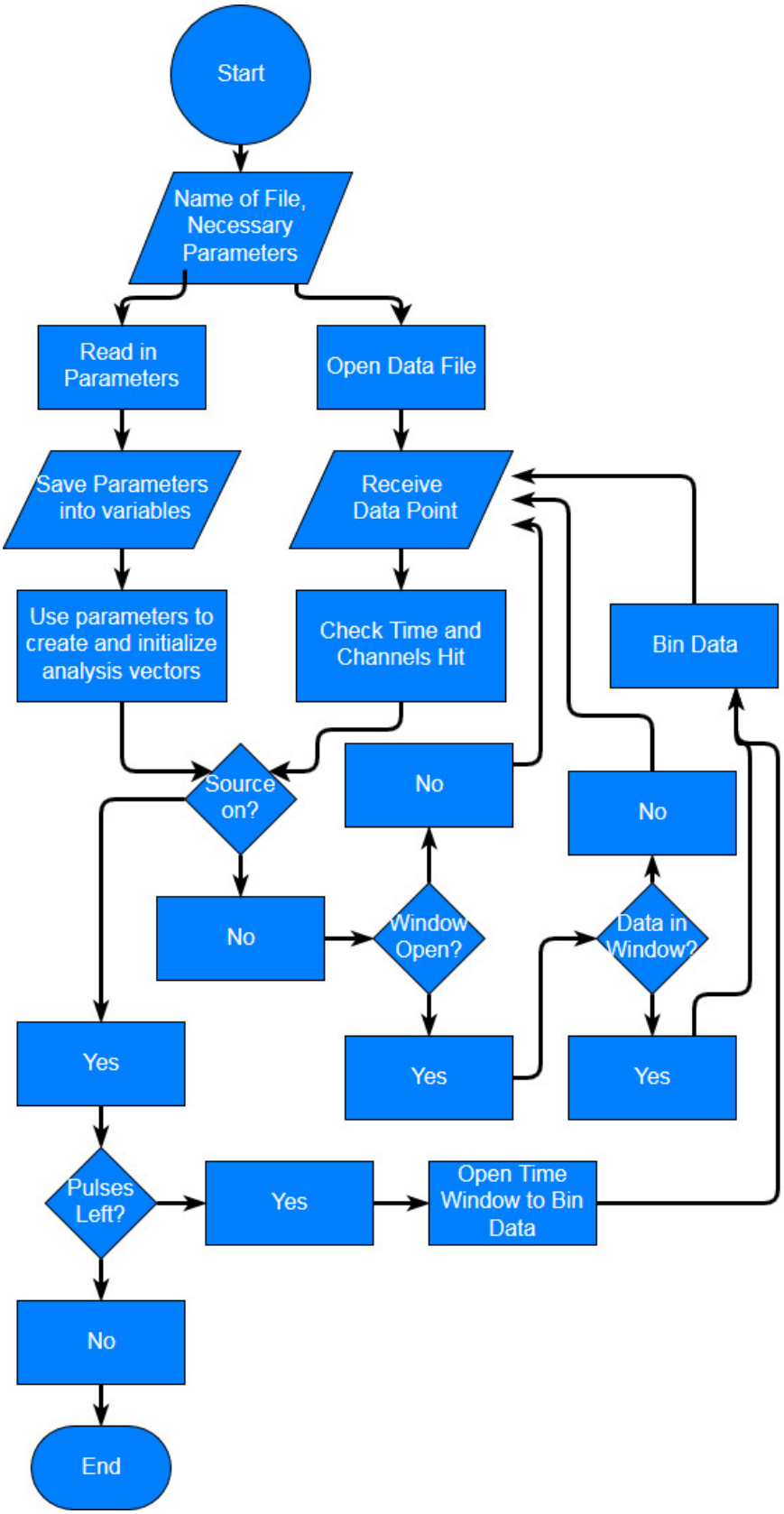

Figure 5.2: Flow chart for pulsed neutron source code analysis software.

reduces the total number of operations the code completes because the data is in ascending time order. Once a time difference passes this limit, the initiating event is moved to the event immediately after the previous initiating event. This process terminates when the time of the initiating event added to the time difference limit exceeds the total measurement time. A flow chart including the logic in this code is shown in Fig. 5.3.

5.3 Determine α

Using the discussed methods, there are two main ways α is determined. The first is a straight calculation using the definition of α method. The second is to fit the prompt neutron decay curve and obtain the value from the fit.

5.3.1 Definition of α Method

Calculations were performed using the MCNP models developed in Chapter 3. These values were converted into their corresponding values of α using Eq. 4.4. For Godiva, the assumed parameters k_{eff} at delayed critical and prompt neutron lifetime l are $k_{eff} = 0.995$ and $l = 7.7 \times 10^{-9}\, s$, respectively. For the Polyethylene Class Foils, the assumed parameters k_{eff} at delayed critical and prompt neutron lifetime l are $k_{eff} = 0.998$ and $l = 4.26 \times 10^{-5}\, s$, respectively.

5.3.2 All Other Methods

In both methods, the histogram of the prompt neutron population was fit to the equation developed in Chapter 2 [53]. The data was fit using a three parameter non-linear exponential fit using a Levenberg-Marquardt fitting algorithm. The three parameters this fit outputs are A, B, and α. In the context of this work, only the parameter α was used to make any determinations about the system.

The program used to fit the data accepts the prompt neutron decay curve histogram and an initial guess for the parameters. Because the fit is exponential, there is only one true

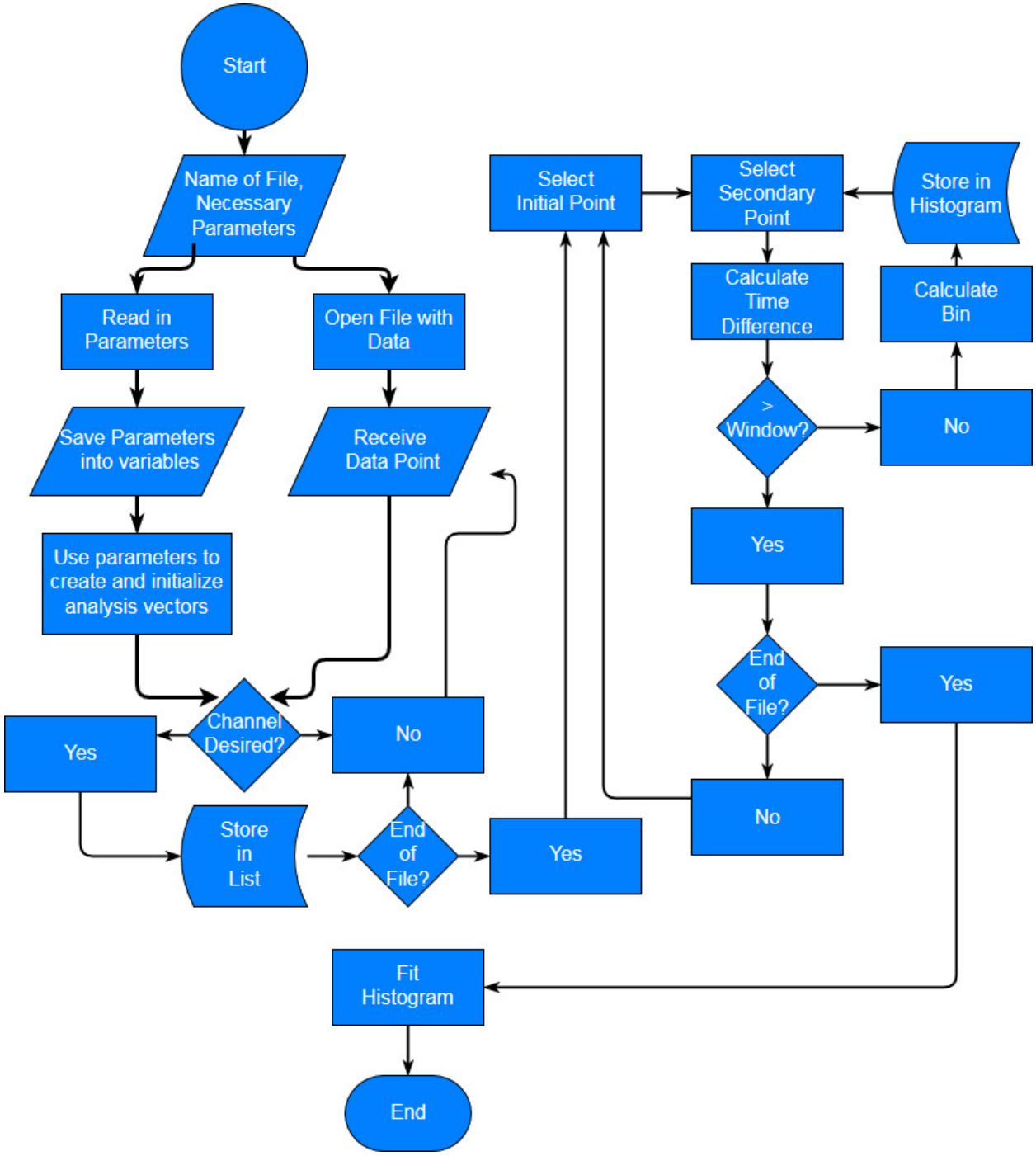

Figure 5.3: Flow chart for Rossi-α code analysis software.

answer so convergence is not an issue when choosing initial values for the parameters, but choosing those values intelligently saves time on convergence. This program allows the user to select an initial value for α which was chosen to be $\alpha = -1000\ s^{-1}$ for all cases. Guesses for the other two parameters are set using values determined differently for each datafile without user input. A is selected to be equal to the largest bin, and B is selected to be the average of the last half of the histogram.

The histogram often has several bins near the beginning that do not exhibit the same exponential behavior as the other bins. These bins are the bins affected by detector dead time. If included, these bins would suppress the value of α of the system. To mitigate against this suppression, the histogram created by the previous code is fit using a Levenberg-Marquardt algorithm ten different times. The first fit is performed on the entire histogram. Each successive iteration is simply a fit of the histogram after removing the first point. The user then selects the fit parameters from the output file based on convergence in the value of α and a decrease in the Chi-Squared of the fit.

5.4 Reactivity from α

To obtain a value that is easy to compare between MCNP and the different experimental and computational methods, the values of α are converted into reactivity ρ. The expectation is that the converted values of reactivity will linearly match the corresponding simulations. It is expected that at some point, the linear relationship will no longer exist. This point of non-linearity is the lower threshold for subcritical reactivity determination.

The measured or calculated subcritical reactivity is determined using Eq. 2.32 from Chapter 2. These reactivity values are then compared to the other methods and the MCNP *KCODE* simulations.

5.5 Uncertainty

Uncertainty is an attempt to quantify unknowns when examining and comparing experimental data. When performing any experiment, it is essential to address the uncertainty

on reported values because uncertainty bounds the true mean value of the parameter. The uncertainty for a measurement is comprised of two main factors. The first is the systematic uncertainty and the second is the uncertainty associated with the statistical nature of the measurement.

5.5.1 Systematic Uncertainty

The systematic uncertainty has to do with how well a system is understood and attempts to address bias based on incomplete knowledge. The systematic uncertainty generally applies equally to all cases examined because it quantifies common unknowns between a measurement and a calculation. For the Polyethylene Class Foils Experiment, several sources of systematic uncertainty are examined. Sources of systematic uncertainty examined are the position of the detectors in the plate, HEU mass, polyethylene plate mass, polyethylene plate dimensions, and the axial air gap. Other parameters have an impact on the systematic uncertainty, but the parameters chosen are judged to have the greatest impact on the systematic uncertainty based on previous experiments.

Simulations were performed to determine the sensitivity of the Polyethylene Class Foils to the position of the detectors in the plate. The sensitivity for the other parameters were taken from a benchmark experiment in the International Handbook of Evaluated Criticality Safety Benchmark Experiments labeled HEU-MET-THERM-001 [70]. This experiment used the same nuclear material and slightly larger polyethylene plates. To confirm the sensitivities from this experiment would be comparative to the experiment performed in this work, simulations were performed to compare the most sensitive parameter, HEU mass. The sensitivity agreed within 7%, so the other sensitivities were assumed to also be adequate estimates. Other sources of systematic uncertainty were also identified, but taken from a benchmark with a similar experimental set-up. These sources of uncertainty include: polyethylene plate mass, polyethylene plate dimensions, and the axial air gap. The benchmark used for these other uncertainty parameters is HEU-MET-THEM-001 which is an experiment using the same foils with 1.00 inch polyethylene interstitial plates.

The uncertainty for the position of the detectors in the measurement plate is attributed to

the manufacturing of the polyethylene plate and of the ^{3}He detectors. This is the uncertainty that the ^{3}He tubes are located where expected. This uncertainty was examined by moving all four detectors to several different positions in the plate. It is likely not physical to have all 4 ^{3}He tubes exactly aligned, but these simulations are aimed at ascertaining the order of magnitude attributed to moving the ^{3}He tubes within the stack rather than obtaining a perfect simulation. In an attempt to minimize the impact of the tubes shifting, the tubes were taped into their positions and the plate holding the tubes was moved minimally.

The HEU mass in each foil is another uncertainty to examine. In the model, all of the foils are assumed to be identical, but in reality there are slight variations on the HEU mass in each foil. To address this concern, an examination of HEU density was performed. Simulations are performed to support the claim that other uncertainty parameters from the benchmark experiment HEU-MET-THEM-001 [70] are similar to those in this experiment. This had the benefit of examining both the uncertainty on the HEU mass which was measured to within ± 0.5 g and the HEU foil dimensions which were not explicitly measured and assumed to have a tolerance of $\pm 0.5\%$. The benchmark states, "as with many fissile systems, the fissile mass was the primary effect." [70].

The polyethylene plate mass was also examined in HEU-MET-THEM-001. The mass of the plates was determined to within ± 0.5 g [70]. This study perturbed the density of polyethylene in the plates by ± 0.00125 g/cm^3. This is equal to an ± 18 gram perturbation in the mass [70]. In this experiment, the uncertainty on the mass of the polyethylene interstitial plates is ± 6 g or a perturbation of ± 0.00042 g/cm^3.

To separate the mass from the density perturbations, dimensional perturbations were also completed. The dimensional measurements of the polyethylene were accurate to within ± 0.01 inch for the width and the thickness [70].

The axial air gaps is one of the largest questions when executing this series of experiments. These gaps are caused by several factors. The first is natural tolerances between the plates. In an attempt to minimize these gaps, a weight was added to the top of the stack. The second is due to slight warping of the polyethylene causing small non-uniform gaps. This source of uncertainty is attempted to be overcome by carefully picking the interstitial pieces when building the experiment. The third is oxidation of the fuel. The oxidation of the

fuel makes the foils thicker than the recessions in the plates and thus create another source of gaps on the edges. This source can be overcome by choosing fuel foils that seem to fit best. Even with attempts to reduce uncertainty in the experiment, no complete reduction is possible. So an axial gap between units is examined. In HEU-MET-THEM-001, a 2 mil (0.00508 cm) air gap was added between the polyethylene plates [70].

5.5.2 Measurement Uncertainty

The uncertainty in the measurement itself is due to natural fluctuations in the measured quantity. For the experimental results, this uncertainty is reported as the standard deviation of a population of measurements taken on the same configuration. This approach will also work for the *PTRAC* MCNP simulations as the data is similar to the experimental data. For the *KCODE* MCNP simulations, the uncertainty is reported by the code in the output file. For the definition of α method, each quantity measured is reported with a standard deviation which is related to fluctuations observed during the simulation. This standard deviation of all calculated quantities is found by propagating this standard deviation to the new parameters.

Experiment Method

The uncertainty applied to the experiment is the same as the uncertainty method applied to the simulated experiment simulations; thus, this method is used for both analyses. The measurement uncertainty in this case is the standard deviation of the population of measurements in a particular configuration. The standard deviation is found using Eq. 5.1.

$$\sigma^2 = \frac{\Sigma_{i=1}^{N} (x_i - \bar{x})^2}{N - 1} \tag{5.1}$$

Where σ is the standard deviation, N is the total number of measurements in the population, i is an iterator going over individual measurements in the population, x_i is the value of the parameter measured at i, and $\bar{x}$ is the mean value of parameter in the population.

Definition of α Method

The uncertainty in a *KCODE* simulation is directly related to the square-root number of particles sampled. Therefore, the uncertainty can be reduced by running more particles. The uncertainty in each value of the prompt neutron decay constant is determined computationally is calculated using standard uncertainty propagation techniques. The uncertainty in each value can be calculated using uncertainty propagation like the example shown in Eq. 5.2 when all parameters are uncorrelated. When the uncertainty on α is calculated for the definition of α method, all parameters are assumed to be independent and Eq. 5.3 is used.

$$\delta\alpha = \sqrt{\left(\frac{\partial\alpha}{\partial k_p}\delta k_p\right)^2 + \left(\frac{\partial\alpha}{\partial k_{eff}}\delta k_{eff}\right)^2 + \left(\frac{\partial\alpha}{\partial l}\delta l\right)^2} \tag{5.2}$$

$$\delta\alpha = \sqrt{\left(\frac{1}{l}\delta k_p\right)^2 + \left(\frac{-1}{l}\delta k_{eff}\right)^2 + \left(\frac{k_{eff}-k_p}{l^2}\delta l\right)^2} \tag{5.3}$$

For the case where all parameters are computationally determined, the individual uncertainties used are the statistical uncertainties given by the code. For the case where an experimental parameter is used, the individual uncertainty on the lifetime becomes more difficult to determine because no uncertainty is given in any of the references where it is quoted. In the cases where an experimental parameter is chosen and not associated with an uncertainty, the uncertainty is assumed to be zero. One such example is the effective delayed neutron fraction, β_{eff}.

CHAPTER 6

RESULTS

6.1 Experimental Analysis Results

6.1.1 Fast System: Godiva IV Experimental Results

For the Godiva IV experiments, both pulsed neutron measurements and Rossi-α measurements are completed. Godiva IV is well characterized, so the baseline reactivity can be determined by removing known amounts of control rod from the system. Additionally, a comparison to Monte Carlo simulations could be included as a secondary tool.

Unfortunately, the scoping experiment indicates that the ^{3}He detection system is not nearly fast enough to capture the prompt neutron decay behavior. Measurements for this type of system will require a detection system with dead-time on the order of tenths of a microsecond while the ^{3}He setup employed has a dead-time of 12-17 microseconds.

Although the planned measurements did not take place, the α-eigenvalue for Godiva IV has been previously measured as $-8.5 \times 10^{-5} s^{-1}$. This can be used to show how much harder the neutron spectrum of Godiva IV is when compared to the Polyethylene Class Foils.

6.1.2 Thermal System: Polyethylene Class Foils Experimental Results

For the Polyethylene Class Foils experiments, the Rossi-α method is used to determine the prompt neutron decay constant. This method is used to facilitate overnight measurements on the systems with low multiplication. The baseline reactivity for the Polyethylene Class Foils is determined using Monte Carlo simulations.

The α-eigenvalue determined for the Polyethylene Class Foils Experiment is $-199.4 \pm$

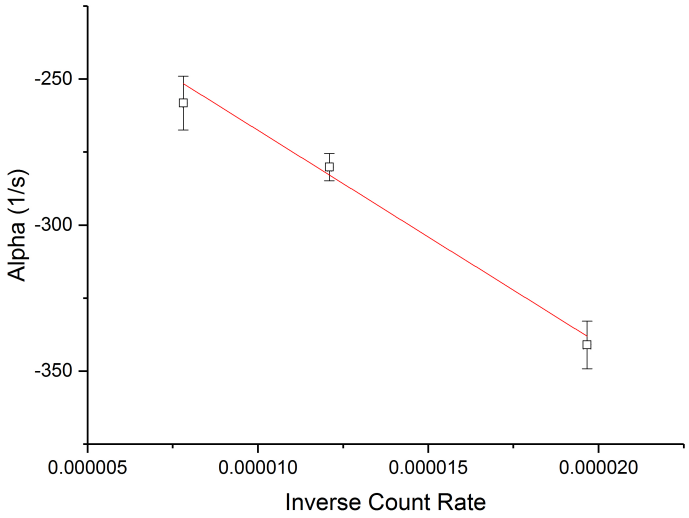

Figure 6.1: Alpha versus Inverse Count Rate Plot used to Determine the Value of the α-eigenvalue for the Polyethylene Class Foils Experiment.

Table 6.1: Average α and inverse count-rate as a function of separation for the 16 foil configuration of the Polyethylene Class Foils Experiment as measured during experimentation.

Mils from Critical	**Inverse CR (s/count)**	$\boldsymbol{\alpha}$ **(s^{-1})**
34	7.809E-6	-258.2
63	1.209E-5	-280.1
94	1.967E-5	-341.0

4.4 s^{-1}. This result is obtained based on measurements made while increasing the separation of the critical configuration, 16 foils, using the Planet critical assembly. The α-eigenvalue is derived based on fitting a line to a plot of α versus the inverse count rate as discussed in Chapter 2. The y-intercept of this linear fit is the α-eigenvalue. For the Polyethylene Class Foils, this result is shown in Fig. 6.1 using data from Table 6.1. The raw experimental data used to construct Table 6.1 is included in Appendix A. The statistical uncertainty quoted on the measurement is obtained using the LINEST function in Excel. Typically, a direct measurement of α for the delayed critical system would also be taken, but the detection system was saturated at delayed critical.

Table 6.2: Experimentally measured results for α on the Polyethylene Class Foils Experiment, and subsequent conversions to reactivity.

# of Units	$\boldsymbol{\alpha}$ **(s^{-1})**	$\boldsymbol{\sigma_\alpha}$ **(s^{-1})**	$\boldsymbol{\rho}$ **(\$)**	$\boldsymbol{\sigma_\rho}$ **(\$)**	$k_{effective}$	$\boldsymbol{\sigma_k}$
15	-340.4	5.3	-0.71	0.05	0.994	3.8E-4
14	-745.8	6.3	-2.74	0.09	0.977	7.2E-4
13	-1253.2	10.5	-5.28	0.15	0.957	1.3E-3
12	-1759.9	21.9	-7.83	0.22	0.938	1.7E-3
11	-2352.2	15.2	-10.80	0.27	0.916	1.9E-3
10	-3063.1	35.5	-14.36	0.38	0.891	2.6E-3
5	-6830.7	140.5	-33.26	1.03	0.780	5.3E-3

Once the α-eigenvalue is defined, subsequent subcritical values of α are measured. Incremental reactivity changes are made to the Polyethylene Class Foils by reducing the total number of units/foils in a given configuration. Measurements are completed on configurations of 5, 10, 11, 12, 13, and 15 units. More measurements were not taken due to time constraints. The data obtained is expected to show both the region of linearity between α and reactivity, and show non-linearity. The data from the measurements performed is compiled in Table 6.2. The raw data used to construct Table 6.2 is included in Appendix B.

6.2 Systematic Uncertainty Results

Several parameters are identified in Chapter 5 which are expected to have the greatest influence on the uncertainty of the measurement. These parameters are detector position, HEU mass, polyethylene plate mass, polyethylene plate dimensions, and the axial air gaps. The sensitivity of the system to each parameter is examined using simulations. In some cases, the sensitivity values are taken from a benchmark from the criticality handbook evaluation HEU-MET-THERM-001 [70].

To support this assumption, a sensitivity study is repeated on the most sensitive parameter, HEU mass, to prove that this assumption is valid. These simulations were performed on the 15 foil case of the Polyethylene Class Foils Experiment. The uncertainty in k_{eff} due to the same change in HEU mass is compared. HEU-MET-THEM-001 obtained ± 0.0053

uncertainty in k_{eff} while the simulations obtained ± 0.0055 which indicates the sensitivities obtained using the benchmark give an adequate representation of the uncertainty in the parameter.

Another assumption made during the systematic uncertainty analysis is that the systematic uncertainty is equal between each configuration. To verify this assumption, additional simulations are performed on one parameter and compared between the largest and smallest cases, 15 and 5 foils, respectively. The uncertainty in HEU mass was compared between these two configurations. The 15 foil case has an uncertainty in k_{eff} of ± 0.0055 while the 5 foil case has an uncertainty of ± 0.0050. So it is assumed that using the uncertainty values from the 15 foil cases would be adequate when discussing all cases in this work.

The contribution to k_{eff} due to each source of uncertainty is examined using MCNP simulations. The results of these simulations are listed in Table 6.3. All of the sources are assumed to be independent and therefore quadratically combined to give a total systematic uncertainty of each measurement. The total systematic uncertainty is ± 0.0060 on k_{eff}. For these measurements, it is often more interesting to examine the uncertainty of α rather than of k_{eff}. This can be completed by uncertainty propagation as discussed in Chapter 5. The question becomes, "Is the uncertainty on k_{eff} significantly different than the uncertainty on α?". To answer this, a simulation is performed using the simulated experiment method examining one parameter. The parameter examined was the detector position. The value of uncertainty on the detector positioning propagated from the k_{eff} simulations is compared to a uncertainty quantification performed directly on α created using the simulated experiment method. The propagated uncertainty on α determined by k_{eff} simulations is $\pm 28.2\ s^{-1}$, and the uncertainty on α determined using the simulated experiment method is $\pm 35.6\ s^{-1}$. The values give similar order of magnitude for the uncertainty. Because calculating k_{eff} is less time intensive, the uncertainty values for α are calculated based on criticality eigenvalue simulations (k_{eff}).. The total uncertainty of ± 0.0060 translates to a ± 0.71\$ uncertainty in reactivity and a $\pm 141.3\ s^{-1}$ uncertainty in α.

Combining the statistical and systematic uncertainty to the experimental data in Table 6.2 generates the data in Table 6.4. The uncertainty bounds on the first couple of measurements are a large percentage of the measured value, but this is mostly an impact of the

Table 6.3: Systematic uncertainty values for parameters of interest produced from calculations and taken from HEU-MET-THEM-001 [70].

Source of Uncertainty	**Parameter Variation in Calculation**	**Calculated Effect of Variation**	**Standard Uncertainty of Parameter**	**Standard Uncertainty in Δk_{eff}**
Detector Position	0.393 in	$\pm$0.0012	0.393 in	$\pm$0.0012
HEU Mass	0.5291 g/cm^3	$\pm$ 0.0055	0.5291 g/cm^3	$\pm$ 0.0055
Poly Plate Mass	$\pm$ 0.00125 g/cm^3	$\pm$ 0.0014	0.00042 g/cm^3	$\pm$ 0.0004
Poly Plate Dim.	0.1 in	$\pm$ 0.0015	$0.01/\sqrt{3}$	$\pm$ 0.00009
Axial Air Gap	0.002 in	$\pm$ 0.0036	$0.002/\sqrt{3}$ in	$\pm$ 0.0021
Total Uncertainty	Combined Total: $\pm$ 0.0060			

Table 6.4: Experimentally measured results for α on the Polyethylene Class Foils Experiment, and subsequent conversions to reactivity.

# of Units	$\boldsymbol{\alpha}$ **(s^{-1})**	$\boldsymbol{\sigma_\alpha}$ **(s^{-1})**	$\boldsymbol{\rho}$ **(\$)**	$\boldsymbol{\sigma_\rho}$ **(\$)**	$k_{effective}$	$\boldsymbol{\sigma_k}$
15	-340.4	141.4	-0.71	0.71	0.994	6.0E-3
14	-745.8	141.4	-2.74	0.72	0.979	6.0E-3
13	-1253.2	141.7	-5.28	0.73	0.959	6.1E-3
12	-1759.9	143.0	-7.83	0.74	0.941	6.2E-3
11	-2352.2	142.1	-10.80	0.76	0.920	6.3E-3
10	-3063.1	145.7	-14.36	0.81	0.897	6.5E-3
5	-6830.7	199.3	-33.26	1.25	0.790	8.0E-3

systematic uncertainty in the measurements. These measurements could be improved by reducing uncertainty in the parameters determined to be sensitive during the simulations. For instance, the systematic uncertainty could be reduced if the mass of the foils were to be measured with a smaller uncertainty. Or if the detector positions in the plate were measured more accurately that would reduce the contribution from detector position.

6.3 Computational Analysis Results

The computations are performed on both a fast and a thermal HEU system. For the fast system, only the results for the definition of α method are presented. This will be addressed

in the results. For the thermal system, both methods are compared.

6.3.1 Fast System: Godiva IV Simulation Results

Using the first method described in Chapter 4, a computational study is completed to determine the value of the prompt neutron decay constant for various reactivities of the Godiva IV assembly. This study is completed using MCNP decks of the assembly in different configurations. Table C.1 in Appendix C includes the prompt neutron decay constant data determined by the MCNP simulations described in Chapter 4.

The reactivity for each position of control rod 1 is given in Table C.2. For each configuration in this table and further tables in this section, the position of each element is given along with the k_{eff} of the configuration. The reactivity in terms of dollars and cents is normalized to a known critical configuration and assumes $\beta_{eff} = 0.0065$. The reactivity for each position of control rod 2 is given in Table C.3. The reactivity for each position of the safety block is given in Table C.4.

The prompt multiplication factor and lifetime for each configuration is also calculated. The prompt multiplication factor and lifetime for the control rod 1 configurations are given in Table C.5. The prompt multiplication factor and lifetime for the control rod 2 configurations are given in Table C.6. The prompt multiplication factor and lifetime for the safety block configurations are given in Table C.7.

6.3.2 Thermal System: Polyethylene Class Foils Simulation Results

For the Polyethylene Class Foils, three different sets of calculations are performed. The first set is used to calculate the effective multiplication factor, k_{eff}. Using Eq. 4.1, the reactivity of each configuration is calculated. The effective delayed neutron fraction, β_{eff}, for these calculations is determined to be 0.0085 from both Eq. 4.2 and using the *KOPTS* card in MCNP. The calculational equivalence to delayed critical k_{eff}, k_{DC} is determined using the known excess reactivity to the critical case and determined to be $k_{DC} = 0.9979$. Using the calculations and these parameters, the baseline reactivity for each configuration between 5

Table 6.5: Computational results determined using *KCODE* MCNP simulations of the Polyethylene Class Foils Experiment.

# of Units	$\mathbf{k}_{effective}$	$\boldsymbol{\sigma_k}$	$\boldsymbol{\rho}$ (\$)	$\boldsymbol{\sigma_\rho}$ (\$)	$\boldsymbol{\alpha}$ ($\mathbf{s^{-1}}$)	$\boldsymbol{\sigma_\alpha}$ ($\mathbf{s^{-1}}$)
15	0.993	2.6E-4	-0.54	0.03	-307.7	9.2
14	0.976	2.8E-4	-2.66	0.03	-729.7	17.5
13	0.954	2.7E-4	-5.45	0.03	-1285.9	29.2
12	0.931	2.5E-4	-8.49	0.03	-1891.4	42.3
11	0.905	2.7E-4	-12.08	0.04	-2608.5	58.1
10	0.876	2.6E-4	-16.38	0.04	-3464.7	76.9
9	0.842	2.6E-4	-21.87	0.04	-4559.4	101.0
8	0.802	2.6E-4	-28.78	0.05	-5937.6	131.4
7	0.757	2.7E-4	-37.60	0.06	-7697.5	170.2
6	0.703	2.4E-4	-49.43	0.06	-10054.7	222.2
5	0.642	2.4E-4	-65.48	0.07	-13256.4	292.8

and 15 units is determined and shown in Table 6.5.

The second set of calculations determines the prompt multiplication factor, k_p. These results are used to determine α using the definition of α method discussed in Chapter 4. The other parameter necessary for these calculations is the neutron lifetime, l. The neutron lifetime is back calculated from the α-eigenvalue and its definition shown in Eq. 2.29. This result agrees well with the neutron lifetime given by the *KOPTS* card for the critical system. The neutron lifetime used is $l = 4.26 \times 10^{-5}\ s$. The values of α for each configuration as determined by the definition of α method are shown in Table 6.6. The raw data used to calculate the information in Table 6.6 is included in Appendix B.

The third set of calculations are MCNP fixed source mode calculations which use tallies and the *PTRAC* file to simulate the experiment. These calculations provide results for the simulated experiment method. This method develops and fits a histogram much like the experimental method. The graphs including the fits are included in Appendix D. The simulated experiment computational results for α are shown in Table 6.7.

In all of these tables, the parameter obtained from the simulation is shown in the first column. Subsequent columns are calculated results based on relationships between reactivity parameters.

Table 6.6: Computational results determined using the definition of α method on the Polyethylene Class Foils Experiment.

# of Units	$\mathbf{k}_p$	$\boldsymbol{\sigma_{k_p}}$	$\boldsymbol{\alpha}$ $(\boldsymbol{s^{-}1})$	$\boldsymbol{\sigma_\alpha}$ $(\boldsymbol{s^{-}1})$	$\boldsymbol{\rho}$ (\$)	$\boldsymbol{\sigma_\rho}$ (\$)	$\mathbf{k}_{eff}$	$\boldsymbol{\sigma_{k_{eff}}}$
15	0.985	2.7E-4	-307.2	8.8	-0.54	0.06	0.995	4.7E-4
14	0.968	2.6E-4	-704.4	8.6	-2.53	0.09	0.979	7.3E-4
13	0.945	2.6E-4	-1235.2	8.6	-5.19	0.14	0.958	1.1E-3
12	0.923	2.6E-4	-1758.6	8.6	-7.82	0.20	0.938	1.5E-3
11	0.897	2.6E-4	-2360.5	8.6	-10.84	0.26	0.916	1.9E-3
10	0.868	2.6E-4	-3041.6	8.5	-14.25	0.34	0.892	2.3E-3
9	0.834	2.7E-4	-3842.2	8.7	-18.27	0.43	0.866	2.7E-3
8	0.795	2.5E-4	-4761.8	8.3	-22.88	0.53	0.837	3.1E-3
7	0.750	2.5E-4	-5802.4	8.3	-28.10	0.64	0.807	3.6E-3
6	0.697	2.5E-4	-7067.6	8.1	-34.44	0.78	0.774	4.0E-3
5	0.634	2.4E-4	-8528.6	8.0	-41.77	0.94	0.738	4.4E-3

Table 6.7: Computational results determined using the simulated experiment method on the Polyethylene Class Foils Experiment.

# of Units	$\boldsymbol{\alpha}$ $(\mathbf{s^{-1}})$	$\boldsymbol{\sigma_\alpha}$ $(\mathbf{s^{-1}})$	$\boldsymbol{\rho}$ (\$)	$\boldsymbol{\sigma_\rho}$ (\$)	$\mathbf{k}_{effective}$	$\boldsymbol{\sigma_k}$
15	-417.8	51.1	-1.10	0.26	0.991	2.2E-3
14	-842.2	34.4	-3.22	0.20	0.973	1.6E-3
13	-1483.9	45.3	-6.44	0.28	0.948	2.1E-3
12	-2060.7	50.5	-9.33	0.34	0.926	2.5E-3
11	-2791.1	81.9	-13.00	0.51	0.901	3.5E-3
10	-3753.3	84.7	-17.82	0.59	0.868	3.8E-3
9	-4878.1	112.3	-23.46	0.78	0.834	4.6E-3
8	-6084.0	145.4	-29.51	0.99	0.799	5.4E-3
7	-7283.5	226.4	-35.53	1.39	0.768	7.0E-3
6	-9362.7	199.4	-45.95	1.44	0.719	6.3E-3
5	-10689.6	299.7	-52.61	1.91	0.691	7.8E-3

6.4 Combined Results

This section shows how the measured value of α compares to the reactivity of the system. This combination is aimed at highlighting the deviation from a linear relationship and explanation of underlying phenomena which create the deviation.

6.4.1 Fast System: Godiva IV Combined Results

The data from the *KCODE* simulations is compared to the simulations performed using the definition of α method. This data is shown graphically in Fig. 6.2. This computational study follows expectations based on historic data of other assemblies. The expectation is that the experimental data would follow a similar trend if a faster detection system were employed. The experiment did not provide results for comparison, so the simulated experiment simulations were not completed.

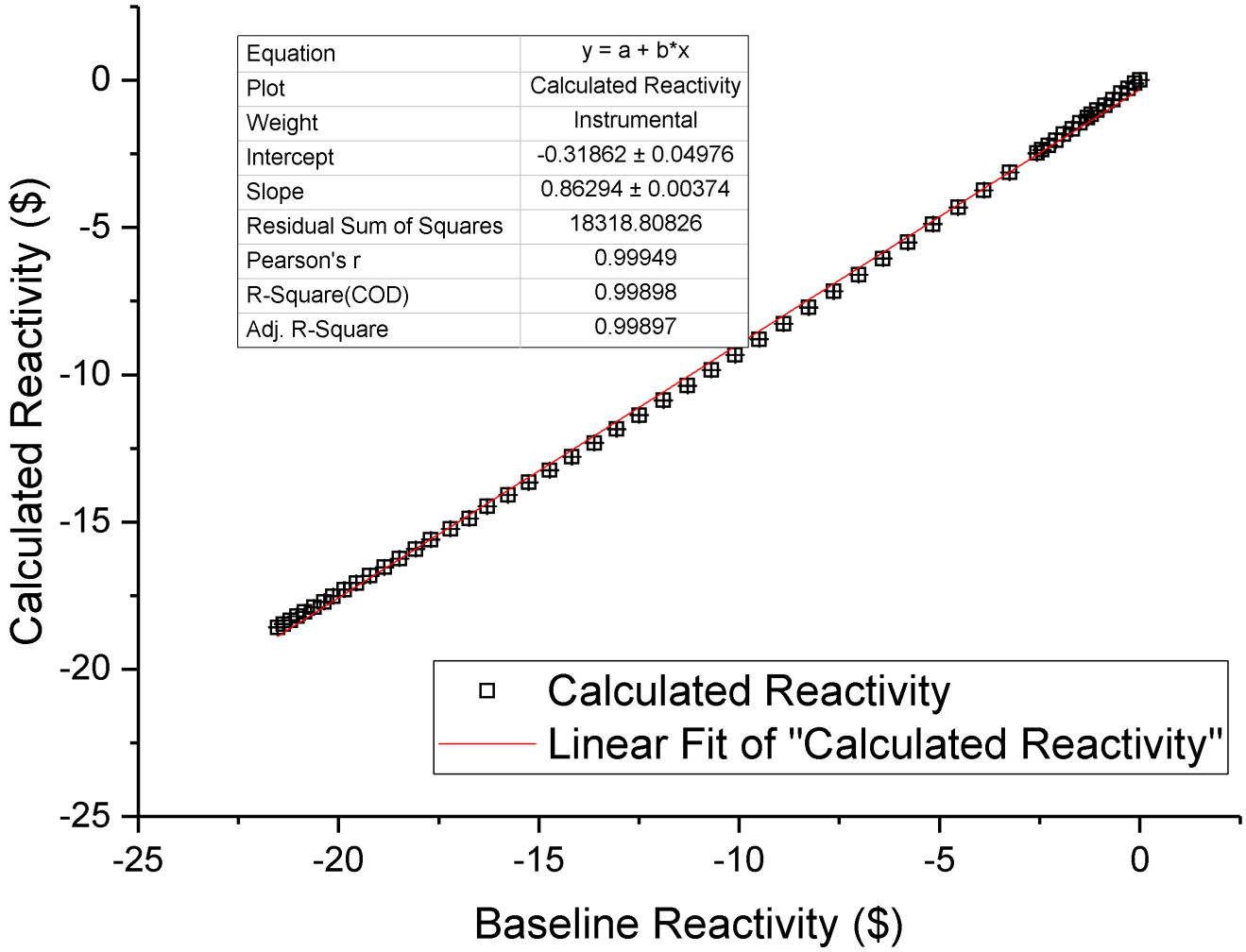

Figure 6.2: The value of the prompt neutron decay constant over the subcritical reactivity range of the Godiva IV assembly.

6.4.2 Thermal System: Polyethylene Class Foils Combined Results

The best method available to calculate the baseline subcritical reactivity for this system is a comparison to *KCODE* MCNP simulations. The O'Dell correlation, shown in Eq. 3.2, could also have been used but does not work well as multiplication decreases. Additionally, MCNP has proven to be quite accurate when calculating the reactivity difference between two configurations. This technique has been well tested, and was used to estimate how many additional fuel units were needed to achieve a critical configuration. This method estimated that 2 additional units would be necessary to achieve the critical configuration of 16 units. So even though there is a bias associated with the model, it is a good assumption that this bias is constant for all models in the experimental series. This may lead to a small deviation of the data comparison from a line with a slope of unity.

As hypothesized, the linear relationship between subcritical reactivity and α is not preserved over the range of experimental configurations. Fig. 6.3 attempts to highlight the inflection point between linear and non-linear transition. In Fig. 6.3, the linear and non-linear portions of the data are plotted using different symbols, and each dataset also has its own color. The linear regions of the data are squares, and the non-linear regions of the data are stars. To better highlight the overlapping data in the linear region of Fig. 6.3, Fig. 6.4 is included.

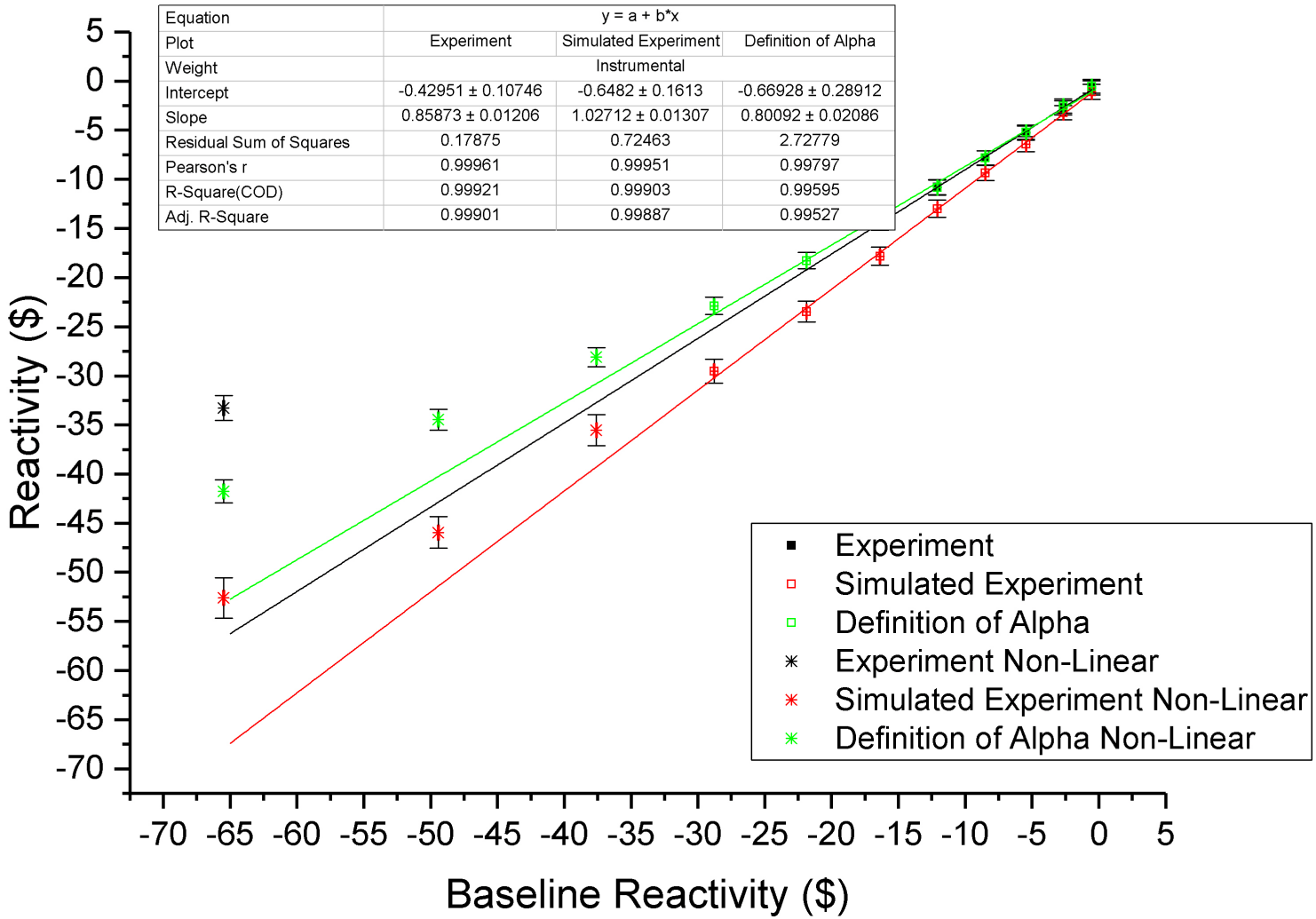

Figure 6.3: Comparison of the reactivity calculated from the measured α to the reactivity calculated by MCNP for different configurations of the Polyethylene Class Foils Experiment.

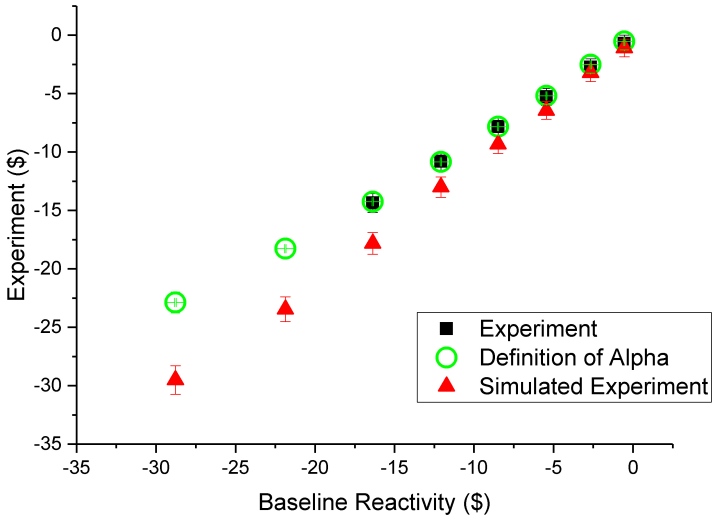

Figure 6.4: The linear region from Fig. 6.3 to better show overlapping data.

For the experimental data, no measurements are taken between 5 and 10 units. The linear to non-linear transition can only be safely assumed to be between $0.64 \leq k_{eff} \leq 0.88$ which corresponds to $-65\$ \leq \rho \leq -16\$$. This behavior is shown by comparing the data in Table 6.8 to the black squares in Fig. 6.3.

The simulation results agreed with this conclusion, and have a higher resolution than the experiment. The subcritical reactivity determined through a linear extrapolation of the α levels off between simulation results for 7 and 8 units for both simulation methods. This corresponds to a k_{eff} below 0.8 and a reactivity of slightly more than $-30\$$. This behavior is seen by comparing the data in Table 6.8 to the red and green symbols in Fig. 6.3.

In an ideal world, the slope of the linear fit in Fig. 6.3 would be unity. The slope differs due to small differences between the calculations and experiment. These deviations are caused by a systematic bias such as air gaps in the stacking, nuclear data, etc.

Confidence in the simulation results is gained because the simulations performed agreed well with the measured data as demonstrated by Fig. 6.5. This allows data gaps to be filled in using simulations, and reinforces their validity. The C/E for the 5 unit case is not shown in Fig. 6.5, and is larger in magnitude when compared to the other calculations.

The deviation from the linear relationship between reactivity and α is caused by a viola-

Table 6.8: Combined results showing the reactivity values determined using all methods discussed in this work for the Polyethylene Class Foils Experiment.

Method	***KCODE***	**Experimental Measurement**	**Simulated Experiment Computation**	**Definition of α Computation**
Equation	**4.1**	**2.32**	**2.32**	**4.4**
# of Units	ρ (\$)			
15	-0.54	-0.71	-1.10	-0.54
14	-2.66	-2.74	-3.22	-2.53
13	-5.45	-5.28	-6.44	-5.19
12	-8.49	-7.83	-9.33	-7.82
11	-12.08	-10.80	-13.00	-10.84
10	-16.38	-14.36	-17.82	-14.25
9	-21.87	N/A	-23.46	-18.27
8	-28.78	N/A	-29.51	-22.88
7	-37.60	N/A	-35.53	-28.10
6	-49.43	N/A	-45.95	-34.44
5	-65.48	-33.26	-52.61	-41.77

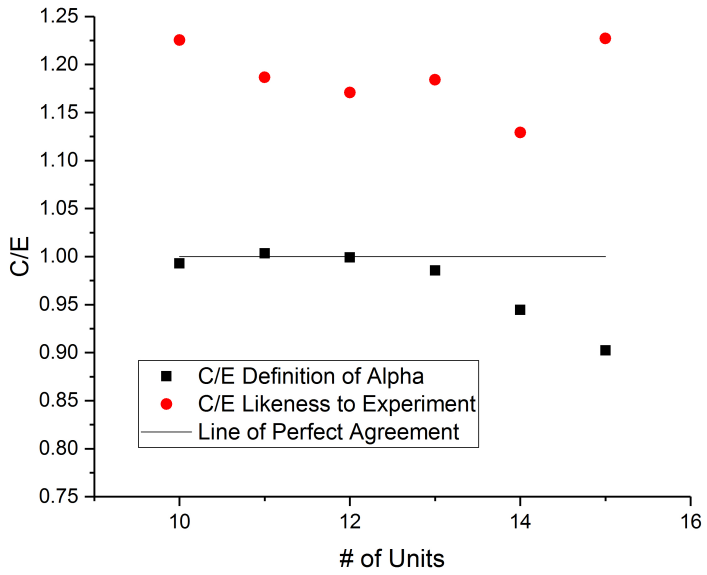

Figure 6.5: C/E comparison between the computed and experimental values of α of the Polyethylene Class Foils Experiment.

tion of the assumptions used to develop the point-reactor kinetics model. The point-reactor kinetics model assumes a fundamental mode because the mathematical derivation assumes the system is a point and the flux has no spatial component. The linear relationship between reactivity and α should also degrade as the system moves away from a fundamental mode distribution. When this happens, the assumption that the neutron flux distribution is independent and separable from the temporal distribution is no longer valid. This invalidates the model of the prompt neutron population which means that the relation described in Eq. 2.8. is no longer valid. If Eq. 2.8 is no longer valid, the linear proportionality between α and reactivity is also no longer valid.

Constant fluctuations in the neutron population exist for all systems, but near critical the time step size to produce a fundamental mode is extremely small. The small time steps allows separate mathematical approximation of the temporal and spacial flux components. In reality, no system has a perfect fundamental mode without averaging over some period of time. The point reactor kinetics framework assumes a single point system, to reduce spatial flux step size and solely examine the temporal flux component.

As the multiplication in the Polyethylene Class Foils decreases, the cosine like neutron population in the fuel will flatten out until the average neutron population is similar to a non-absorbing, non-multiplying media. At low multiplication, each position in the fuel experiences large variations in the flux as a function of time, averaged over longer periods this flux will appear flat and constant. Tallies in the fuel cells are used to produce graphically representations of the neutron flux in the fuel region for several configurations. As the multiplication in the system decreased, the neutron flux in the fuel region flattened. Fig. 6.6 shows a graphical representation of the fuel region neutron flux profiles on either side of the breakdown of the linear relationship between reactivity and α. Fig. 6.6 is created by normalizing the flux values shown in Appendix F so that the profiles have overlapping magnitudes. The neutron flux values for all configurations are These profiles are not the perfect cosine shape that is typically expected from neutron flux; this is mainly attributed to the absorption in the ^{3}He detectors which suppress the flux where the gas is present.

Fig. 6.6 does not show the flux completely flatten immediately as the non-linear relationship between reactivity and α begins, but it is clear from Fig. 6.6 that the trend is toward a

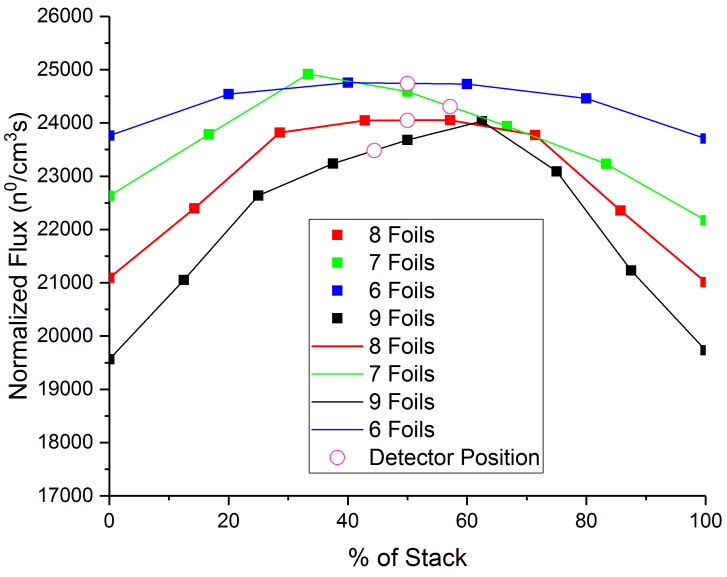

Figure 6.6: The flux profiles for 4 different configurations of the Polyethylene Class Foils Experiment near the linear to non-linear transformation.

linear profile. This supports the idea that a reactivity based threshold is a better indicator of the linear relationship; while, Fig. 6.6 supports the claim that the fundamental mode for the system is deteriorating.

CHAPTER 7

CONCLUSIONS

This work successfully measures prompt neutron decay constants on a series of configurations utilizing a thermal HEU system, and performed preliminary measurements on a fast HEU system. The thermal system consists of about 1 kg of HEU in foil form between polyethylene plates and is typically referred to as the Polyethylene Class Foils. The Polyethylene Class Foils is designed to act similarly to a solution system with an optimized H/^{235}U ratio to minimize critical mass. These measurements span a reactivity range of about -70$ to delayed-critical (0$). The fast system intended for measurements has a measurement range of -25$ to delayed-critical, but the decay constants were too large for the current measurement system.

This work is novel and interesting because it explores the extent to which subcritical measurements of α remain linearly related to the system reactivity for a given configuration. This work presents a threshold of non-linearity at which these type of measurements can be completed in thermal HEU systems.

The threshold of non-linearity for these measurements exists when the system deviates too far from its critical state. For the measurements on the thermal system, it is quite clear that near critical linear proportionality is observed. So the question becomes, "What does near critical mean?". Near critical is an assumption made by point reactor kinetics related to spatial and temporal separability. Near critical is the region where neutron multiplication is sufficient that the spatial population is stable as a function of time. This typically occurs when a system has a high neutron multiplication, and can sustain an average neutron population similar to the mathematically derived fundamental mode. This work took measurements on several well defined thermal HEU systems to better understand the lower limit to the linear relationship between α and reactivity.

Through analysis of this data, the prompt neutron decay constant at each point is de-

termined. Using the linear extrapolation of α as shown in Chapter 2, the experimental subcritical reactivity for each measurement was determined. This reactivity is then compared to a baseline reactivity of the system as given by the MCNP Monte Carlo code.

Through comparison of the simulations and experiments, the prompt neutron decay constant decouples from its linear relation to reactivity for a thermal HEU system near a $k_{eff} = 0.80$. This result is observed in Fig. 6.3 which uses the data values from Table 6.8. Measurements taken of α linearly relate to reactivity for $k_{eff} > 0.80$ because the underlying assumption of separability has not been violated. If this were to translate identically to the fast system, all configurations possible would have provided a linear relationship to reactivity. This can be seen using the simulated results shown in Fig. 6.2.

The monotonic relationship between α and reactivity can be explained by a violation of one of the core assumptions made during the development of the point reactor kinetics model. The assumption that has been violated to create this non-linearity is that the system being measured has a constant fundamental mode. This originates with the assumption used when developing the point reactor kinetics model that the time and space components of the flux are independent and are thus separable. This assumption works well near critical when fission chains are long and the spatial neutron flux distribution is well defined, but as reactivity decreases the spatial neutron flux becomes less stable as a function of time and is no longer independent of the time.

This result can be extended to other systems with some additional work. A computational proof of systems with different properties would make an excellent research project going forward, with supporting experiments being required to validate the results. This would require technological upgrades to the detection systems used in this work as systems with fast neutron populations have much faster time constants, far smaller than the ^{3}He detector dead-time.

CHAPTER 8

FUTURE WORK

In the future it would be interesting to perform an extension of this work to determine if some other relationship to reactivity can be determined at a low multiplication. This work would be similar to work John Orndoff performed at Los Alamos National Laboratory in the 1960s, with the main difference being Orndoff measured α above prompt critical and found its relation to reactivity at the high end of the spectrum whereas this work would examine the low end of the spectrum.

Another interesting spin-off of this work would be to measure the overlap between different multiplication measurement techniques. Namely the methods examined would be the Feynman Variance-to-Mean and the Rossi-α (or pulsed neutron source method). This comparison would make an excellent journal article and seminal work in neutron noise analysis. This work can be completed using data from this thesis along with additional data taken at the same time using a tri-lab (Los Alamos National Laboratory, Lawrence Livermore National Laboratory, and Sandia National Laboratory) designed multiplicity counter called the NoMAD. This paper would examine when the uncertainty on Variance-to-Mean measurements become so large that the method cannot accurately determine the multiplication of a system, and when the Rossi-α (or pulsed neutron source technique) can no longer be related to reactivity (and therefore multiplication). It is our (experts at each technique respectively) expectation that the methods would have significant overlap. The overlap is sufficient that users who typically measure systems with low multiplication tend toward using Variance-to-Mean, and users who typically measure reactor type systems near, at, or above critical will tend to use the Rossi-α technique. This constitutes one of the reasons this work has not previously been documented.

Additionally, a potentially interesting problem to address is the calculation of statisti-

cal uncertainty on a single Rossi-α measurements. This work would require a significant knowledge of statistics to complete, but would have great impact in this field.

CHAPTER 9

REFERENCES

[1] R. E. Uhrig, *Random Noise Techniques in Nuclear Reactor Systems.* New York, NY: Ronald, 1970.

[2] M. M. R. Williams, *Random Processes in Nuclear Reactors.* Elmsford, NY: Maxwell House, 1974.

[3] F. de Hoffman, "Statistical fluctuations in the water boiler and time dispersion of neutrons emitted per fission," Los Alamos National Laboratory, Los Alamos, NM, Tech. Rep. LA-101, June 1944.

[4] J. Orndoff and C. Johnstone, "Time scale measurements by the Rossi method," Los Alamos National Laboratory, Los Alamos, NM, Tech. Rep. LA-744, November 1949.

[5] J.-L. Muñoz-Cobo, R. Perez, and G. Verdu, "Stochastic neutron transport theory: neutron counting statistics in nuclear assemblies," *Nuclear Science and Engineering*, vol. 95, no. 2, pp. 83–105, 1987.

[6] C. P. Baker, "Time scale measurements by the Rossi method," Los Alamos National Laboratory, Los Alamos, NM, Tech. Rep. LA-617, January 1947.

[7] J. D. Orndoff, "Prompt neutron periods of metal critical assemblies," *Nuclear Science and Engineering*, vol. 2, no. 4, pp. 450–460, 1957.

[8] K. M. Kupferberg, "Lifetime of neutrons in reflectors," Los Alamos National Laboratory, Tech. Rep. LA-02743, 1962.

[9] L. Passell, J. Bengston, and D. C. Blair, "The application of pulsed neutron sources to criticality measurements," California. Univ., Livermore. Radiation Lab., Tech. Rep., 1957.

[10] B. Simmons and J. King, "A pulsed neutron technique for reactivity determination," *Nuclear Science and Engineering*, vol. 3, no. 5, pp. 595–608, 1958.

[11] J. Brown, *Measurements of subcritical reactivity using a pulsed-neutron source*, Jan 1964.

[12] E. Garelis and J. L. Russell Jr, "Theory of pulsed neutron source measurements," *Nuclear Science and Engineering*, vol. 16, no. 3, pp. 263–270, 1963.

[13] E. Garelis, "Survey of pulsed neutron source methods for multiplying media," *Pulsed Neutron Research*, vol. II, pp. 3–24, 1965.

[14] P. Meyer, "An experimental study of the (kβ/) pulsed neutron source technique in light water assemblies," *Pulsed Neutron Research*, vol. II, pp. 25–46, 1965.

[15] T. Gozani, P. Demarmels, T. Hürlimann, and H. Winkler, "Modified pulsed source techniques," *Pulsed Neutron Research*, vol. II, pp. 49–62, 1965.

[16] S. Scott, "Reactivity by the pulsed measurement neutron method," *Pulsed Neutron Research*, vol. II, pp. 63–75, 1965.

[17] F. Storrer, "Pulsed neutron experiments on fast and intermediate systems," in *Pulsed Neutron Research. Vol. II. Proceedings of the Symposium on Pulsed Neutron Research*, 1965.

[18] L. Kostic, "Reactivity determination in accelerator driven reactors using reactor noise analysis," *Nuclear Technology and Radiation Protection, XVII (1–2)*, 2002.

[19] I. PÁZSIT, "Neutron fluctuations in traditional and accelerator driven reactors [abstract]," *Fluctuation and Noise Letters*, vol. 1, no. 02, pp. R101–R118, 2001.

[20] S. Degweker, "Reactor noise in accelerator driven systems," *Annals of Nuclear Energy*, vol. 30, no. 2, pp. 223 – 243, 2003.

[21] I. Pázsit and Y. Yamane, "The backward theory of feynman-and rossi-alpha methods with multiple emission sources," *Nuclear science and engineering*, vol. 133, no. 3, pp. 269–281, 1999.

[22] Z. Kuang and I. Pázsit, "The general backward theory of neutron fluctuations in subcritical systems with multiple emission sources," *Il Nuovo Cimento*, vol. 112 A, no. 10, pp. 1067–1092, 1999.

[23] Y. Rugama, J. MUNOZ-COBO, and J. Kloosterman, "Application of the stochastic theory to reactivity measurements in a subcritical assembly driven by a pulsed source," *Submitted to M&C*, 2003.

[24] P. Baeten, "Heuristic derivation of the rossi-alpha formula for a pulsed neutron source," *Annals of Nuclear Energy*, vol. 31, no. 1, pp. 43 – 53, 2004.

[25] Y. Kitamura, K. Taguchi, T. Misawa, I. Pazsit, A. Yamamoto, Y. Yamane, C. Ichihara, H. Nakamura, and H. Oigawa, "Calculation of the stochastic pulsed rossi-alpha formula and its experimental verification," *Progress in Nuclear Energy*, vol. 48, no. 1, pp. 37 – 50, 2006.

[26] Y. Kitamura, I. Pzsit, J. Wright, A. Yamamoto, and Y. Yamane, "Calculation of the pulsed feynman- and rossi-alpha formulae with delayed neutrons," *Annals of Nuclear Energy*, vol. 32, no. 7, pp. 671 – 692, 2005.

[27] G. J. Arnone, G. S. Brunson, and K. L. Coop, "A pulse arrival-time recording module for analyzing neutron multiplicities," in *IEEE Conference on Nuclear Science Symposium and Medical Imaging*, Oct 1992, pp. 369–371 vol.1.

[28] W. L. Myers, G. J. Arnone, and S. G. Melton, "Use of list-mode data acquisition systems for performing benchmark subcritical neutron measurements," Los Alamos National Laboratory, Los Alamos, NM, Tech. Rep. LA-UR-09-00231, June 2009.

[29] Y. Kitamura, M. Matoba, T. Misawa, H. Unesaki, and S. Shiroya, "Reactor noise experiments by using acquisition system for time series data of pulse train," *Journal of nuclear Science and Technology*, vol. 36, no. 8, pp. 653–660, 1999.

[30] C. Jammes, G. Perret, and G. Imel, "First muse-4 experimental results based on time series analysis," in *International Conference PHYSOR*, 2002.

[31] J. Lebrat, R. Soule, and M. Martini, "Experimental investigation of multiplying subcritical media in presence of an external source operating in pulsed or continuous mode: the muse-3 experiment [abstract]," *International Conferecne on Accelerator Driven Transmutation Technologies and Applications 3*, June 1999.

[32] R. Soule, W. Assal, P. Chaussonnet, C. Destouches, C. Domergue, C. Jammes, J. Laurens, J. Lebrat, F. Mellier, G. Perret et al., "Neutronic studies in support of ads: The muse experiments in the masurca facility," *in Nuclear Science and Engineering*, 2003.

[33] A. Gandini and M. Salvatores, "The physics of subcritical multiplying systems," *Journal of Nuclear Science and Technology*, vol. 39, no. 6, pp. 673–686, 2002.

[34] G. Aliberti, G. Rimpault, R. Jacqmin, J. Lebrat, P. Finck, G. Imel, A. Rineiski, P. Ravetto, and J. Sens, "Dynamic measurements and control of an accelerator driven system (ads)," *Physor 2002*, 2002.

[35] N. Messaoudi and E. M. Malambu, "MUSE-4 benchmark calculations using MCNP-4C and different nuclear data libraries," in *Actinide and fission product partitioning and transmutation*, 2003.

[36] A. Billebaud, R. Brissot, D. Heuer, M. Kerveno, C. Le Brun, E. Liatard, J. Loiseaux, O. Meplan, E. Merle, F. Perdu et al., "The muse-4 experiment: prompt reactivity and neutron spectrum measurements," *PHYSOR-2002, Seoul, Korea, Oct*, pp. 7–10, 2002.

[37] D. Villamarín and E. González-Romero, "First ciemat measurements of the muse-4 kinetic response," *PHYSOR-2002, Seoul, Korea, Oct*, pp. 7–10, 2002.

[38] Y. Rugama, J. Kloosterman, and A. Winkelman, "Preliminary measurements of the prompt neutron decay constant in masurca," *Progress in Nuclear Energy*, vol. 43, no. 1, pp. 421–428, 2003.

[39] Y. Rugama, J. Kloosterman, and A. Winkelman, "Experimental results from noise measurements in a source driven subcritical fast reactor," *Progress in Nuclear Energy*, vol. 44, no. 1, pp. 1 – 12, 2004.

[40] P. Baeten and H. A. Abderrahim, "Measurement of kinetic parameters in the fast subcritical core MASURCA," *Nuclear Engineering and Design*, vol. 230, no. 13, pp. 223 – 232, 2004.

[41] V. Grabezhnoi, V. Dulin, G. Mikhailov, and O. Pavlova, "α-rossi determination of deeply subcritical states of multiplying media," *Atomic Energy*, vol. 101, no. 2, pp. 593–601, 2006.

[42] C.-M. Persson, P. Seltborg, A. Åhlander, W. Gudowski, T. Stummer, H. Kiyavitskaya, V. Bournos, Y. Fokov, I. Serafimovich, and S. Chigrinov, "Analysis of reactivity determination methods in the subcritical experiment yalina," *Nuclear Instruments and Methods in Physics Research Section A: Accelerators, Spectrometers, Detectors and Associated Equipment*, vol. 554, no. 1, pp. 374–383, 2005.

[43] P. Saracco, R. Marotta, G. Lomonaco, D. Chersola, and L. Mansani, "A preliminary study of an improved area method, adapted to short time transients in sub-critical systems," in *Proceedings of the International Conference PHYSOR*, 2014.

[44] G. McKenzie, "Modern Rossi-alpha Measurements," 2015.

[45] R. Sanchez, J. Bounds, T. Bredeweg, J. Goda, T. Grove, D. Hayes, K. Jackman, G. McKenzie, and W. Myers, "Reaction rate, fission product yield, and rossi-alpha measurements using a heu metal, copper reflected critical assembly," *JOURNAL OF NUCLEAR SCIENCE AND TECHNOLOGY*, vol. 52, no. 7-8, pp. 1018–1025, 2015.

[46] R. G. Sanchez, T. J. Grove, G. E. McKenzie, J. M. Goda, J. A. Bounds, T. E. Cutler, and D. K. Hayes, "Prompt neutron decay constants in a highly enriched uranium-lead copper reflected system," 2016 ANS Winter Meeting and Nuclear Technology Expo ; 2016-11-06 - 2016-11-10 ; Las Vegas, Nevada, United States, Tech. Rep., 2016, sponsor: USDOE National Nuclear Security Administration (NNSA). Office of Defense Programs (DP) (NA-10).

[47] G. E. McKenzie, J. M. Goda, T. J. Grove, and R. G. Sanchez, "Rossi-alpha for a thermal system: Comparison of experiment and calculation," Tech. Rep., 2017, sponsor: USDOE National Nuclear Security Administration (NNSA).

[48] G. E. McKenzie, J. D. Hutchinson, and W. L. Myers, "Prompt neutron decay constant measurements on a polyethylene-reflected sphere of highly enriched uranium," Winter ANS ; 2017-10-29 - 2017-10-29 ; Washington, District Of Columbia, United States, Tech. Rep., 2017, sponsor: USDOE, LDRD.

[49] W. Uyttenhove, *Reactivity Monitoring of Accelerator-Driven Nuclear Reactor Systems*. TU Delft, Delft University of Technology, 2016.

[50] K. Behringer and P. Wydler, "On the problem of monitoring the neutron parameters of the fast energy amplifier," *Annals of Nuclear Energy*, vol. 26, no. 13, pp. 1131–1157, 1999.

[51] J. L. Alwin and S. P. Monahan, "United States Department of Energy (NCSP) hands-on experimental tranining," Los Alamos National Laboratory, Los Alamos, NM, Tech. Rep. LA-UR-13-21945, 2013.

[52] M. Hayashi, "Comments on" neutron lifetime, fission time, and generation time"," *Nuclear Science and Engineering*, vol. 121, pp. 492–492, 1995.

[53] R. Feynman, "Statistical behavior of neutron chains," Los Alamos National Laboratory, Los Alamos, NM, Tech. Rep. LA-591(DEL), July 1946.

[54] H. C. Paxon and G. E. Hansen, "Critical assemblies and associated measurements," unpublished.

[55] G. R. Keepin, *Physics of Nuclear Kinetics*. Reading, MA: Addison-Wesley, 1965.

[56] G. I. Bell and S. Glasstone, *Nuclear Reactor Theory*. 1970, Oct 1970.

[57] G. Hansen, H. H. Helmick, and J. D. Orndoff, "Neutron counting statistics in basic fast critical assemblies," Los Alamos National Laboratory, Los Alamos, NM, Tech. Rep. LA-UR-85-3859, 1985.

[58] G. Spriggs, G. Hansen, E. Martin, E. Plassman, R. Pederson, J. Schlesser, T. Krawczyk, G. Smolen, and J. Tanner, "Subcritical measurements of the winco slab tank experiment using the source-jerk technique," *ANS Conference Proceedings*, November 1989.

[59] F. de Hoffmann, "Criticality of the water boiler and effective number of delayed neutrons," Los Alamos Scientific Lab., Tech. Rep. LA-183, 1944.

[60] R. P. Feynman, F. De Hoffmann, and R. Serber, "Dispersion of the neutron emission in u-235 fission," *Journal of Nuclear Energy (1954)*, vol. 3, no. 1-2, pp. 64IN9–69IN10, 1956.

[61] T. Wimet, R. White, and R. Wagner, "Godiva IV," University of Califronia and Los Alamos National Laboratory, Los Alamos, NM, Tech. Rep., 1970.

[62] *International Handbook of Evaluated Criticality Safety Benchmark Experiments*, Nuclear Energy Agency Std. HEU-MET-FAST-086, 2014.

[63] T. Cutler, J. Bounds, T. Grove, J. Hutchinson, D. Hayes, and R. Sanchez, "A new critical experiment in support of the nuclear criticality safety class," *ICNC Conference Preceedings*, 2015.

[64] General Electric, *RS-P4-0203-201*, April 2010.

[65] General Electric, *SS-P4-0203-201*, August 2010.

[66] R. O'Dell, "k_{eff} vs. fraction of critical mass," Los Alamos National Laboratory, Tech. Rep., 1996.

[67] J. D. Hutchinson, T. E. Cutler, R. G. Sanchez, M. V. Mitchell, and D. K. Hayes, "Investigation of keff versus fraction of critical mass," *ANS Conference Proceedings*, June 2014.

[68] J. F. Briesmeister, *MCNP - A General Monte Carlo N-Particle Transport Code*, March 2000.

[69] G. E. Hansen, "The Rossi alpha method," Los Alamos National Laboratory, Los Alamos, NM, Tech. Rep. LA-UR-85-4176, August 1985.

[70] *International Handbook of Evaluated Criticality Safety Benchmark Experiments*, Nuclear Energy Agency Std. HEU-MET-THERM-001, 2014.

APPENDIX A

SEPARATION MEASUREMENTS OF α

This appendix includes the prompt neutron population histograms from the determination of the α-eigenvalue. These include three measurements made very near delayed critical which are used to infer the α-eigenvalue. The average value of the parameters determined by the fits is shown in Table A.1.

Table A.1: Parameters obtained from the fits of the experimental data for as a function of separation for the Polyethylene Class Foils.

Mils from Critical	$\boldsymbol{\alpha}$ **(s^{-1})**	**A**	**B**
34	-258.2	4.9E7	5.5E5
63	-280.1	7.6E6	3.6E5
94	-341.0	2.9E6	2.7E5

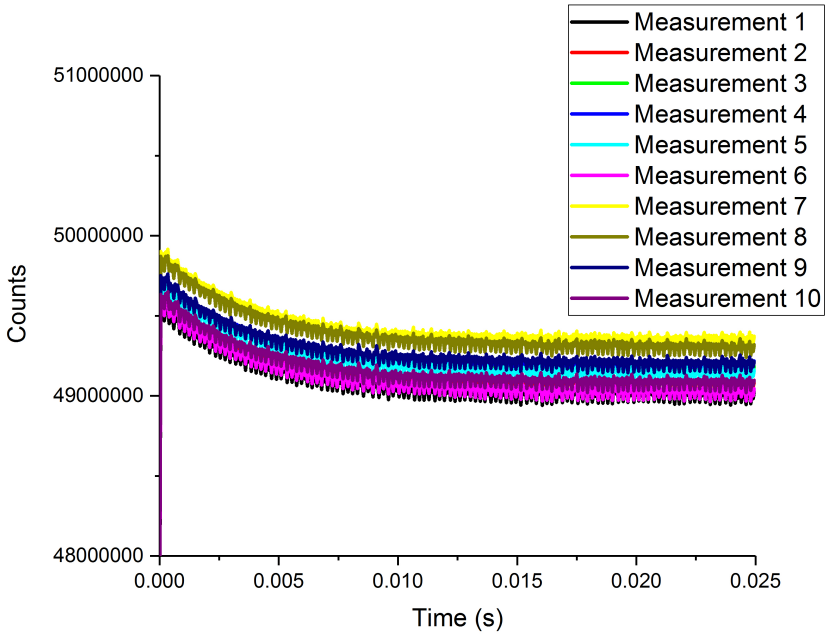

Figure A.1: This figure shows the 10 different prompt neutron population histograms obtained for the configuration 34 mils separated from delayed-critical on the Polyethylene Class Foils.

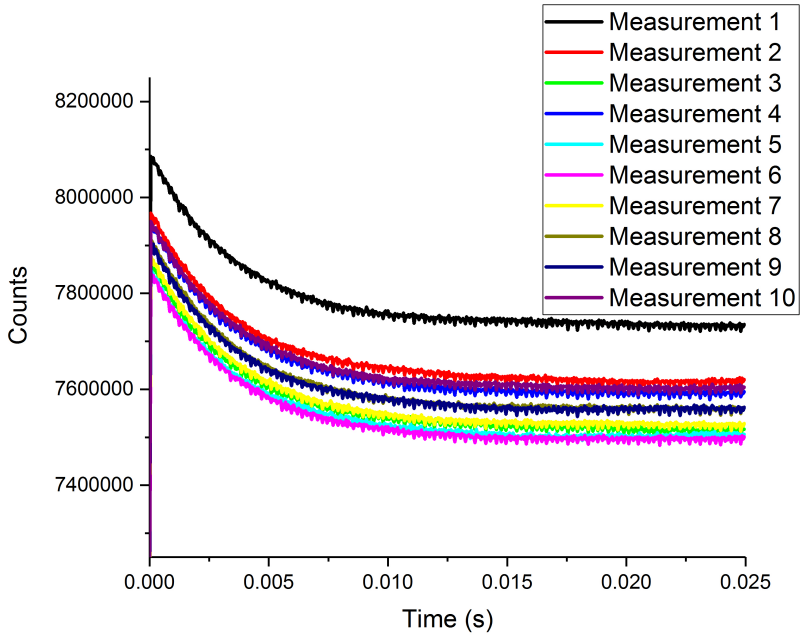

Figure A.2: This figure shows the 10 different prompt neutron population histograms obtained for the configuration 63 mils separated from delayed-critical on the Polyethylene Class Foils.

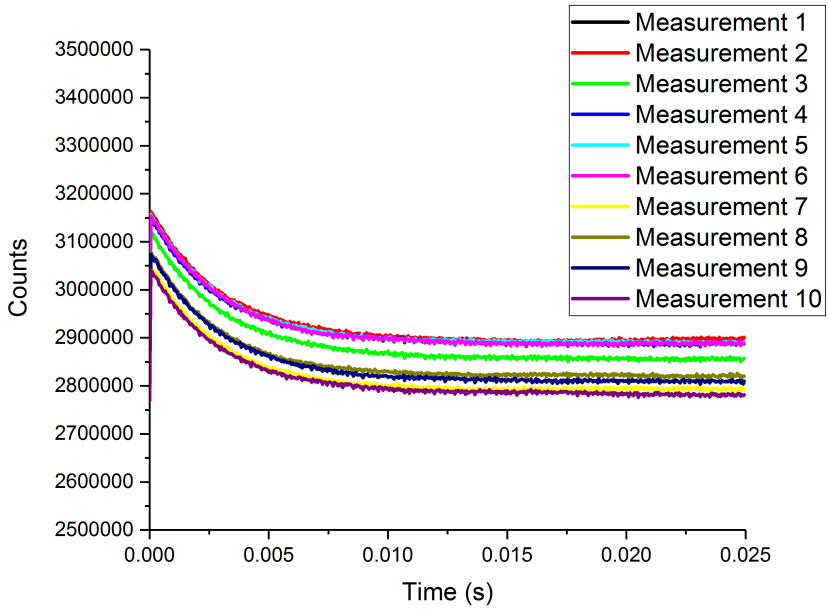

Figure A.3: This figure shows the 10 different prompt neutron population histograms obtained for the configuration 94 mils separated from delayed-critical on the Polyethylene Class Foils.

APPENDIX B

FULLY ASSEMBLED UNIT MEASUREMENTS

This appendix contains the data obtained from the fully assembled Polyethylene Class Foils stacks examined, between 5-15 units.

Table B.1: Parameters obtained from the fits of the experimental data for the Polyethylene Class Foils Experiment.

# of Units	$\boldsymbol{\alpha}$ **(s^{-1})**	**A**	**B**
15	-340.4	3.2E6	1.4E5
14	-745.8	4.1E5	4.8E4
13	-1253.2	2.4E5	3.3E4
12	-1759.9	3.9E5	5.5E4
11	-2352.2	3.0E6	4.4E4
10	-3063.1	2.6E5	3.8E4
5	-6830.7	2.4E4	4.0E3

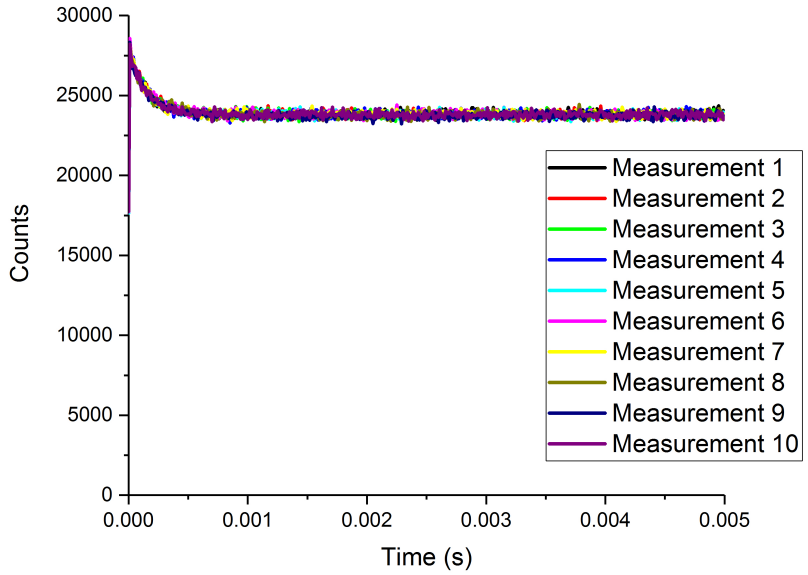

Figure B.1: This figure shows the 10 different prompt neutron population histograms obtained for the Polyethylene Class Foils Experiment configuration with 5 units.

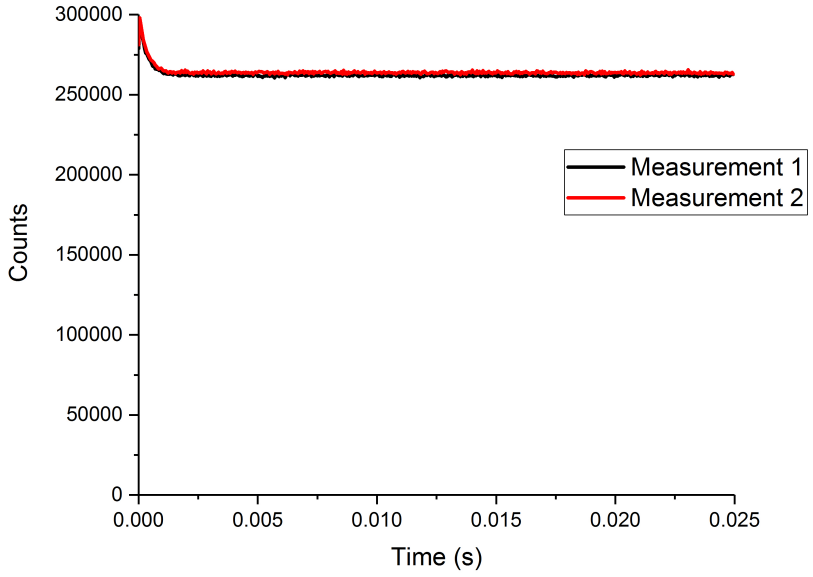

Figure B.2: This figure shows the 2 different prompt neutron population histograms obtained for the Polyethylene Class Foils Experiment configuration with 10 units.

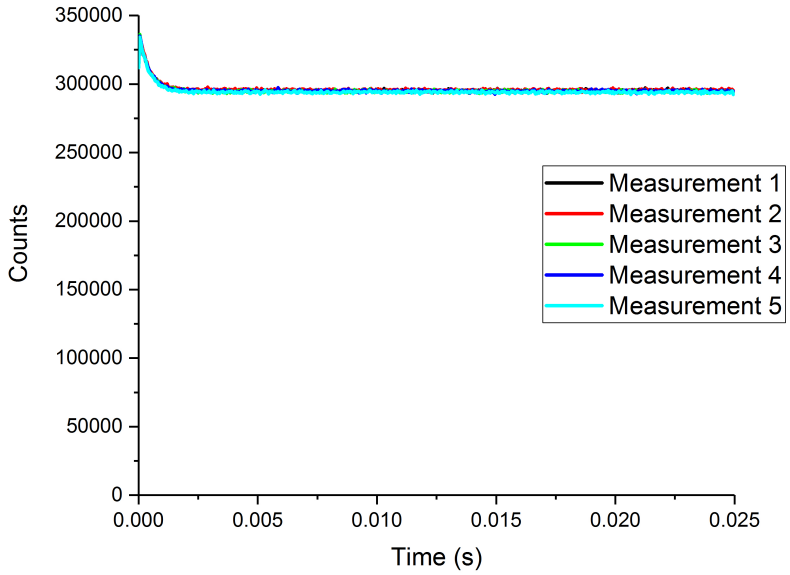

Figure B.3: This figure shows the 5 different prompt neutron population histograms obtained for the Polyethylene Class Foils Experiment configuration with 11 units.

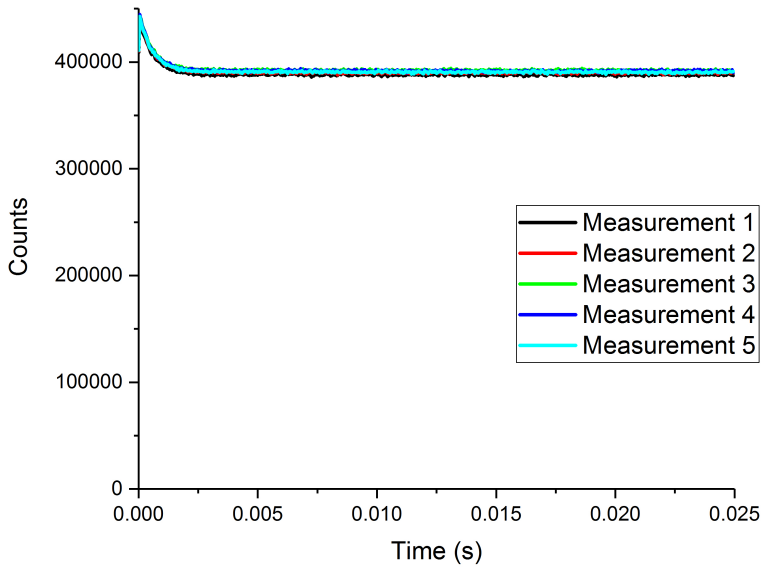

Figure B.4: This figure shows the 5 different prompt neutron population histograms obtained for the Polyethylene Class Foils Experiment configuration with 12 units.

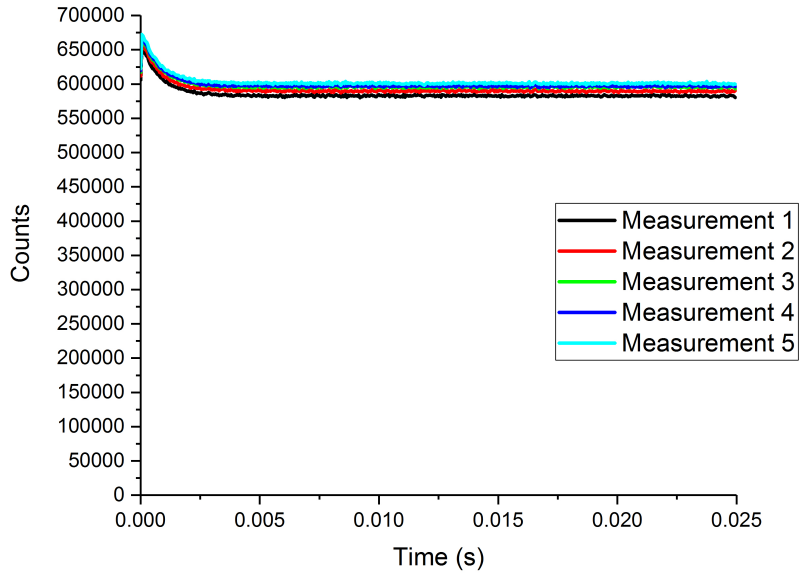

Figure B.5: This figure shows the 5 different prompt neutron population histograms obtained for the Polyethylene Class Foils Experiment configuration with 13 units.

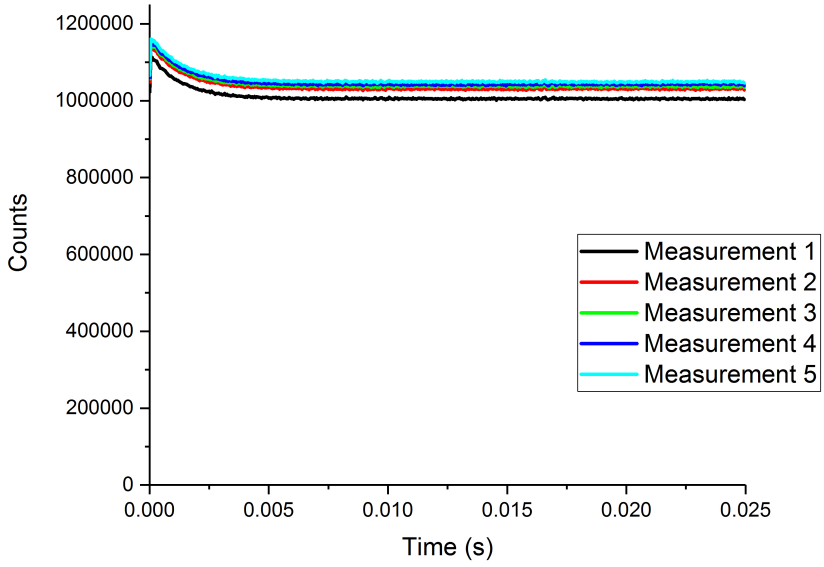

Figure B.6: This figure shows the 5 different prompt neutron population histograms obtained for the Polyethylene Class Foils Experiment configuration with 14 units.

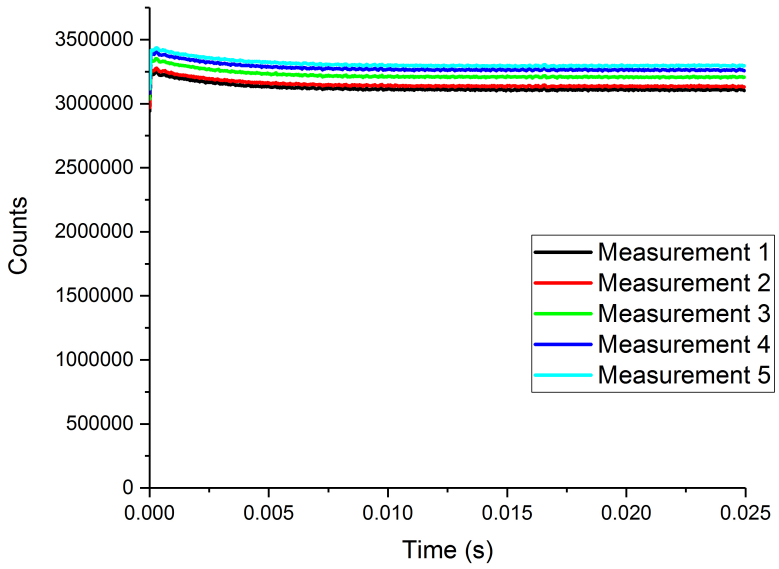

Figure B.7: This figure shows the 5 different prompt neutron population histograms obtained for the Polyethylene Class Foils Experiment configuration with 15 units.

APPENDIX C

COMPUTATIONAL STUDY RAW DATA

This appendix consists of all of the information used in making Fig. 6.2. The data collected here was found using MCNP6 and the method described in Section 4.

Table C.1: Computationally calculated value of the prompt neutron decay constant using both the experimentally determined lifetime and the computationally calculated lifetime.

Reactivity ($)	**Computational**		**Experimental**	
	$\boldsymbol{\alpha}$ $(\boldsymbol{s^{-1}})$	$\boldsymbol{\sigma}$ $(\boldsymbol{s^{-1}})$	$\boldsymbol{\alpha}$ $(\boldsymbol{s^{-1}})$	$\boldsymbol{\sigma}$ $(\boldsymbol{s^{-1}})$
0.00	-930804	11376	-838961	10143
-0.13	-1037100	11367	-937662	10143
-0.29	-1192149	12342	-1080519	11019
-0.46	-1347780	11451	-1220779	10143
-0.67	-1559042	12503	-1409090	11019
-0.87	-1718200	12506	-1561038	11019
-1.06	-1875008	11644	-1706493	10143
-1.21	-2010481	12659	-1825974	11019
-1.30	-2110906	11766	-1920779	10143
-1.49	-2257837	12734	-2059740	11019
-1.68	-2449481	11922	-2236363	10143
-1.90	-2615057	12061	-2388311	10143
-2.09	-2807672	12165	-2567532	10143
-2.28	-2956697	13123	-2710389	11019
-2.44	-3103244	12417	-2838961	10143
-2.57	-3202397	12478	-2933766	10143

Table C.1: Computationally calculated value of the prompt neutron decay constant using both the experimentally determined lifetime and the computationally calculated lifetime.

Reactivity ($)	**Computational**		**Experimental**	
	$\boldsymbol{\alpha}$ $(\boldsymbol{s^{-1}})$	$\boldsymbol{\sigma}$ $(\boldsymbol{s^{-1}})$	$\boldsymbol{\alpha}$ $(\boldsymbol{s^{-1}})$	$\boldsymbol{\sigma}$ $(\boldsymbol{s^{-1}})$
-3.25	-3768067	13702	-3484415	11019
-3.89	-4278464	13297	-3992207	10143
-4.53	-4802372	13765	-4487012	10143
-5.16	-5263890	14337	-4961038	10143
-5.79	-5785279	15566	-5485714	11019
-6.41	-6217050	15446	-5945454	10143
-7.02	-6653509	15994	-6414285	10143
-7.63	-7101776	17259	-6884415	11019
-8.26	-7553947	17280	-7346753	10143
-8.89	-7977915	17777	-7810389	10143
-9.49	-8381892	18371	-8253246	10143
-10.09	-8818973	19026	-8709090	10143
-10.69	-9176801	19728	-9135064	10143
-11.29	-9609239	20368	-9587012	10143
-11.89	-9986518	21475	-10005194	10143
-12.50	-10353120	22602	-10427272	11973
-13.06	-10757806	22393	-10829870	10143
-13.62	-11134804	22889	-11223376	10143
-14.18	-11467534	23461	-11622077	10143
-14.73	-11806131	24567	-12005194	10143
-15.25	-12174547	25190	-12361038	10143
-15.77	-12506958	25403	-12720779	10143
-16.29	-12831338	25989	-13044155	10143
-16.74	-13162194	26647	-13392207	10143
-17.21	-13438458	27206	-13690909	10143

Table C.1: Computationally calculated value of the prompt neutron decay constant using both the experimentally determined lifetime and the computationally calculated lifetime.

Reactivity ($)	**Computational**		**Experimental**	
	$\boldsymbol{\alpha}$ $(\boldsymbol{s^{-1}})$	$\boldsymbol{\sigma}$ $(\boldsymbol{s^{-1}})$	$\boldsymbol{\alpha}$ $(\boldsymbol{s^{-1}})$	$\boldsymbol{\sigma}$ $(\boldsymbol{s^{-1}})$
-17.69	-13701625	27578	-13996103	10143
-18.07	-13973419	28217	-14267532	10143
-18.48	-14270927	29064	-14538961	10143
-18.86	-14606104	29779	-14789610	10143
-19.21	-14866508	30146	-15033766	10143
-19.55	-15020547	30800	-15237662	10143
-19.85	-15324380	30888	-15427272	10143
-20.13	-15523460	31420	-15616883	10143
-20.36	-15714119	31903	-15779220	10143
-20.61	-15872317	32491	-15935064	10143
-20.84	-16109294	32502	-16070129	10143
-21.03	-16220556	32675	-16185714	10143
-21.19	-16354214	32501	-16305194	10143
-21.38	-16403422	33630	-16411688	10143
-21.51	-16589289	33421	-16506493	10143

Table C.2: Reactivity of the various control rod 1 positions.

Control Rod/Safety Block Position			$\boldsymbol{k_{eff}}$		**Reactivity ($)**	
			Value	$\boldsymbol{\sigma}$	***KCODE***	**Adjusted**
DC mod 6 Benchmark			0.99507	6.00E-5	-0.76	0
CR1 500 mils	CR2 DC	SB In	0.99422	6.00E-5	-0.89	-0.13
CR1 1000 mils	CR2 DC	SB In	0.99319	6.00E-5	-1.06	-0.29
CR1 1500 mils	CR2 DC	SB In	0.99207	6.00E-5	-1.23	-0.47
CR1 2000 mils	CR2 DC	SB In	0.99077	6.00E-5	-1.43	-0.67
CR1 2500 mils	CR2 DC	SB In	0.98950	6.00E-5	-1.63	-0.87
CR1 3000 mils	CR2 DC	SB In	0.98826	6.00E-5	-1.83	-1.07
CR1 3500 mils	CR2 DC	SB In	0.98734	5.00E-5	-1.97	-1.21
CR1 Fully Out	CR2 DC	SB In	0.98675	5.00E-5	-2.06	-1.31

Table C.3: Reactivity of the various control rod 2 positions.

Control Rod/Safety Block Position			k_{eff}		**Reactivity ($)**	
			Value	σ	***KCODE***	**Adjusted**
CR1 Out	CR2 500 mils	SB In	0.98555	5.00E-5	-2.25	-1.50
CR1 Out	CR2 1000 mils	SB In	0.98434	6.00E-5	-2.45	-1.69
CR1 Out	CR2 1500 mils	SB In	0.98299	6.00E-5	-2.66	-1.90
CR1 Out	CR2 2000 mils	SB In	0.98177	6.00E-5	-2.86	-2.10
CR1 Out	CR2 2500 mils	SB In	0.98058	6.00E-5	-3.05	-2.29
CR1 Out	CR2 3000 mils	SB In	0.97958	5.00E-5	-3.21	-2.45
CR1 Out	CR2 Fully Out	SB In	0.97882	6.00E-5	-3.33	-2.57

Table C.4: Reactivity of the various safety block positions.

Control Rod/Safety Block Position			k_{eff}		**Reactivity ($)**	
			Value	σ	***KCODE***	**Adjusted**
CR1 Out	CR2 Out	SB 100 mils	0.97458	6.00E-5	-4.01	-3.25
CR1 Out	CR2 Out	SB 200 mils	0.97067	5.00E-5	-4.65	-3.89
CR1 Out	CR2 Out	SB 300 mils	0.96675	5.00E-5	-5.30	-4.53
CR1 Out	CR2 Out	SB 400 mils	0.96294	5.00E-5	-5.93	-5.17
CR1 Out	CR2 Out	SB 500 mils	0.95920	5.00E-5	-6.55	-5.79
CR1 Out	CR2 Out	SB 600 mils	0.95550	5.00E-5	-7.17	-6.41
CR1 Out	CR2 Out	SB 700 mils	0.95189	5.00E-5	-7.78	-7.02
CR1 Out	CR2 Out	SB 800 mils	0.94828	6.00E-5	-8.40	-7.64
CR1 Out	CR2 Out	SB 900 mils	0.94464	5.00E-5	-9.02	-8.27
CR1 Out	CR2 Out	SB 1000 mils	0.94101	5.00E-5	-9.66	-8.89
CR1 Out	CR2 Out	SB 1100 mils	0.93755	5.00E-5	-10.26	-9.50
CR1 Out	CR2 Out	SB 1200 mils	0.93415	5.00E-5	-10.86	-10.10
CR1 Out	CR2 Out	SB 1300 mils	0.93076	5.00E-5	-11.46	-10.70
CR1 Out	CR2 Out	SB 1400 mils	0.92742	5.00E-5	-12.05	-11.29
CR1 Out	CR2 Out	SB 1500 mils	0.92406	5.00E-5	-12.66	-11.90
CR1 Out	CR2 Out	SB 1600 mils	0.92073	5.00E-5	-13.26	-12.50
CR1 Out	CR2 Out	SB 1700 mils	0.91764	5.00E-5	-13.83	-13.06
CR1 Out	CR2 Out	SB 1800 mils	0.91459	5.00E-5	-14.38	-13.62
CR1 Out	CR2 Out	SB 1900 mils	0.91156	5.00E-5	-14.94	-14.18
CR1 Out	CR2 Out	SB 2000 mils	0.90859	5.00E-5	-15.50	-14.73
CR1 Out	CR2 Out	SB 2100 mils	0.90581	5.00E-5	-16.02	-15.26
CR1 Out	CR2 Out	SB 2200 mils	0.90305	5.00E-5	-16.54	-15.77
CR1 Out	CR2 Out	SB 2300 mils	0.90031	5.00E-5	-17.05	-16.29
CR1 Out	CR2 Out	SB 2400 mils	0.89797	5.00E-5	-17.50	-16.73
CR1 Out	CR2 Out	SB 2500 mils	0.89549	5.00E-5	-17.98	-17.21
CR1 Out	CR2 Out	SB 2600 mils	0.89298	5.00E-5	-18.46	-17.70
CR1 Out	CR2 Out	SB 2700 mils	0.89104	5.00E-5	-18.84	-18.07
CR1 Out	CR2 Out	SB 2800 mils	0.88893	5.00E-5	-19.23	-18.48
CR1 Out	CR2 Out	SB 2900 mils	0.88700	5.00E-5	-19.62	-18.86
CR1 Out	CR2 Out	SB 3000 mils	0.88517	5.00E-5	-19.98	-19.22
CR1 Out	CR2 Out	SB 3100 mils	0.88348	5.00E-5	-20.31	-19.55
CR1 Out	CR2 Out	SB 3200 mils	0.88193	5.00E-5	-20.62	-19.85
CR1 Out	CR2 Out	SB 3300 mils	0.88053	5.00E-5	-20.89	-20.13
CR1 Out	CR2 Out	SB 3400 mils	0.87941	5.00E-5	-21.12	-20.36
CR1 Out	CR2 Out	SB 3500 mils	0.87814	5.00E-5	-21.37	-20.61
CR1 Out	CR2 Out	SB 3600 mils	0.87699	5.00E-5	-21.60	-20.84
CR1 Out	CR2 Out	SB 3700 mils	0.87602	5.00E-5	-21.80	-21.03
CR1 Out	CR2 Out	SB 3800 mils	0.87522	5.00E-5	-21.95	-21.19
CR1 Out	CR2 Out	SB 3900 mils	0.87431	5.00E-5	-22.14	-21.38
CR1 Out	CR2 Out	SB 4000 mils	0.87363	5.00E-5	-22.28	-21.51

Table C.5: Prompt multiplication factor and lifetime for various configurations of control rod 1.

Control Rod/Safety Block Position			k_p		**Lifetime (s)**	
			Value	σ	**Value**	σ
DC mod 6 Benchmark			0.98862	5.00E-5	6.940E-9	1.243E-11
CR1 500 mils	CR2 DC	SB In	0.98785	5.00E-5	6.961E-9	1.230E-11
CR1 1000 mils	CR2 DC	SB In	0.98675	6.00E-5	6.978E-9	1.245E-11
CR1 1500 mils	CR2 DC	SB In	0.98568	5.00E-5	6.974E-9	1.240E-11
CR1 2000 mils	CR2 DC	SB In	0.98423	6.00E-5	6.959E-9	1.238E-11
CR1 2500 mils	CR2 DC	SB In	0.98306	6.00E-5	6.995E-9	1.241E-11
CR1 3000 mils	CR2 DC	SB In	0.98194	5.00E-5	7.007E-9	1.261E-11
CR1 3500 mils	CR2 DC	SB In	0.98102	6.00E-5	6.993E-9	1.256E-11
CR1 Fully Out	CR2 DC	SB In	0.98028	5.00E-5	7.006E-9	1.250E-11

Table C.6: Prompt multiplication factor and lifetime for various configurations of control rod 2.

Control Rod/Safety Block Position			k_p		**Lifetime (s)**	
			Value	σ	**Value**	σ
CR1 Out	CR2 500 mils	SB In	0.97921	6.00E-5	7.024E-9	1.254E-11
CR1 Out	CR2 1000 mils	SB In	0.97785	5.00E-5	7.030E-9	1.242E-11
CR1 Out	CR2 1500 mils	SB In	0.97668	5.00E-5	7.032E-9	1.265E-11
CR1 Out	CR2 2000 mils	SB In	0.97531	5.00E-5	7.041E-9	1.253E-11
CR1 Out	CR2 2500 mils	SB In	0.97421	6.00E-5	7.058E-9	1.257E-11
CR1 Out	CR2 3000 mils	SB In	0.97321	5.00E-5	7.044E-9	1.269E-11
CR1 Out	CR2 Fully Out	SB In	0.97248	5.00E-5	7.054E-9	1.268E-11

Table C.7: Prompt multiplication factor and lifetime for various configurations of the safety block.

Control Rod/Safety Block Position			k_p		**Lifetime (s)**	
			Value	σ	**Value**	σ
CR1 Out	CR2 Out	SB 100 mils	0.96825	6.00E-5	7.120E-9	1.278E-11
CR1 Out	CR2 Out	SB 200 mils	0.96433	5.00E-5	7.184E-9	1.286E-11
CR1 Out	CR2 Out	SB 300 mils	0.96052	5.00E-5	7.194E-9	1.268E-11
CR1 Out	CR2 Out	SB 400 mils	0.95687	5.00E-5	7.256E-9	1.306E-11
CR1 Out	CR2 Out	SB 500 mils	0.95284	6.00E-5	7.301E-9	1.307E-11
CR1 Out	CR2 Out	SB 600 mils	0.94930	5.00E-5	7.363E-9	1.330E-11
CR1 Out	CR2 Out	SB 700 mils	0.94569	5.00E-5	7.423E-9	1.344E-11
CR1 Out	CR2 Out	SB 800 mils	0.94206	6.00E-5	7.464E-9	1.365E-11
CR1 Out	CR2 Out	SB 900 mils	0.93850	5.00E-5	7.488E-9	1.366E-11
CR1 Out	CR2 Out	SB 1000 mils	0.93493	5.00E-5	7.538E-9	1.365E-11
CR1 Out	CR2 Out	SB 1100 mils	0.93152	5.00E-5	7.581E-9	1.376E-11
CR1 Out	CR2 Out	SB 1200 mils	0.92801	5.00E-5	7.604E-9	1.381E-11
CR1 Out	CR2 Out	SB 1300 mils	0.92474	5.00E-5	7.664E-9	1.411E-11
CR1 Out	CR2 Out	SB 1400 mils	0.92125	5.00E-5	7.682E-9	1.411E-11
CR1 Out	CR2 Out	SB 1500 mils	0.91803	5.00E-5	7.714E-9	1.463E-11
CR1 Out	CR2 Out	SB 1600 mils	0.91478	7.00E-5	7.755E-9	1.440E-11
CR1 Out	CR2 Out	SB 1700 mils	0.91169	5.00E-5	7.751E-9	1.441E-11
CR1 Out	CR2 Out	SB 1800 mils	0.90866	5.00E-5	7.761E-9	1.433E-11
CR1 Out	CR2 Out	SB 1900 mils	0.90559	5.00E-5	7.803E-9	1.444E-11
CR1 Out	CR2 Out	SB 2000 mils	0.90264	5.00E-5	7.829E-9	1.489E-11
CR1 Out	CR2 Out	SB 2100 mils	0.89990	5.00E-5	7.817E-9	1.485E-11
CR1 Out	CR2 Out	SB 2200 mils	0.89712	5.00E-5	7.831E-9	1.463E-11
CR1 Out	CR2 Out	SB 2300 mils	0.89463	5.00E-5	7.827E-9	1.464E-11
CR1 Out	CR2 Out	SB 2400 mils	0.89195	5.00E-5	7.834E-9	1.471E-11
CR1 Out	CR2 Out	SB 2500 mils	0.88966	5.00E-5	7.844E-9	1.478E-11
CR1 Out	CR2 Out	SB 2600 mils	0.88731	5.00E-5	7.865E-9	1.477E-11
CR1 Out	CR2 Out	SB 2700 mils	0.88522	5.00E-5	7.862E-9	1.486E-11
CR1 Out	CR2 Out	SB 2800 mils	0.88312	5.00E-5	7.844E-9	1.501E-11
CR1 Out	CR2 Out	SB 2900 mils	0.88119	5.00E-5	7.796E-9	1.497E-11
CR1 Out	CR2 Out	SB 3000 mils	0.87931	5.00E-5	7.786E-9	1.489E-11
CR1 Out	CR2 Out	SB 3100 mils	0.87775	5.00E-5	7.811E-9	1.515E-11
CR1 Out	CR2 Out	SB 3200 mils	0.87629	5.00E-5	7.751E-9	1.477E-11
CR1 Out	CR2 Out	SB 3300 mils	0.87483	5.00E-5	7.746E-9	1.485E-11
CR1 Out	CR2 Out	SB 3400 mils	0.87358	5.00E-5	7.319E-9	1.489E-11
CR1 Out	CR2 Out	SB 3500 mils	0.87238	5.00E-5	7.730E-9	1.504E-11
CR1 Out	CR2 Out	SB 3600 mils	0.87134	5.00E-5	7.681E-9	1.472E-11
CR1 Out	CR2 Out	SB 3700 mils	0.87044	5.00E-5	7.683E-9	1.471E-11
CR1 Out	CR2 Out	SB 3800 mils	0.86953	5.00E-5	7.676E-9	1.449E-11
CR1 Out	CR2 Out	SB 3900 mils	0.86870	5.00E-5	7.703E-9	1.506E-11
CR1 Out	CR2 Out	SB 4000 mils	0.86797	5.00E-5	7.661E-9	1.470E-11

APPENDIX D

COMPUTATIONAL DATA FITS

This appendix includes the plots of the data fits used to produce Table 6.7. A fit for each configuration, 5-15 units, are shown in this appendix. All of the parameters determined from the fit are shown in Table D.1.

Table D.1: Parameters obtained from the fits of the simulated experiment computations for the Polyethylene Class Foils.

# of Units	α (s^{-1})	A	B
15	-417.8	1.6E7	5.2E7
14	-842.2	5.7E6	2.6E7
13	-1483.9	3.2E6	1.1E7
12	-2060.7	2.1E6	6.8E6
11	-2791.1	1.7E6	5.1E6
10	-3753.3	1.9E6	4.6E6
9	-4878.1	1.6E6	3.7E6
8	-6084.0	1.2E6	2.9E6
7	-7283.5	1.4E6	3.5E6
6	-9362.7	1.9E6	5.8E6
5	-10689.6	2.0E6	6.1E6

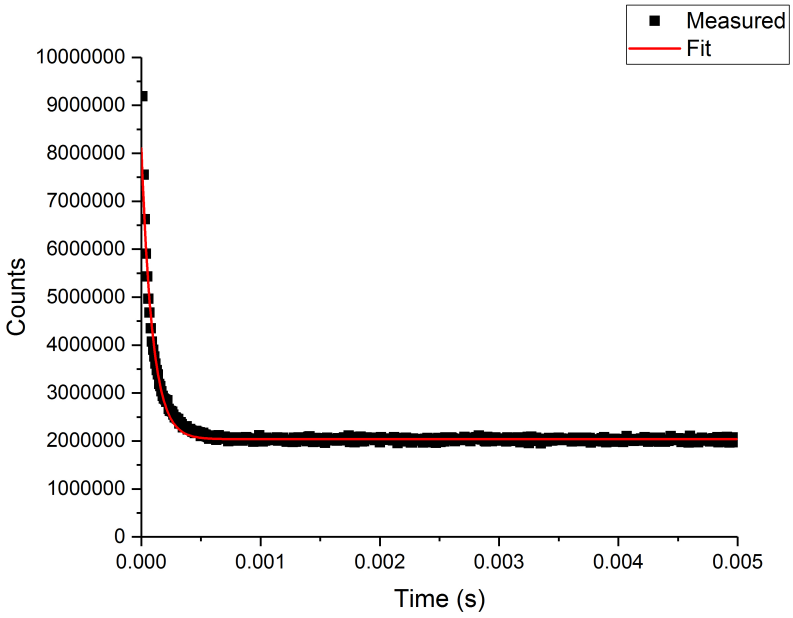

Figure D.1: Rossi-α histogram and fit for the Polyethylene Class Foils 5 unit calculation using the simulated experiment method.

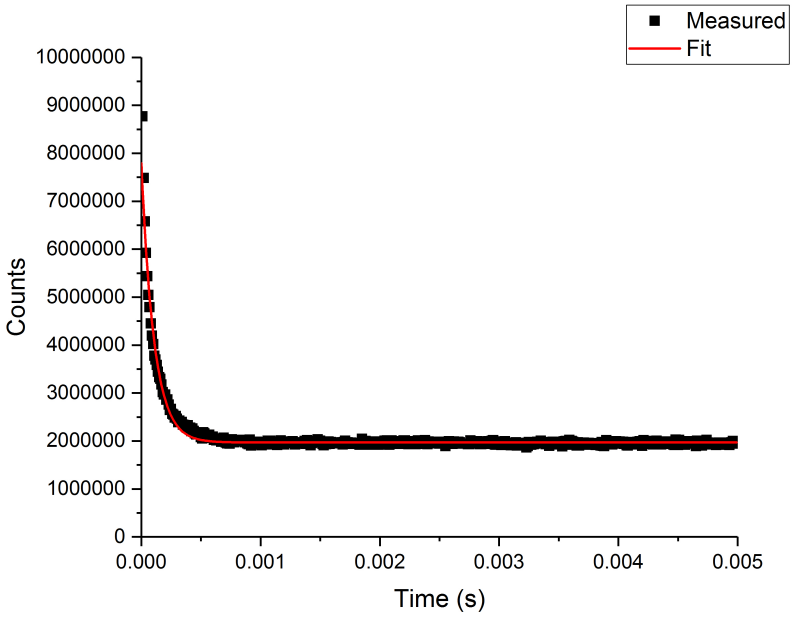

Figure D.2: Rossi-α histogram and fit for the Polyethylene Class Foils 6 unit calculation using the simulated experiment method.

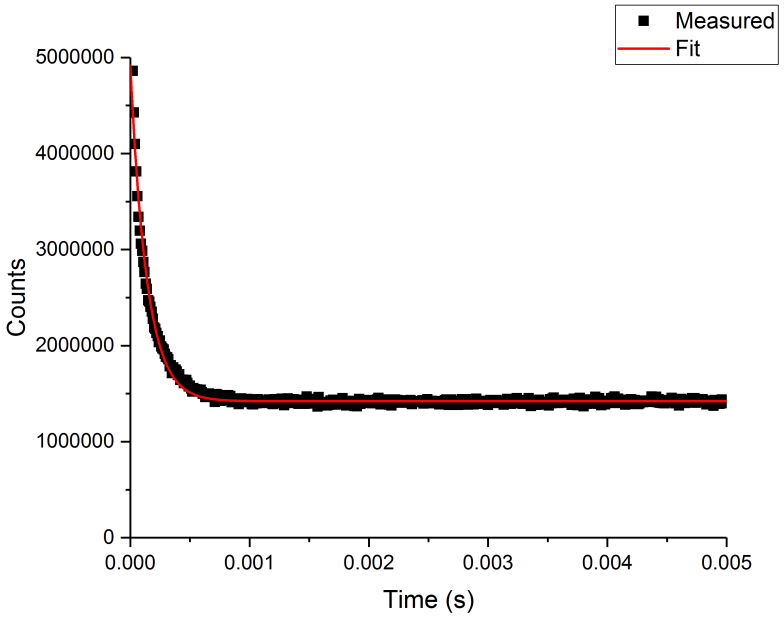

Figure D.3: Rossi-α histogram and fit for the Polyethylene Class Foils 7 unit calculation using the simulated experiment method.

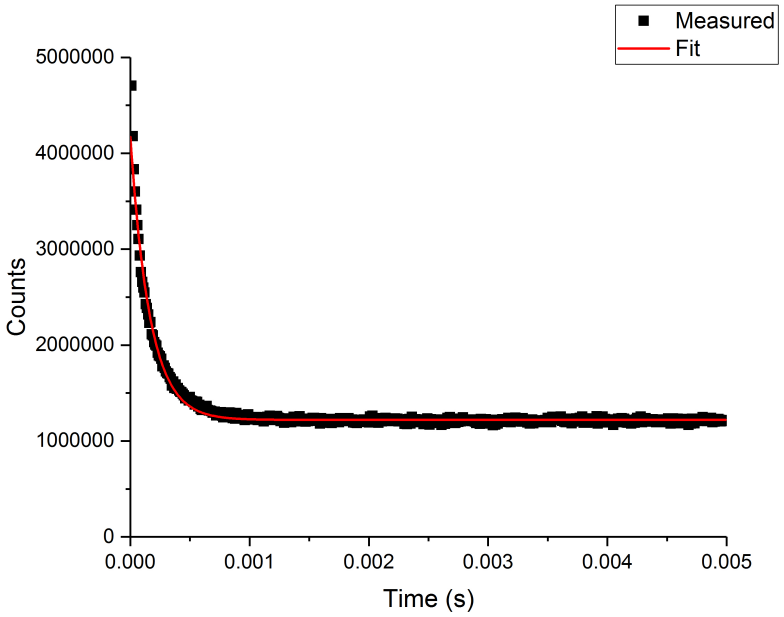

Figure D.4: Rossi-α histogram and fit for the Polyethylene Class Foils 8 unit calculation using the simulated experiment method.

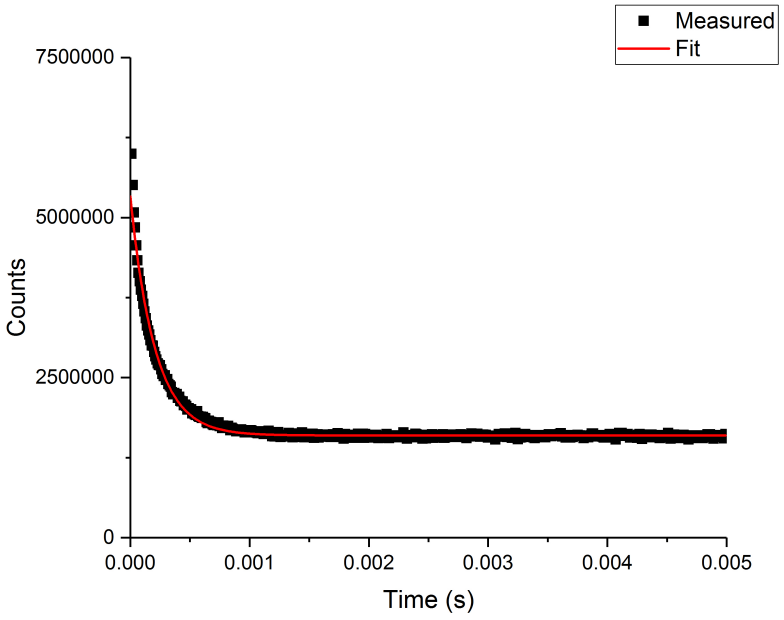

Figure D.5: Rossi-α histogram and fit for the Polyethylene Class Foils 9 unit calculation using the simulated experiment method.

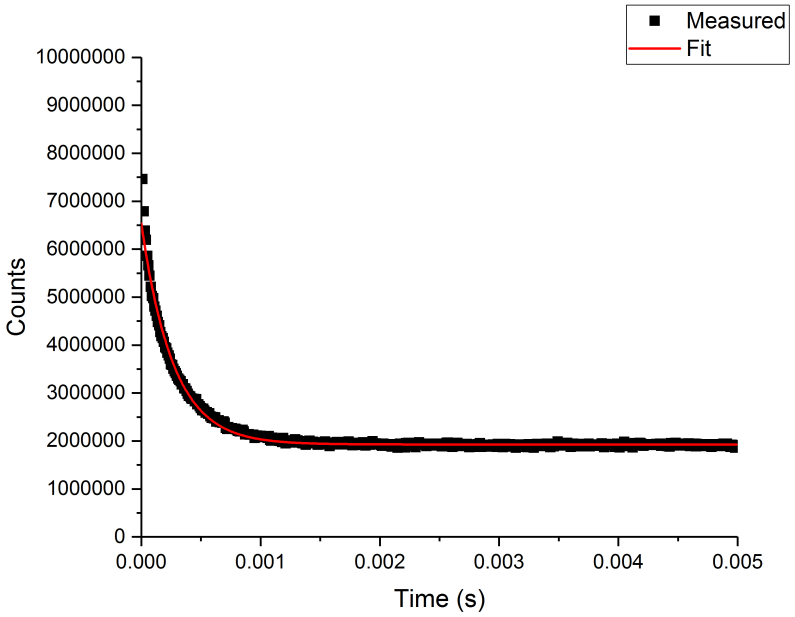

Figure D.6: Rossi-α histogram and fit for the Polyethylene Class Foils 10 unit calculation using the simulated experiment method.

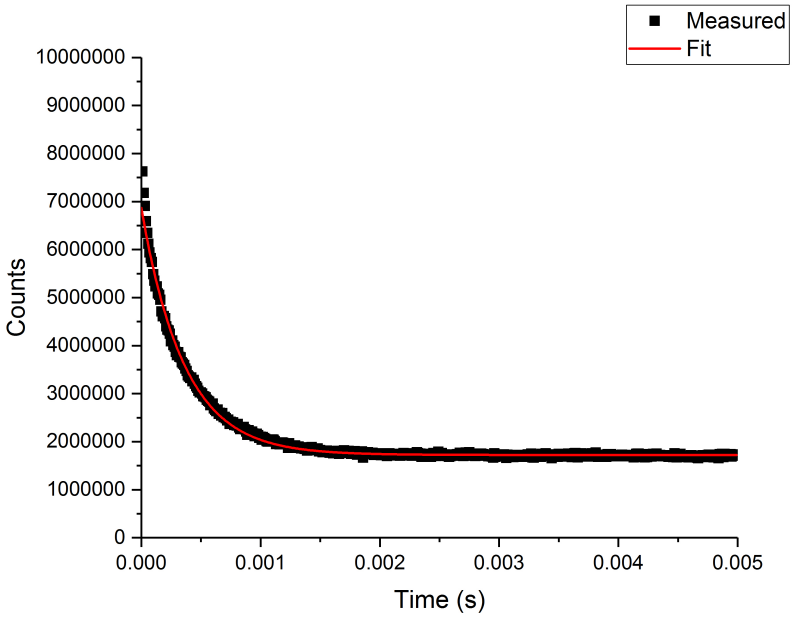

Figure D.7: Rossi-α histogram and fit for the Polyethylene Class Foils 11 unit calculation using the simulated experiment method.

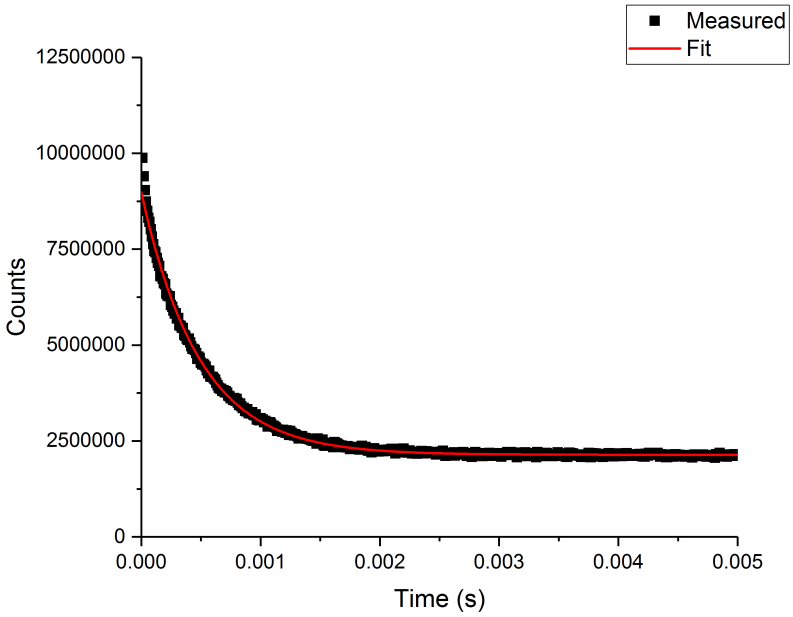

Figure D.8: Rossi-α histogram and fit for the Polyethylene Class Foils 12 unit calculation using the simulated experiment method.

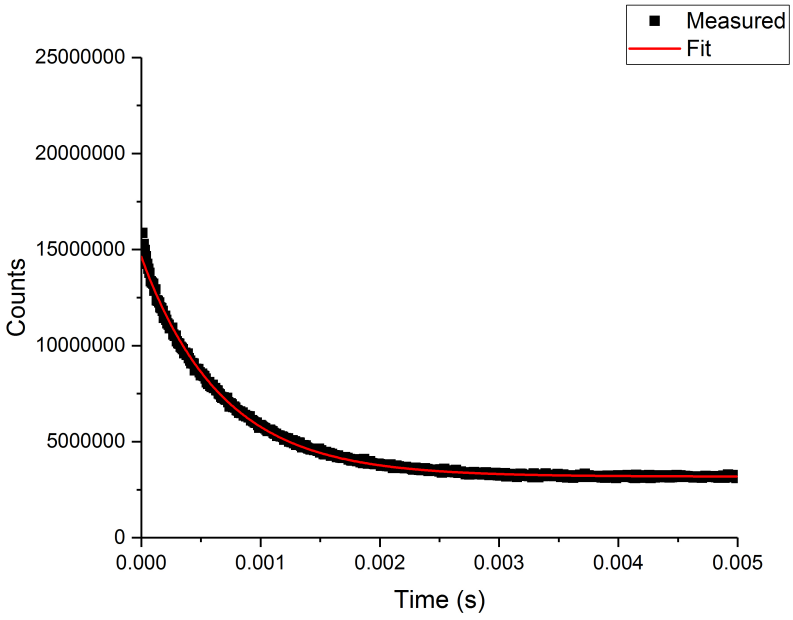

Figure D.9: Rossi-α histogram and fit for the Polyethylene Class Foils 13 unit calculation using the simulated experiment method.

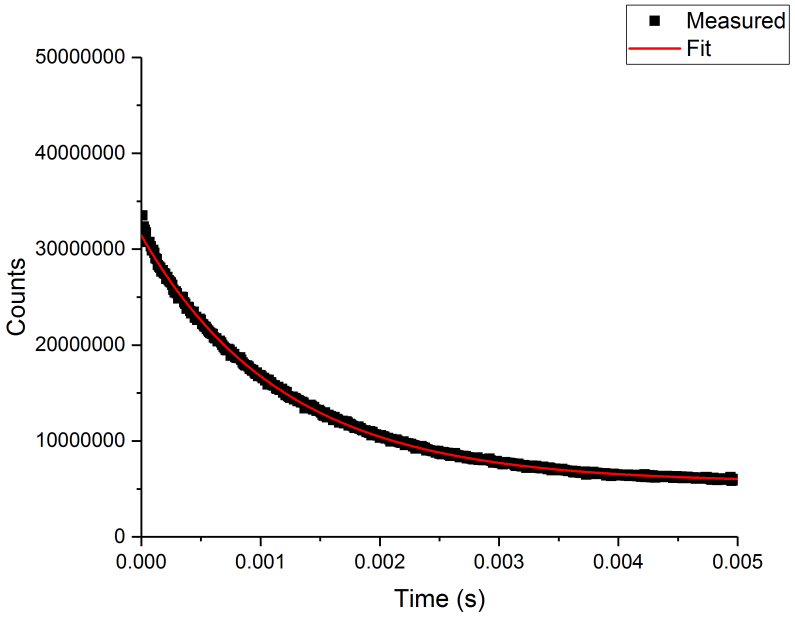

Figure D.10: Rossi-α histogram and fit for the Polyethylene Class Foils 14 unit calculation using the simulated experiment method.

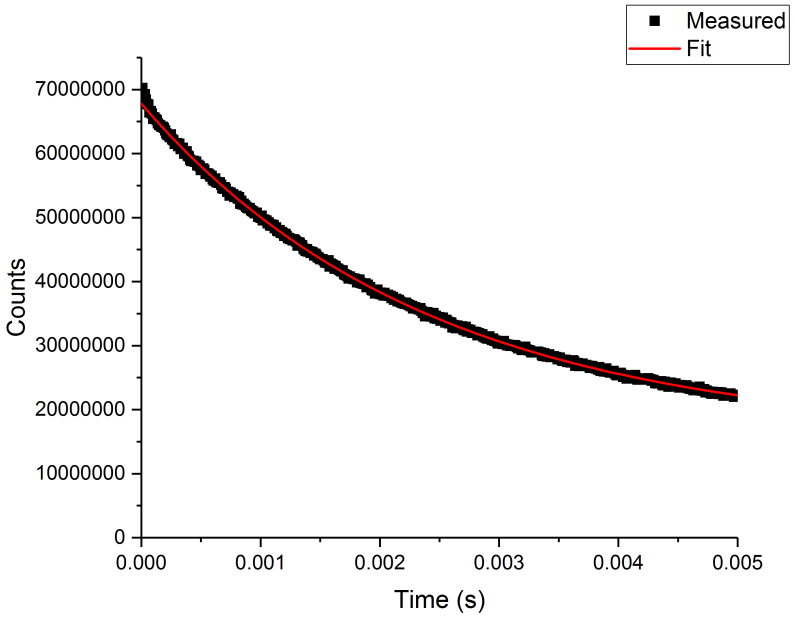

Figure D.11: Rossi-α histogram and fit for the Polyethylene Class Foils 15 unit calculation using the simulated experiment method.

APPENDIX E

UNCERTAINTY PROPAGATION

In Chapter 5, uncertainty propagation for several quantities using the method shown in Eq. 5.2 is used. This section will show the propagation for all quantities reported in this work. The main parameters listed in this work are α, k_{eff}, and ρ. As the propagation for α is already defined in Chapter 5, only the derivations for k_{eff} and ρ are listed in this appendix. The uncertainty propagations for k_{eff} and ρ are shown in Eqs. E.1 - E.9. During the actual calculation of uncertainty, the neutron lifetime, l, and effective delayed neutron fraction, β_{eff}, are assumed to have no variation so $\delta l = 0$ and $\delta\beta_{eff} = 0$. These parameters were not determined using methods which easily supply uncertainty, and their input is a constant such that their uncertainty is not quantified in this work.

$$k_{eff} = \frac{1}{1 - \rho\beta_{eff}} \tag{E.1}$$

$$\delta k_{eff} = \sqrt{\left(\frac{\partial k_{eff}}{\partial \rho}\delta\rho\right)^2 + \left(\frac{\partial k_{eff}}{\partial \beta_{eff}}\delta\beta_{eff}\right)^2} \tag{E.2}$$

$$\delta k_{eff} = \sqrt{\left(\frac{\beta_{eff}}{(1 - \rho\beta_{eff})^2}\delta\rho\right)^2 + \left(\frac{\rho}{(1 - \rho\beta_{eff})^2}\delta\beta_{eff}\right)^2} \tag{E.3}$$

$$\rho = \frac{k_{eff} - k_{DC}}{k_{eff}k_{DC}\beta_{eff}} \tag{E.4}$$

$$\delta\rho = \sqrt{\left(\frac{\partial \rho}{\partial \beta_{eff}}\delta\beta_{eff}\right)^2 + \left(\frac{\partial \rho}{\partial k_{eff}}\delta k_{eff}\right)^2 + \left(\frac{\partial \rho}{\partial k_{DC}}\delta k_{DC}\right)^2} \tag{E.5}$$

$$\delta\rho = \sqrt{\left(\frac{k_{DC} - k_{eff}}{k_{eff}k_{DC}\beta_{eff}^2}\delta\beta_{eff}\right)^2 + \left(\frac{1}{k_{eff}^2\beta_{eff}}\delta k_{eff}\right)^2 + \left(\frac{-1}{k_{DC}^2\beta_{eff}}\delta k_{DC}\right)^2} \tag{E.6}$$

$$\rho = \frac{\alpha_{DC} - \alpha}{\alpha_{DC}} \tag{E.7}$$

$$\delta\rho = \sqrt{\left(\frac{\partial\rho}{\partial\alpha}\delta\alpha\right)^2 + \left(\frac{\partial\rho}{\partial\alpha_{DC}}\delta\alpha_{DC}\right)^2} \tag{E.8}$$

$$\delta\rho = \sqrt{\left(\frac{-1}{\alpha_{DC}}\delta\alpha\right)^2 + \left(\frac{\alpha}{\alpha_{DC}^2}\delta\alpha_{DC}\right)^2} \tag{E.9}$$

APPENDIX F

AXIAL NEUTRON FLUX PROFILES

This appendix includes the neutron flux in each fuel cell for the measured configurations of the Polyethylene Class Foils. Table F.1 includes the neutron flux values as calculated by MCNP simulations. The values in Table F.1 assume 10 million fissions occur in the system.

Table F.1: Total neutron flux values for each fuel unit as determined using MCNP simulations.

Position in the Stack	Number of Units in the Configuration (10^4 $\frac{n^0}{cm^3 s}$)										
	15	14	13	12	11	10	9	8	7	6	5
15	1.34										
14	1.29	1.47									
13	1.43	1.38	1.58								
12	1.60	1.53	1.73	1.72							
11	1.75	1.71	1.93	1.88	1.88						
10	1.88	1.87	2.11	2.09	2.05	2.13					
9	1.93	1.96	2.22	2.25	2.25	2.30	2.34				
8	2.01	2.06	2.28	2.34	2.39	2.52	2.52	2.62			
7	2.09	2.18	2.23	2.34	2.45	2.67	2.74	2.79	2.93		
6	2.11	2.21	2.21	2.36	2.49	2.71	2.86	2.96	3.07	3.37	
5	2.06	2.19	2.19	2.35	2.53	2.63	2.81	3.00	3.16	3.48	3.83
4	1.97	2.12	2.08	2.25	2.45	2.54	2.76	3.00	3.25	3.52	3.83
3	1.84	1.99	1.91	2.09	2.29	2.43	2.69	2.97	3.29	3.52	3.92
2	1.67	1.82	1.72	1.88	2.08	2.24	2.50	2.79	3.14	3.49	3.97
1	1.49	1.62	1.56	1.72	1.91	2.06	2.32	2.63	2.99	3.38	3.94